A Two-dimensional Vortex Sheet Model for a Temporal Free Shear Layer: Integrating Beyond the Moore Singularity by the Technique of Viscosity Switch Smoothing

A Thesis Submitted for the Degree of
Doctor of Philosophy

Engineering Mechanics Unit
Jawaharlal Nehru Centre for Advanced Scientific Research
Bangalore 560064

Ujjayan Paul

February 2016

DECLARATION

I hereby declare that the matter embodied in the thesis entitled 'A **Two-dimensional Vortex Sheet Model for a Temporal Free Shear Layer: Integrating Beyond the Moore Singularity by the Technique of Viscosity Switch Smoothing**' is the result of investigations carried out by me at the Engineering Mechanics Unit, Jawaharlal Nehru Centre for Advanced Scientific Research, Bangalore, India under the supervision of **Prof. Roddam Narasimha** and that it has not been submitted elsewhere for the award of any degree or diploma. In keeping with the general practice in reporting scientific observations, due acknowledgement has been made whenever the work described is based on the findings of other investigations.

Ujjayan Paul

CERTIFICATE

I hereby certify that the matter embodied in the thesis entitled 'A Two-dimensional Vortex Sheet Model for a Temporal Free Shear Layer: Integrating Beyond the Moore Singularity by the Technique of Viscosity Switch Smoothing' has been carried out by Ujjayan Paul at the Engineering Mechanics Unit, Jawaharlal Nehru Centre for Advanced Scientific Research, Bangalore, India under my supervision and that it has not been submitted elsewhere for the award of any degree or diploma.

Prof. Roddam Narasimha

Abstract

The Navier-Stokes equations are the fundamental equations governing the dynamics of Newtonian fluids, if one neglects theirs derivation from the Boltzmann equation of molecular dynamics. The inviscid Navier-Stokes equations are known as the Euler equations. The Reynolds number of the flow, which is the ratio of inertial to frictional forces in the fluid, is infinite for an inviscid fluid. For very low Reynolds number flows it is possible to obtain some exact and approximate solutions of the Navier-Stokes equations.

Modelling turbulent flows is a difficult problem in fluid dynamics. The Navier-Stokes equations are not amenable to mathematical analysis, and they cannot be used to predict detailed consequences or the emergence of randomness at high Reynolds number. The theory of Richardson and Kolmogorov views turbulence as a cascade of eddies or coherent structures. However, most of these studies are statistical and are not likely to answer the lack of universality. The theory of chaos in fluid flows, originated by Lorenz, views turbulence as a sensitive dependence on initial conditions. Simple nonlinear equations with analytical solutions and prescribed initial conditions were found to exhibit chaotic and apparently random behaviour. Turbulent scales have a fractal like distribution. However, the randomness generated by the Navier-Stokes equations may be due to (hidden) intrinsic reasons. This framework cannot be used to predict global variables in a turbulent flow, for example the Reynolds number dependence of the resistance coefficient, in a pipe of given radius and pressure gradient.

The advent of high-speed digital computing has made it possible to resolve intractable theoretical problems in turbulence (at modest to moderate Reynolds number). Today many results on turbulent flows depend critically on computer results - there is no other way to do it. The direct numerical simulation of simple physical problems is a useful tool in turbulence research. For homogeneous turbulence with periodic boundaries the maximum spatial resolution achieved was 4096^3 performed by the Earth Simulator supercomputer in 2003. It has been exceeded since. Unfortunately engineering simulations at high Reynolds number or with complex boundaries cannot be solved by DNS on the current generation of computers. There are various ad-hoc turbulence models to account for the wide range of scales generated at high Reynolds number. Another interesting way to handle such problems is through Lattice Boltzmann simulations.

We study the time evolution of a temporal free shear layer, modelled by an inviscid vortex sheet with periodic boundaries. A wide range of practically important and naturally occurring turbulent flows are generated by shear. Jets, wakes and mixing layers are examples of shear flows. These flows have been found to contain large scale coherent structures amidst chaos. The experiments of Brown and Roshko (1974) showed that a turbulent free shear layer is dominated by large spanwise vortices. The framework of homogeneous isotropic turbulence is therefore not appropriate for studying these type of turbulent flows. For two dimensional turbulent shear flows modelling with point vortices or a vortex sheet mimics the growth of coherent structures. These models are strictly two dimensional. It has been shown by Wygnanski and Brownand (1979) that the coherent structures in a free shear layer are quasi-two dimensional, and independent of Reynolds number at sufficiently high Reynolds number.

A free flat inviscid vortex sheet is unstable to infinitesimal disturbances. Linear perturbation analysis shows that a disturbance with wavenumber k grows exponentially at a rate proportional

to k. The vortex sheet is ill-posed and gives rise to a finite time singularity. Since this linear theory cannot be extended much beyond the initial time, a nonlinear analysis is required to make this conclusion. An estimate of the singular time (critical time) was first given by Moore (1980) using asymptotic analysis. He further showed that the coefficients of Fourier modes of the sheet decay like $k^{-5/2}$ for wavenumber k. The vortex sheet loses analyticity, and the singularity is known as the Moore singularity. At the critical time there is a cusp in vortex sheet circulation density and a blow-up in curvature of the vortex sheet.

It is well-known that inviscid vortex sheet computations cannot proceed past the Moore singularity. The singularity formation is not restricted to two dimensions as shown by Ishihara and Kaneda (1995). There have been extensive studies on an inviscid vortex sheet, most of them by point vortex approximations, with or without desingularization. The spontaneous appearance of singularity is a consequence of mathematical modelling, since a real fluid with viscosity, however small, will never develop any singular properties. The reason for desingularization is to obtain a smooth roll-up of a vortex sheet. Some remarkable smoothing techniques were given by Krasny (1986), Holms, Nitsche and Putkaradze (2006) and Hou, Lowengrub and Shelley (1997). A weak solution to the Euler equations is recovered in the limit of vanishing smoothing parameter. A fundamental weak point of desingularization is that it introduces a smoothing parameter that does not have physical meaning like viscosity or surface tension. It also leads to suppression or delay of chaos in a system of point vortices, see Suryanarayanan and Narasimha (2014). Since a turbulent free shear layer is inherently chaotic, desingularization makes it extremely difficult to simulate a limiting solution which represents a turbulent free shear layer.

The discrete approximation to vortex sheets has low computational efficiency for a given degree of convergence on moments when compared to continuous approximation to vortex sheets, for example the vortex panel method of Basu, Narasimha and Prabhu (1995). On the other hand, point vortex system codes are easily parallelized. The vortex panel method was used to simulate a spatial free shear layer with appropriate inflow and outflow boundaries. The boundary condition on the splitter plate is satisfied rigorously using a doublet sheet. The roll-up of the sheet was smoother compared to point vortex models and the well known invariants of vortex dynamics were conserved. The mean streamwise velocity profile, the growth rate, and the values of stress and moments are in close agreement to experiments. However, the vortex panel method suffered from self intersection of panels due to low resolution power of computers. Thus, continuous models are effective in simulating a free shear layer and the convergence of computed variables is faster than discrete models.

In the present vortex sheet model for a temporal free shear layer the velocity fields generated are computed from the kinematic Biot-Savart equation. The adaptive split of panels or vortex sheet segments used in the vortex panel method is used to maintain resolution. The previous technique appears in the work of Basu, Narasimha and Prabhu (1995). There is no self-intersection of vortex sheet segments in this case. The problem of singularity formation prevents the roll-up of the vortex sheet. The introduction of small amount of physical viscosity in a vortex sheet problem does not lead to a smooth roll-up. This vortex sheet is harder to compute than an inviscid vortex sheet. The limited computations of Tryggvasson, Dahm and Sbeih (1991) showed that the Navier-Stokes solution in the limit ν goes to zero is similar to

desingularized point vortex solution in the limit δ goes to zero. Another type of physical re-gurlarization is provided by surface tension as in Pullin (1982). Surface tension tends to reduce the interface thus smoothing out very fine-scale structures. However, these physical effects are weak and the close approach of singularities in the complex plane to the real axis induces high sensitivity, and breakdown in computations.

Tangential diffusion of vorticity is added to the vortex sheet equations at points where Moore singularity appears, which enables us to take computations past the critical time. This is an adaptive procedure and the regularization is switched on only when gradients along the vortex sheet are above a cut-off or threshold. We shall call this (method) as the *viscosity switch*. The cusp in circulation density is not removed entirely, but the peak is analytic. Importantly, there is no finite-time blow up as the peak circulation is controlled at each time step. The viscosity switch is not an arbitrary parameter inserted to supress the singularity. This is a restricted form of viscous diffusion. In real fluids, viscosity and surface tension are responsible for regularizing the vortex sheet equations. In the limit of zero vortex sheet layer thickness, the diffusing vortex sheet has properties that are different from the inviscid vortex sheet.

The viscosity switch method gives a smooth roll-up of the vortex sheet starting with random initial conditions. This is the main result of the thesis. The rest are applications and conclusions. The vortex sheet rolls-up and forms coherent structures. These structures are long lived and of different sizes. They are either absorbed by a bigger structure or they merge with each other at different times. The periodic boundaries limit the growth of coherent structures. The accuracy of computation is checked by verifying the conservation of mass, momentum and energy. Since there is some form of diffusion, the invariance is approximate: there is loss of energy. The growth rate of the free shear layer is obtained from an ensemble of simulations. The enumeration of singular regions is required to identify coherent structures. The singular regions occur in clusters giving rise to superstructures.

In Chapter 1, we review the point vortex model and associated desingularization techniques. This provides the basis for extension into more complicated systems like the vortex sheet element model. In Chapter 2, the vortex sheet element model is built with periodic boundaries and no viscosity or smoothing of any type. The numerical method for the model is outlined in Chapter 3. There is also a brief study about the nature of singularity that prevents the vortex sheet element model from being able to simulate a vortex sheet roll-up. The viscosity switch solution of the vortex sheet solution is presented in Chapter 4. The method of variable viscosity smoothing (viscosity switch) is introduced in this chapter. The tools developed in Chapters 2 and 4, enable us to simulate a temporal free shear layer. The results are summarized in Chapter 5. It also contains an ensemble study for the growth of a temporal free shear layer. Chapter 6 contains discussion and conclusions.

Acknowledgements

I want to thank Prof. Roddam Narasimha for all the time, patience and energy he spent supervising my thesis. I would also like to thank friends and mentors: Vinay K Gupta, Ryan Chaterjee, Anubhab Roy, Saikat Saha, Prof. Meheboob Alam, Priyanka Shukla, Mahan R Banerjee, Partha P Kundu, Gautam Chaterjee, Shahjhan S Hasanali, Vicky K Verma, Ramakrishna Rongali and Prasanth Prabhakaran. The names are in no particular order.

The equations that mattered

$$\pi \cot(\pi z) = \frac{1}{z} + 2z \sum_{n=1}^{\infty} \frac{1}{z^2 - n^2}$$

$$A_{\left[\frac{\mathrm{d}B}{\mathrm{d}t}\right]}(k) = \imath k A_{[B]}(k)$$

Contents

List of Figures

Chapter 0

Introduction to Free Shear Layers

The governing equations for an incompressible viscous fluid, also known as the incompressible Navier-Stokes equations, are a set of nonlinear partial differential equations:

$$\nabla \cdot \boldsymbol{u} = 0 \tag{1}$$

$$\frac{\partial \boldsymbol{u}}{\partial t} + \underbrace{\boldsymbol{u} \cdot \nabla \boldsymbol{u}}_{\text{advection}} = -\rho^{-1} \nabla p + \underbrace{\nu \nabla^2 \boldsymbol{u}}_{\text{diffusion}} + \underbrace{\rho^{-1} \boldsymbol{f}}_{\text{body force}} \tag{2}$$

These equations are mathematical formulation of the conservation of mass and momentum respectively. The velocity field is expressed as $\boldsymbol{u}$, the density of the fluid ρ is a constant and the kinematic viscosity is ν. The external body force $\boldsymbol{f}$ is imposed on the fluid. Since there is no external force in this thesis we set $\boldsymbol{f} = 0$ identically. The pressure p is not a thermodynamic quantity, as it cannot be related to temperature and density of an incompressible fluid. From equation (1) and (2) we get,

$$\nabla^2 p = -\rho \frac{\partial u_i}{\partial x_j} \frac{\partial u_j}{\partial x_i}$$

The pressure term is a solution of the Poisson equation and is determined upto a constant. The material or convective derivative is denoted as $\frac{\mathrm{d}}{\mathrm{d}t}$. The material derivative is defined as $\frac{\mathrm{d}}{\mathrm{d}t} = \frac{\partial}{\partial t} + \boldsymbol{u} \cdot \nabla$. Using this notation, equation (2) can be written as

$$\frac{\mathrm{d}\boldsymbol{u}}{\mathrm{d}t} = -\rho^{-1} \nabla p + \nu \nabla^2 \boldsymbol{u} \tag{3}$$

If the viscosity ν of fluid is zero, then equation (2) becomes

$$\frac{\mathrm{d}\boldsymbol{u}}{\mathrm{d}t} = -\rho^{-1} \nabla p \tag{4}$$

Equation (4) is of the hyperbolic type, whereas the addition of viscosity as in equation (3) makes it parabolic. The inviscid version of the Navier-Stokes equations are also known as the Euler equations.

The Navier-Stokes equations are often written in dimensionless form by rescaling the length, time, velocity and pressure variables. The system parameters are then all subsumed in a single dimensionless parameter called the *Reynolds number*

$$\mathrm{Re} = \frac{UL}{\nu} \tag{5}$$

where U is a charecteristic velocity scale and L a charecteristic length scale. The non-dimensional momentum equation is then

$$\frac{\mathrm{d}\boldsymbol{u}}{\mathrm{d}t} = -\nabla p + \frac{1}{\mathrm{Re}}\nabla^2\boldsymbol{u} \tag{6}$$

The Reynolds number is interpreted as the ratio of inertial forces to viscous forces. High Reynolds number flows are usually turbulent, while low Reynolds number flows are usually laminar. The Euler equations are the Navier-Stokes equations without the viscous term, limit of Re going to infinity in equation (6).

0.1   Free Shear Layers

A (spatially developing) free shear layer is usually obtained in the laboratory by letting two initially separated streams of different velocities, U_1 above and U_2 below a semi-infinite length splitter plate, come in contact at the trailing edge of the plate. The term 'free' is used to indicate that the shear layer is not attached to any solid boundary. Sometimes the term 'plane' is added to 'free shear layer' to imply that its mean velocity is two-dimensional. Mixing layers are type of free shear layers, although the converse is not true. However, the distinction between 'mixing' free shear layers and 'non-mixing' free shear layers is often not enforced. Figure 1 illustrates a two-dimensional free shear layer.
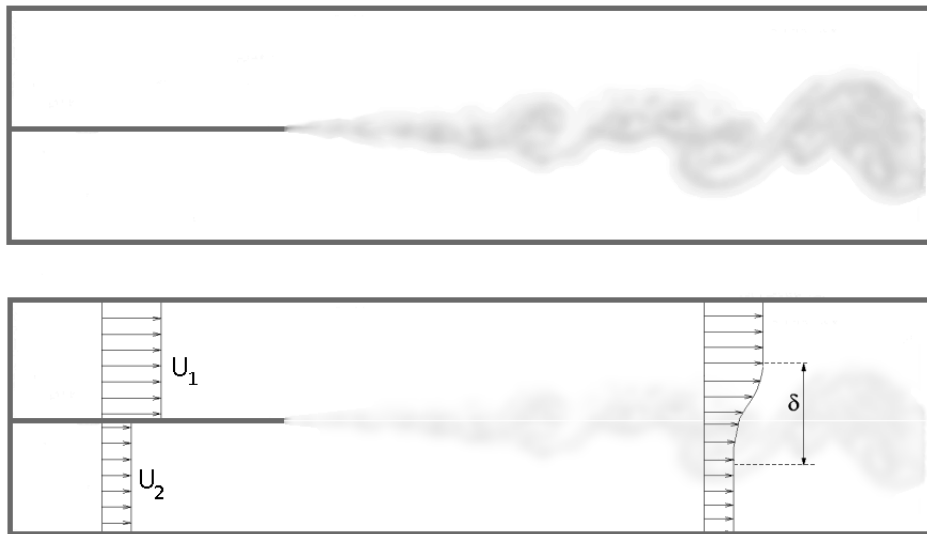
Figure 1: A schematic diagram of a spatial shear layer at high Reynolds number. Top: the interface between the top and the bottom fluids is marked in a colour contour. Bottom: upstream and downstream time averaged velocity profile. The thickness of the free shear layer is δ. The extent of the layer is the region where the y-derivative of the mean velocity profile is non-zero. The boundary layer on either sides of the splitter plate is not shown.

Free shear layers belong to the general class of inhomogeneous flows known as free shear flows. Apart from free shear layers, other examples of free shear flows are jets and wakes (behind bodies). A free shear flow can be either laminar or turbulent. However, most free shear flows that occur naturally are turbulent[1]. Their importance lies in the fact that they are highly

---

[1]Another type of turbulent flow considered widely in texts is the statistically homogenous isotropic turbulence. This may not be a a very simple example as opposed to a free shear layer. Further details on homogenous isotropic turbulence can be found in the textbooks by Batchelor (1953) and Davidson (2004).

instructive from a theoretical point of view. Jets, wakes and free shear layers can be realized in the laboratory without difficulty. They are also important in technology because they dissipate energy, cause mixing of fluids, lead to entrainment and are a source of drag or thrust. Most of the ideas on free shear layers can be extended, with suitable modifications, to jets and wakes, and vice-versa. For more on jets and wakes refer to Carazzo, Kaminski and Tait (2006) and Narasimha and Prabhu (1972).

We shall work with a free shear layer with initial conditions $U_2 = -U_1$ and periodic boundaries in the streamwise direction. This is known as the temporal free shear layer. Note that in Figure 2 the interface between the two streams (marked in red) have a slight perturbation. The other assumptions are:

1. The flow is two-dimensional. It is the same as assuming that the flow is homogeneous in the third dimension.

2. The fluid is incompressible and has uniform density.

3. The Reynolds number is sufficiently large, so that the flow is turbulent and the dynamics of 'large scales' is independent of viscosity.

4. There are no solid boundaries.

5. External forces including gravity are absent.

The temporal free shear layer resembles a spatial free shear layer in a moving frame of reference. The spatial shear layer and the temporal shear layer can be related by a Galilean transformation under certain limiting conditions that are given in Corcos and Sherman (1984). In the canonical scenario presented here, the temporal shear layer involves a single parameter: the velocity difference across the layer. The flow is also inviscid due to the lack of viscosity in the model. Laboratory experiments and theoretical studies have shown that a free shear layer is not stable. Any infinitesimal disturbance causes the interface to roll-up and give rise to complicated vortex structures. This is known as the *Kelvin-Helmholtz instability* or *K-H instability*. Analytical details related to Kelvin-Helmholtz instability are given in Section 3.2. In general for spatially developing non-parallel flows, a growing layer is stable for Re less than about 30, and is only weakly dependent on the free stream velocity ratio, but not including cases with counterflow, see Bhattacharya et al. (2006).

0.2 Large-scale Structures in Free Shear Layers

Given the chaotic and disordered nature of turbulence, it was at first strange that free shear layers contain large-scale structures. The key observation was made by Brown and Roshko (1974), and further validations have been obtained in later experiments. They found that the interface between the two streams consists of large, quasi-two-dimensional 'coherent' structures and they span the whole width of the layer. These large eddies play an important role in the entrainment process, by which momentum and energy are extracted from the free-stream region and fed into the turbulent 'mixing' region.
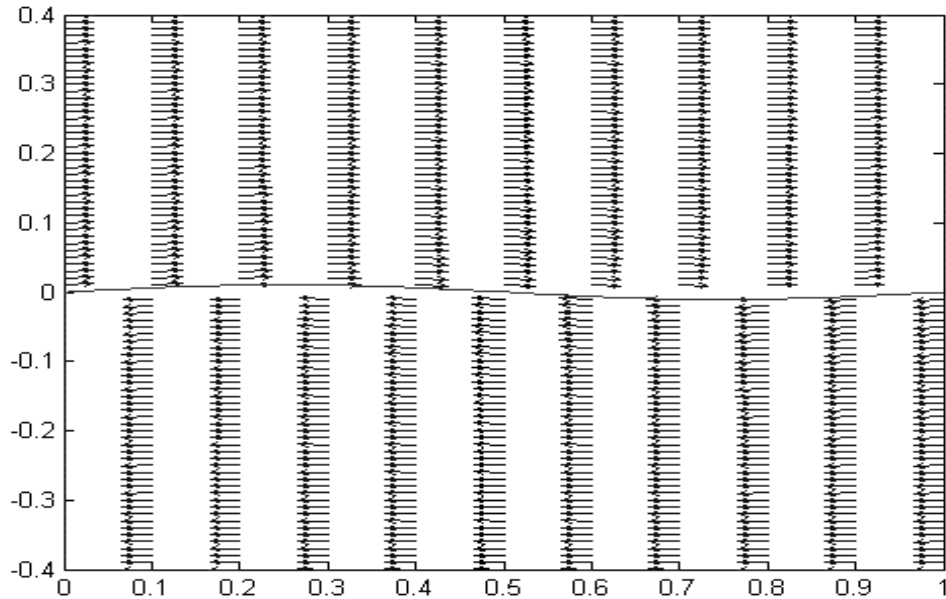
Figure 2: A quiver plot depicting a temporal free shear layer generated by a free flat vortex sheet with x-periodic boundaries. There is a slight perturbation on the interface at time $t = 0$. The period length in x is 1. There is no periodicity in the y-direction. The flow shown here can be either laminar or turbulent. For a turbulent flow the velocities are time-averaged.

This is remarkably similar to what we obtain if we approximate a free shear layer with a vortex sheet[2]. The infinite flat vortex sheet generates a flow profile of the type $\pm U$, which is a temporal free shear layer. This may be superimposed with other background flows to generate spatial free shear layers. A schematic temporal free shear layer with periodic boundaries is shown in Figure 0.2. The Reynolds number of the flow is infinite since viscosity is zero. The flat vortex sheet is an unstable configuration due to K-H instability. It rolls up to generate structures whose scales, shape and internal organization mimic the 'coherent' structures of a free shear layer at high Reynolds number.
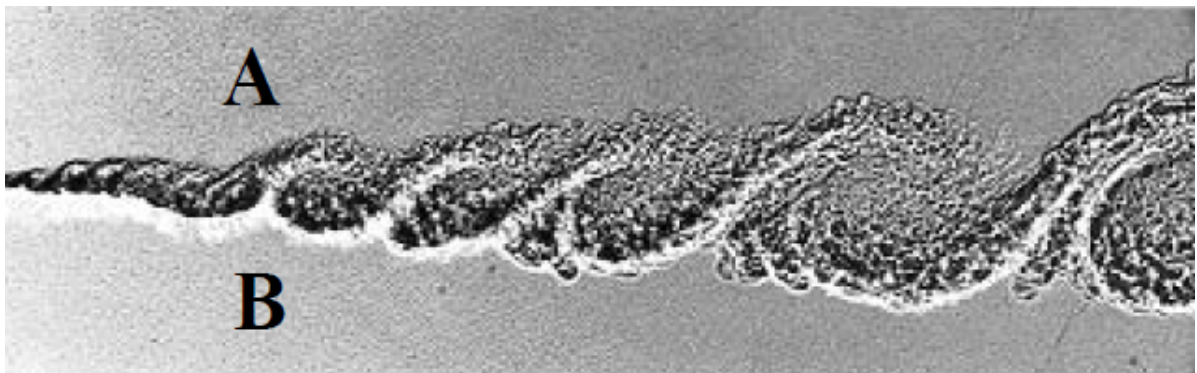
Figure 3: An example of spatial free shear layer at high Reynolds number between two different streams of gases - nitrogen and helium (Brown and Roshko 1974). The fast stream is labelled A and the slow stream is labelled B.

This is fundamentally different from homogeneous isotropic turbulence where there is no large scale 'coherent' structure in the flow. The homogeneous isotropic turbulence is an idealized

---

[2]Vortex sheets are formally introduced in Section 0.3. A vortex sheet is amenable to detailed mathematical treatment. It is used to model velocity jumps across an interface, provided the thickness of the jump is small compared to the streamwise scale.

example of turbulence, but most real turbulent flows are neither homogeneous nor isotropic. This makes free shear flows a better and more relevant example in technology and geophysical studies. The free shear layer therefore provides a good starting point for the understanding of a turbulent shear flow problem.

0.3 Vortex Sheets

A vortex sheet (in a two dimensional flow) is a discontinuity of tangential velocity across a curve in the plane of the flow. The vorticity distribution is singular: it is infinite on the curve and zero elsewhere. In a viscous flow the vorticity field becomes automatically free from singularities, but in the Euler limit the vorticity is confined to the sheet at all times as a Dirac delta function in the coordinate normal to the sheet. A corollary of Kelvin's circulation theorem the vortex sheet separates regions of fluid in irrotational motion.

The formulation of the problem is given in terms of a complex coordinate $z = x + \imath y$. The vortex sheet is described parametrically by $z(s,t)$ where s is the arc length between coordinate z and any reference material point, and t is the time. Let $\gamma(s,t)$ denote the strength of the sheet, that is, the jump in the tangential discontinuity. Then the velocity field induced by the sheet is

$$\frac{\partial z^*}{\partial t} = -\frac{\imath}{2\pi} \int_{-\infty}^{\infty} \frac{\gamma(s',t)ds'}{z(s,t) - z(s',t)} \tag{7}$$

The integral in (7) is a Cauchy principal value integral. Greater details on vortex sheets and vorticity dynamics can be found in the textbook by Saffman (1977).

We now define Γ as the integrated sheet strength or circulation between a point with arc length s and the reference material point $s = 0$ in the sheet:

$$\Gamma(s,t) = \int_{0}^{s} \gamma(s',t)\mathrm{d}s' \qquad \text{and} \qquad \frac{\mathrm{d}\Gamma}{\mathrm{d}s} = \gamma(s,t) \tag{8}$$

As a consequence of Kelvin's circulation theorem, in the absence of external forces on the sheet, the circulation between any two material points in the sheet remains conserved, so

$$\frac{\mathrm{d}\Gamma}{\mathrm{d}t} = 0 \tag{9}$$

The equation of the sheet can be rewritten in terms of Γ and t by a change of variable. The parameter s is replaced by Γ. That is,

$$z(s,t) = z(\Gamma,t)$$

is the locus of the sheet and $\gamma = |\partial z/\partial \Gamma|^{-1}$. Also $\gamma\,\mathrm{d}s = \mathrm{d}\Gamma$ and (7) can be expressed as

$$\frac{\partial z^*}{\partial t} = -\frac{\imath}{2\pi} \int_{-\infty}^{\infty} \frac{d\Gamma'}{z(\Gamma,t) - z(\Gamma',t)} \tag{10}$$

This nonlinear integro-differential equation is called the *Birkoff-Rott equation*. It describes the evolution of the sheet given its initial shape and strength. It is an elegant formulation, but is not necessarily the most suitable for numerical computation of sheet evolution.

When initial conditions are given, the solution to equation (10) can be obtained by integration. At $t = 0$, the undisturbed vortex sheet extends from $-\infty$ to $+\infty$ with uniform velocity on either side given by

$$u(x, y) = \begin{cases} U & y > 0 \\ -U & y < 0 \end{cases} \tag{11}$$

which in circulation coordinate representation becomes

$$z(\Gamma, 0) = \Gamma \tag{12}$$

A slight perturbation is given to the vortex sheet at time $t = 0$. Specifically, we impose a sinusoidal disturbance of amplitude ϵ and wavelength $\lambda = L$.

$$z(\Gamma, 0) = \Gamma + i\epsilon \sin \frac{2\pi\Gamma}{L} \tag{13}$$

Note that boundary conditions are periodic. It is advantageous to take $L = 1$. The admissible range of solutions are those which have Γ varying monotonically along the sheet. This condition may be written explicitly as

$$\frac{\mathrm{d}\Gamma}{\mathrm{d}s} \geq 0 \tag{14}$$

The present vortex sheet problem is ill-posed and a singularity known as Moore's singularity occurs in finite time. Further discussions on Moore's singularity and the problem arising in vortex sheet computation can be found in Section 0.5.

0.4   Compressibility in Free Shear Layers

One of the assumptions we make is that the fluid is not compressible. An incompressible fluid will not behave like any real fluid, because disturbances in incompressible fluids travel at infinite speed, like in rigid bodies. Miles (1958) used a vortex sheet model to study the two-dimensional instabilities of a free shear layer. For an experimental study on compressible free shear layers refer to Papamoschou and Roshko (1988). The growth rate of compressible free shear layers was found be lower than those of incompressible free shear layers.

In compressible fluids ρ is also a variable, which adds another equation - the energy conservation equation connecting p, ρ and another variable T being the temperature. The closure is obtained by the equation of state. The compressible version of inviscid Navier-Stokes equations are as follows:

$$\text{Continuity} \quad : \quad \frac{\partial \rho}{\partial t} + \nabla \cdot (\rho \boldsymbol{u}) = 0 \tag{15}$$

$$\text{Momentum Equation} \quad : \quad \rho \frac{\mathrm{d}\boldsymbol{u}}{\mathrm{d}t} = -\frac{1}{\gamma M^2}\nabla p \tag{16}$$

$$\text{Energy Equation} \quad : \quad \rho \frac{\mathrm{d}T}{\mathrm{d}t} = \frac{\gamma - 1}{\gamma}\frac{\mathrm{d}p}{\mathrm{d}t} \tag{17}$$

$$\text{Equation of State} \quad : \quad p = \rho T \tag{18}$$

where M is the Mach number[3] and γ is the ratio of the constant pressure and constant volume heat capacity. The equation of state given in (18) is for a perfect gas.

---

[3]Mach number is the ratio of freestream velocity U_∞ and the speed of sound waves $c = \sqrt{\gamma R T}$ in the medium. In an incompressible fluid $M = 0$. For $M < 0.3$ density changes in the fluid are minute and can be treated as nearly incompressible.

The linear stability theory of a compressible free shear layer tends to be complicated. However, a number of experiments have shown that a compressible free shear layer becomes more stable with increasing Mach number. The flow variables are decomposed into a base state and a fluctuating component that oscillates,

$$\begin{aligned}
\boldsymbol{u} &= \left[U(y) + u'(x, y, t), v'(x, y, t)\right] \\
p &= P(y) + p'(x, y, t) \\
\rho &= D(y) + \rho'(x, y, t) \\
T &= \Theta(y) + \theta'(x, y, t)
\end{aligned}$$

The base state and perturbed state must satisfy the compressible Navier-Stokes equations. A normal modes solution is found by substituting

$$[u', v', p', \rho', \theta'](x, y, t) = [f, g, \Pi, r, \theta](y)e^{\imath\alpha(x-ct)}$$

into the linearized disturbance equations. In the above relation, α is identified as the wavenumber in x-direction, c is identified as the wave velocity[4]. For a free shear layer with uniform temperature $\Theta = 1$, the stability of normal modes is governed by the equation

$$\Pi_{yy} - \frac{2U_y}{U - c}\Pi_y - \alpha^2[1 - M^2(U - c)^2]\Pi = 0 \tag{19}$$

and the boundary conditions $\Pi(y) = 0$ as $y \to \pm\infty$. For more details on equation (19) refer to Lees and Lin (1946) and Blumen, Billings and Drazin (1975). When $M = 0$ equation (19) reduces to the Rayleigh equation.

The stability equation (19) together with its boundary conditions is an eigenvalue problem. Nontrivial solutions of Π exist only for certain values of the parameters α and $c = c_R + \imath c_I$. The solution is called an unstable mode if the corresponding eigenvalue c_I is greater than zero. A flow may have several unstable modes. Unfortunately, for equation (19) no general results are known and the number of unstable modes is usually determined empirically, by solving the equations numerically and searching for eigenvalues. However, a few situations are tractable. For example, in a hyperbolic-tangent velocity profile $U(y) = \tanh y$, a root is given by

$$c = 0, \qquad c = \sqrt{1 + \frac{1}{M^2} - \frac{1}{M^2}\sqrt{1 + 4M^2}} = c_0 \quad \text{(say)}$$

The above eigenvalues (phase velocities) are exact for $\alpha = 0$. The solution c_0 is imaginary, zero or real depending on whether M is less than, equal to or more than $\sqrt{2}$ respectively. This illustrates that the flow becomes more stable as the value of M increases. The physical reasoning for an increase in stability of a compressible fluid is that a certain amount of work is required to overcome the elasticity of the medium, before it can initiate instability. Buoyancy due to gravity shows a similar stabilizing feature.

0.5   Moore's Singularity

A vortex sheet model for a free shear layer poses interesting mathematical problems concerning singular integrals, weak limits and nonlinear dynamics. It was conjectured by Birkhoff (1962)

---

[4]Note that in temporal stability theory α is real and c is complex.

that nonlinearity would cause a vortex sheet to form a singularity at a finite time. That is, variables tend to infinity at a finite time. Infinities do not occur physically, but the behaviour near the singularity is of interest. An asymptotic analysis by Moore (1979) supported Birkhoff's conjecture. Further analysis by Meiron, Baker and Orszag (1983) obtained results consistent with Moore, by studying the Taylor series expansion of the Birkhoff-Rott integral in time. Using a point vortex approximation and a Fourier filter to control the growth of round-off error, Krasny (1986) studied direct simulations of vortex sheet motion. The resulting conclusions were consistent with Moore's. It was found that the point vortex approximation converges upto the vortex sheet's critical time. The resultant vortex sheet does not depend on any numerical parameters. For a study on special solutions refer to Caflisch and Orellana (1989).

A vortex sheet becomes singular at a finite time well before the appearance of large scale roll-up commonly associated with free shear layers. The curvature of the sheet diverges and the circulation density develops a cusp but remains finite. Moore's analysis indicated the presence of a branch singularity of order 3/2. Whether this is true or not cannot be said as theoretical proof is lacking. But numerical evidence presented by Krasny (1986) supports Moore's result. Because of this finite time blow up, the existence and evolution of the vortex sheet beyond the critical time t_c is in question and the solutions are not trivial. Commonly utilized techniques like regularization are effective in solving ill-posed problems. The initial condition of the vortex sheet is given in equation (13). The singularity manifests itself as a spike in circulation density and a jump discontinuity in curvature. While it can be shown that vortex sheets starting from analytic initial data will develop a finite time singularity (see Moore, 1984), proving that a singularity appears for any initial data remains an open problem.

Computer solutions of vortex sheets require an additional parameter to be introduced in order to avoid a finite time singularity. Such a parameter is also known as the regularization parameter. In Chapter 4 we introduce a regularization parameter which we shall call as *viscosity switch*. This parameter has a physical significance resembling but not identical to that of viscosity. Since the parameter is nonzero at some locations in time and space, and zero otherwise, it is called a switch. Some analogous numerical problems are shock waves in compressible flows, see Lax(1973), where introduction of a smoothing parameter produces physically relevant solutions.

0.6 Background: Two Dimensional Euler Solutions

We shall consider two-dimensional motion of a fluid $\boldsymbol{u}(x_1, x_2) = (u_1, u_2)$ at high Reynolds number and periodic boundaries. There are no external force fields. The discussion is not specific to a temporal free shear layer with periodic boundaries, but valid for any flow in two-dimensions with periodic boundaries and non-zero viscosity. The velocity and scalar vorticity fields are governed by

$$\frac{\mathrm{d}\boldsymbol{u}}{\mathrm{d}t} = -\frac{1}{\rho}\nabla p + \nu\nabla^2\boldsymbol{u} \tag{20}$$

$$\frac{\mathrm{d}\omega}{\mathrm{d}t} = \nu\nabla^2\omega \tag{21}$$

Equation (21) represents the diffusion of vorticity. This equation includes an additional term known as vortex stretching in three-dimensions. The presence of vortex stretching in the vorticity

equation leads to the formation of intense vortex filaments in three-dimensional flows, which is not possible in two-dimensional flows. This is a fundamental difference between two and three dimensions. From equations (20) and (21) it is easy to derive the equations for kinetic energy per unit mass and enstrophy respectively,

$$\frac{\mathrm{d}}{\mathrm{d}t}\left\langle\frac{1}{2}u^2\right\rangle = -2\nu\left\langle\frac{1}{2}\omega^2\right\rangle \tag{22}$$

$$\frac{\mathrm{d}}{\mathrm{d}t}\left\langle\frac{1}{2}\omega^2\right\rangle = -\nu\langle(\nabla\omega)^2\rangle \tag{23}$$

The angled brackets mean spatial averaging (which is also equal to the ensemble average if the system is ergodic). Therefore in an inviscid two-dimensional flow both energy and enstrophy are conserved.

The point to note is that enstrophy decreases monotonically when ν is nonzero. So $\langle\frac{1}{2}\omega^2\rangle$ is bounded from above by its initial value. In the absence of a vortex stretching mechanism, there is no way for enstrophy to increase. Therefore in the limit Re $\to \infty$ it follows that

$$\lim_{\nu\to 0}\frac{\mathrm{d}}{\mathrm{d}t}\left\langle\frac{1}{2}u^2\right\rangle = 0$$

since $\langle\frac{1}{2}\omega^2\rangle$ is always greater than or equal to zero. It implies that energy is conserved to within a margin of order Re^{-1}. On the other hand, $\langle\frac{1}{2}\omega^2\rangle$ is fixed by its initial value and cannot grow to compensate for small values of ν.

While the dissipation of energy is a prolonged process, dissipation of enstrophy is not bound to be slow. In equation (21) we see that vorticity is advected and diffused like a passive scalar. In the limit of large Re, diffusion is small except in the regions of large vorticity gradients. However, if a blob of vorticity is extended into thin vortex sheets, it can amplify vorticity gradients and $(\nabla\omega)^2$ will increase with time. Thus even if a two-dimensional flow cannot enhance its enstrophy, it does have a mechanism to generate fine-scale structures where high vorticity gradients lead to destruction of enstrophy. In the theory of two-dimensional turbulent flows enstrophy plays a role similar to that of energy in three dimensions. The enstrophy is passed down from large to small scales, until viscosity destroys it by diffusion of vorticity when gradients become large enough. This process is often refered to as the *enstrophy cascade*, by analogy with the energy cascade in three dimensions.

Based on the evidence that dynamical systems with large degrees of freedom tend to evolve to a state which is independent of initial conditions, Batchelor (1969) and Kraichnan (1967) put forward a non-trivial hypothesis that in fully developed two-dimensional turbulence $\frac{\mathrm{d}}{\mathrm{d}t}\langle\frac{1}{2}\omega^2\rangle$ is independent of ν when Re is large. Batchelor (1969) showed from here that the energy spectrum should have a self-similar form valid at all times other than the initial period. The energy spectrum function is written as $E(k)$,

$$\frac{\mathrm{d}}{\mathrm{d}t}\left\langle\frac{1}{2}u^2\right\rangle = \int_0^\infty E(k)\,\mathrm{d}k \qquad \frac{\mathrm{d}}{\mathrm{d}t}\left\langle\frac{1}{2}\omega^2\right\rangle = \int_0^\infty k^2 E(k)\,\mathrm{d}k \tag{24}$$

Computer simulations do not support this theory entirely. A detailed discussion can be found in Davidson (2003) where it is mentioned that strong regions of vorticity survive filamentation and eventual viscous dissipation. These patches of vorticity behave like a point vortex system showing cluster formation and local intensification. The time dependence of $E(k)$ follows from

equations (24). Since $\langle\frac{1}{2}u^2\rangle$ is almost conserved and $\langle\frac{1}{2}\omega^2\rangle$ decreases at a finite rate, the area under the curve of $E(k)$ is nearly constant and the integral of $k^2 E(k)$, which is weighted more towards large values of k, falls with time. It means that $E(k)$ must grow at small k and deplete at large k. This is interpreted as the flow of energy from small to large scale structurces.

0.7 Terminilogy

Attractor: A set in the phase space invariant under the dynamics, toward which neighbouring orbits approach asymptotically. An attractor can be a single point, a curve, a manifold or a complicated set with fractal structure.

Chaos: A particular behaviour of dynamical systems where two points in phase space, initially very close, will separate exponentially.

Coherent structures. The best way to describe coherent structures (in free shear layers) is in a qualitative fashion: as relatively long-lived objects of generally circular topology. It should be clearly distinguishable from the background within which they evolve.

Compressibility: A measure of relative volume or density change of a fluid as a response to pressure change. The factor is defined as

$$\beta = \frac{1}{\rho}\frac{\mathrm{d}\rho}{\mathrm{d}p}$$

The parameter β for incompressible flows is zero.

Curvature: For a plane curve, it is a local measure of the rate of change of tangential angle with respect to arclength. The curvature κ of a parametric curve $(x(t), y(t))$ is given by

$$\kappa = \frac{|x'y'' - y'x''|}{(x'^2 + y'^2)^{3/2}} \tag{25}$$

The primes denote derivatives with respect to t.

Ensemble: Also known as probability space in the domain of probability theory. In fluid mechanics the term is usually interpreted as a set of experiments or realizations with identical macroscopic conditions, but different microscopic conditions.

Ill-posed problem: Hadamard defines a problem as well-posed if a solution exists, is unique and depends continuously on initial data. Problems that are not well-posed in the sense of Hadamard are termed ill-posed.

Regularization: In the context of vortex sheets it is a process of providing additional information or parameters that will solve an otherwise ill-posed problem.

Vorticity and Enstrophy: The vorticity field in a fluid flow is given by $\boldsymbol{\omega} = \nabla \times \boldsymbol{u}$. It is interpreted as measure of local rotation of fluid elements. The evolution of vorticity field $\boldsymbol{\omega}$ is derived by taking the the curl of the Navier-Stokes equation:

$$\frac{\mathrm{d}\boldsymbol{\omega}}{\mathrm{d}t} = (\boldsymbol{\omega} \cdot \nabla)\boldsymbol{u} + \nu\nabla^2\boldsymbol{\omega} \tag{26}$$

The term $(\boldsymbol{\omega} \cdot \nabla)\boldsymbol{u}$ is called the *vortex stretching and tilting* term. Enstrophy is the squared modulus of vorticity.

Weak solution: A weak solution to a differential equation is one which does not satisfy the equation in the usual sense (derivatives of the function may not exist), but in some defined

notion: integrating the left and right hand sides of the equation against any test functions must give the same number, with all derivatives taken in the weak sense.

Chapter 1

Point Vortex Systems

It is possible to build a model of the free shear layer, using a finite collection of point vortices. Rosenhead (1931) approximated the motion of a two-dimensional vortex sheet by the motion of a system of point vortices. While a vortex sheet approximation of a free shear layer restricts the vorticity distribution to a curve, the point vortex approximation contracts vorticity even further into a finite number of points. Studies have shown that a system of point vortices is not an exact prototype for a free shear layer that occurs in experiments, in the sense that it evolves into a chaotic cluster of points and the vortex sheet cannot be reconstructed at a later time. However, despite its simplicity it can give nontrivial insights into quasi two-dimensional flows and a useful starting point of vortex sheet models. The system also provides a weak solution to the Euler equations. Modern computers have made it possible to study the (chaotic) evolution of a large point vortex system over a long time. Regardless of its relevance to free shear layers, this model has important theoretical implications as it offers the possibility of establishing a connection between statistical mechanics and 'coherent structures' of turbulent shear flows, see Suryanarayanan, Narasimha and Dass (2014).

1.1   Biot-Savart Law

A point vortex is a singular distribution of vorticity given by $\boldsymbol{\omega} = \gamma\delta(\boldsymbol{x} - \boldsymbol{x}_0)\boldsymbol{k}$, where $\boldsymbol{k}$ is a unit vector orthogonal to $(\boldsymbol{x} - \boldsymbol{x}_0)$. The point vortex is located at $\boldsymbol{x}_0$ and has strength (also known as circulation) equal to γ. The velocity field generated by this point vortex is obtained by inverting the definition of vorticity.

$$\boldsymbol{u}(\boldsymbol{x}, t) = \frac{\gamma}{2\pi}\frac{\boldsymbol{k} \times (\boldsymbol{x} - \boldsymbol{x}_0)}{|\boldsymbol{x} - \boldsymbol{x}_0|^2} + \boldsymbol{u}_F(\boldsymbol{x}, t) \tag{1.1}$$

This is known as the *Biot-Savart law*. It is named after its exact analogue in electrodynamics. It is a kinematic relation that contains all the dynamical information contained in the Euler equations for a point vortex. The velocity field $\boldsymbol{u}$ is unique up to a potential component $\boldsymbol{u}_F$, that represents the velocity at infinity and the effect of walls or boundaries. The presence of boundaries needs the addition of an image vortex of opposite strength, satisfying the kinematic boundary condition of zero normal velocity at the wall.

In two dimensions, vorticity is always perpendicular to the plane of the flow, and therefore it

can be considered a scalar field. Equation (1.1) then takes a simple form

$$u_r(\boldsymbol{x}, t) = 0, \qquad u_\theta(\boldsymbol{x}, t) = \frac{\gamma}{2\pi|\boldsymbol{x} - \boldsymbol{x}_0|} \tag{1.2}$$

where u_r and u_θ are the radial and tangential components of the velocity in polar coordinates. The effect of boundaries is not taken into consideration in the present work as we shall study problems like temporal free shear layers with no solid boundaries. The Biot-Savart law is used in Chapter 2 to derive the velocity field equations for a vortex sheet model.

1.2 Point Vortex Systems

A point vortex system consists of N points in a plane with the Cartesian coordinate of the ith point vortex denoted by $\boldsymbol{x}_i = (x_i, y_i)$. If the ith vortex carries a circulation γ_i, then the equations of motion can be written in the form

$$\gamma_i \frac{\mathrm{d}x_i}{\mathrm{d}t} = \frac{\partial \mathcal{H}}{\partial y_i}, \quad \gamma_i \frac{\mathrm{d}y_i}{\mathrm{d}t} = -\frac{\partial \mathcal{H}}{\partial x_i} \tag{1.3}$$

where

$$\mathcal{H} = -\frac{1}{4\pi} \sum_{i \neq j} \gamma_i \gamma_j \log r_{ij}, \quad r_{ij} = |\boldsymbol{x}_i - \boldsymbol{x}_j| \tag{1.4}$$

$\mathcal{H}$ is the Hamiltonian or *energy function* of the unbounded point vortex system. It should be noted that r_{ij} is a non-dimensional quantity as its logarithmic value is taken.

An alternate way to represent a point vortex system is in a complex plane. The vortices are located at $z_i = x_i + \imath y_i$ and have an equal circulation γ. The equations of motion are

$$\frac{\mathrm{d}z_i^*}{\mathrm{d}t} = -\frac{i\gamma}{2\pi} \sum_{j=1, j \neq i}^{N} \frac{1}{z_i - z_j} \tag{1.5}$$

Note that the sum does not include the effect of a vortex on itself. This is a system of $2N$ ODEs that can be solved as an initial value problem. They can be easily programmed on a computer and studied for various sets of initial conditions.

The equations (1.5) are conservative, since they are inviscid, and conserve the linear and angular momenta of the velocity field, as well as its kinetic energy. Some of these quantities diverge formally, but they can be regularized by considering the changes in the invariants as the vortices move around, instead of the invariants themselves. In a point vortex system the conservation of linear and angular momenta corresponds to the invariance of the centroid and of the moment of inertia of the vortex system, where each vortex is treated as a point of mass γ.

$$Linear\,Momentum \quad : \quad M = \gamma \sum_{i=1}^{N} z_j \tag{1.6}$$

$$Angular\,Momentum \quad : \quad I = \gamma \sum_{i=1}^{N} |z_j|^2 \tag{1.7}$$

$$Energy \quad : \quad E = -\gamma^2 \sum_{i \neq j} \log |z_i - z_j|^2 \tag{1.8}$$

More on the behaviour of point vortex systems are described in Batchelor (1967) and Newton (2001). The invariance of angular momentum ensures that the points stay confined to an area comparable to the initial extent of the system, while invariance of energy prevents points from coming too close to each other[1].

An N-point vortex system has $2N - 4$ degrees of freedom. Therefore, when N is small the system is constrained to be simple. When the value of N is four or more, the system behaves in a very complex way and the generic behaviour starts to get chaotic. Since the influence of initial conditions get lost quickly, statistics becomes relevant. Observing many realizations with different initial conditions is equivalent to observing a single realization for a long time in a statistically steady state. It should also be noted that the behaviour of all the points are equivalent and it is of little interest to follow one particular vortex in a high-dimension system.

1.3 The Spontaneous Appearance of Large-scale and Long-lived Vortices in Two-dimensional Flows

The modern explanation of the commonly observed feature of nearly two dimensional flows: the spontaneous appearance of large-scale and long-lived vortices, was initiated by Onsager (1949). Like-signed vortices in an ideal two-dimensional flow tend to attract over long time scales. While the initial ideas of Onsager have now been modified, extended or made rigorous, his primary contribution of *negative temperature states* remains unchanged. Most systems have the property that entropy increases monotonically with energy. The temperature[2] of such systems is therefore always positive. A point vortex system in an enclosed area, however, has the unusual property that entropy of the system starts to decrease when energy is added after a critical value. When temperature is positive, the most probable state will be that in which point vortices are well mixed and disorganized. But when temperature is negative, clustering of like-signed vortices are favoured and large 'organized structures' come into picture. For a recent review refer to Eyink and Sreenivsan (2006).

---

[1] If the strength of the vortices are not same, energy conservation prevents points of same sign from coming too close to each other. However, pairs can form of vortices of opposite signs, which carry very little momentum and very little energy. Such dipoles form spontaneously and decouple from rest of the system. They can escape to infinity or come very close to another vortex.

[2] The temperature of a system is defined as $T = \frac{\partial E}{\partial S}$, where E is the internal energy and S is the entropy of the system. For usual material systems temperature is never negative.

Statistical mechanics of point vortex systems have been used to study atmospheric problems, like the Great Red Spot on Jupiter. But application of such theory to free shear flows have been limited. Marchioro and Pulvirenti (1994) addressed the problem imposed by the point vortex approximation. Lundgren and Pointin (1976) conducted numerical simulations with initial state corresponding to several point vortex clusters. The evolution of concentrated blobs of vorticity in an ideal incompressible fluid is similar as long as the distance between the blobs is much greater than their diameters. The equilibrium theory predicts that they will finally coalescence into a single large supervortex. For a statistical mechanics description of a free shear layer and 'vortex gas' computations refer to Suryanarayanan, Narasimha and Dass(2014). The term vortex gas is an alternate for a collection of large number of point vortices (delta functions in vorticity) in an inviscid fluid.

Figure 1.1: A composite Cassini image of Jupiter. The large oval shaped vortex south of the equator is known as the Great Red Spot. The spot is large enough to contain three Earth-sized planets and has been in existence since 1665. Similar large-scale, long-lived vortices exist in the atmospheres of the other gas giant planets of our solar system.

1.4 Ergodicity

The essential ingredient of all statistical treatments of a point vortex system is ergodicity, which theorizes that long-time averages are equal to ensemble averages. The ideas presented here can be extended to a vortex sheet. The approximation of a vortex sheet by a system of panels or linear segments is given in Chapter 2.

Let us consider a probability space (Ω, Σ, p) and a transformation $T : \Omega \to \Omega$. It will suffice to note that p is defined on Borel sets of Ω known as the Σ algebra or simply Σ. We assume that the map T is one-one and invertible. The map T will be used to characterize the time evolution of the system. Consider the orbit of the map ω, $T\omega$, $T^2\omega$, ... and the image of each iterate $f(\omega)$, $f(T\omega)$, $f(T^2\omega)$, ... corresponding to a measurable function. The long-time or temporal average is defined as

$$\bar{f}(x) = \lim_{N \to \infty} \frac{1}{N} \sum_{k=0}^{N-1} f(T^k x) \tag{1.9}$$

The ensemble average of f is defined as

$$\langle f \rangle(\omega) = \int_\Omega f \, \mathrm{d}p \tag{1.10}$$

Depending upon the nature of a particular experiment, it is often difficult to compute both the averages together. However, this is not an impossible task. In numerical simulations estimates

of both these averages can be obtained without difficulty.

For our purpose the flow equations (1.3) define a flow map $T(\boldsymbol{x}) : \mathbb{R}^{2n} \to \mathbb{R}^{2n}$. The flow map is volume preserving i.e. the determinant of the Jacobian

$$J = \frac{\partial T(\boldsymbol{x})}{\partial \boldsymbol{x}}$$

is unity. For brevity of notation we shall denote $T(\boldsymbol{x})$ as $\boldsymbol{w}$. Taking the determinant of J and differentiating w.r.t time t gives us

$$
\begin{aligned}
\frac{\mathrm{d}|J|}{\mathrm{d}t} &= \frac{\mathrm{d}\,\mathrm{e}^{\mathrm{tr}\log J}}{\mathrm{d}t} \\
&= \mathrm{e}^{\mathrm{tr}\log J} \mathrm{tr}\left(J^{-1}\frac{\mathrm{d}J}{\mathrm{d}t}\right) \\
&= |J|\,\mathrm{tr}\left(\frac{\partial \boldsymbol{x}}{\partial \boldsymbol{w}}\frac{\partial \dot{\boldsymbol{w}}}{\partial \boldsymbol{x}}\right) \qquad (J^{-1} \text{ is obtained by inverse function}) \\
&= |J|\,\frac{\partial \dot{\boldsymbol{w}}_j}{\partial \boldsymbol{w}_j} = |J|\,\nabla_{\boldsymbol{w}} \cdot \dot{\boldsymbol{w}} = 0
\end{aligned}
$$

since the system of equations (1.3) is Hamiltonian. Since the initial condition of the differential equation is $J(0) = 1$, we can say $J(t) = 1$. From this it follows that T preserves measure p in the sense that $p(T\mathcal{B}) = p(\mathcal{B})$ where $\mathcal{B}$ is a Borel subset of $\mathbb{R}^{2n}$.

It seems that for any measure preserving transformation T, the long-time average and ensemble average of any measurable function f are equal. Unfortunately this conclusion is not true. It is also necessary to assume that the orbit of T fills out the phase space densely and uniformly. Such transforms T are known as *ergodic* transforms. For more details on ergodic transforms interested readers are asked to look in Petersen (1983).

1.5 The Point Vortex Approximation

Early attempts to model a free shear layer used a finite number of point vortices and periodic boundaries. Rosenhead (1931) used 10 vortices and a first order Euler method with time step 0.05. In the 1950s computations were performed using a larger number of points and a more accurate time integration scheme. Contrary to expectation, the later computations resulted in chaotic and irregular motion, see Birkhoff and Fischer (1959), and Hama and Burke (1960). Other methods to get a convergent and smooth solution had limited success. No matter how good the order of accuracy of the numerical method, noise introduced by round-off error is amplified, that scatters the points to form a 'cloud', see Higdon and Pozrikidis (1985) and Shelley (1992). Aref and Siggia (1980) used 4096 points and a cloud-in-cell method for a point vortex approximation to a free shear layer[3]. The computed solution showed a smooth roll-up initially. But the method also introduces some numerical viscosity into the system. The general conclusion is that the point vortex approximation degenerates into chaotic clusters of points. A point vortex system with more than 3 vortices always becomes chaotic providing a valid description of two-dimensional turbulence. However, point vortex systems can reproduce some

---

[3]The idea of the 'cloud-in-cell' method comes from the 'particle-in-cell' method, which has been used in plasma simulation by Birdsall and Fuss (1969). It retains the Lagrangian treatment of the vorticity field and solve Poisson equation for the velocity field. This method is time efficient compared to a direct method when the number of vortices N is large, but have some grid dependent features. Sometimes the cloud-in-cell method may not reproduce the original flow correctly.

dominant features of a free shear layer. For example, the formation of 'coherent structures' and amalgamation of 'coherent structures'.

The point vortex approximation of a temporal shear layer leads us to a set of ordinary differential equations. Note that the boundaries are periodic. There are N points of strength γ in the main domain. The length of domain is $[0,1]$. They are initially located along the x-axis with a slight perturbation. Let the location of the points be $z_i = x_i + \iota y_i$ in the complex plane.

$$\frac{\mathrm{d}z_i^*}{\mathrm{d}t} = -\frac{i\gamma}{2} \sum_{j=1, j\neq i}^{N} \cot \pi (z_i - z_j) \tag{1.11}$$

The sum omits the singular term. The difference in the kernel of equation (1.5) and equation (1.11) is due to periodicity. Separating the real and imaginary part of equation (1.11) gives a set of two equations, which seem to have been first mentioned by Friedman and Polubarinova (1928),

$$\frac{\mathrm{d}x_i}{\mathrm{d}t} = -\frac{\gamma}{2} \sum_{j=1, j\neq i}^{N} \frac{\sinh(2\pi(y_i - y_j))}{\cosh(2\pi(y_i - y_j)) - \cos(2\pi(x_i - x_j))} \tag{1.12}$$

$$\frac{\mathrm{d}y_i}{\mathrm{d}t} = \frac{\gamma}{2} \sum_{j=1, j\neq i}^{N} \frac{\sin(2\pi(y_i - y_j))}{\cosh(2\pi(y_i - y_j)) - \cos(2\pi(x_i - x_j))} \tag{1.13}$$

This is a system of $2N$ ODEs that can be solved as an initial value problem. The strength of each point (γ) is set to be $2U/N$ so that the induced velocity profile is $\pm U$ initially. The Hamiltonian corresponding to this system is

$$\mathcal{H} = -\frac{\gamma^2}{8\pi} \sum_{i\neq j} \log \frac{\cosh 2\pi(y_i - y_j) - \cos 2\pi(x_i - x_j)}{2} \tag{1.14}$$

Evidently, equation (1.14) is a special case of equation (1.4). The logarithmic term of the Hamiltonian must be non-dimensional. Here, the domain length equal to unity is used as a lengthscale. Another type of lengthscale often used for the purpose of non-dimensionalizing is the radius of gyration of the point vortex system,

$$R_g = \sqrt{\frac{1}{N} \sum_{1}^{N} (x_i^2 + y_i^2)}$$

The Hamiltonian is a conserved quantity in a point vortex system. Hamiltonian conservation in a point vortex free shear layer simulation was assessed by Delcourt and Brown (1979) using 750 point vortices. The reported drop in value was 10^{-2} per $t\Delta U/L$. Conservation to the order of 10^{-5} has been obtained in the computations of Suryanarayanan, Narasimha and Dass (2014) using 32,000 point vortices.
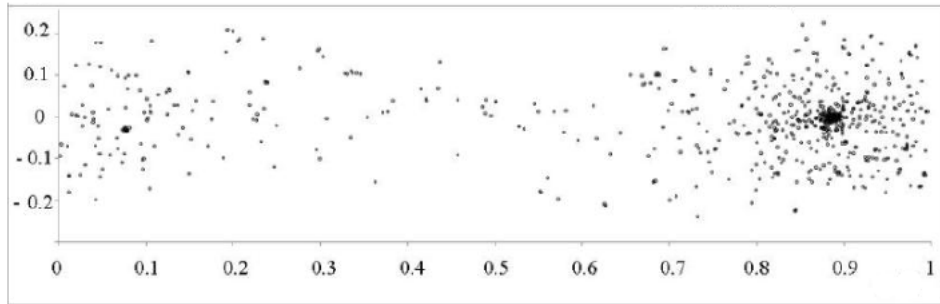
Figure 1.2: The position of point vortices in a temporal free shear layer simulation with 800 points by Suryanarayanan and Narasimha (2014). The vortices were initially placed randomly in the horizontal layer $\pm 10^{-6}$. Beyond time $t = 4.0$ there is a single structure left in each periodic domain. The current value of t is 8.0.

1.6 Desingularization

It has been mentioned that an increase in the number of vortices makes the system more chaotic. This happens because Kelvin-Helmholtz instability of a vortex sheet makes the smallest wavelength grow at the fastest rate. Therefore, as the inter-vortex spacing decreases errors of any type tend to magnify. For N evenly spaced near-aligned points noise generated from round-off error will grow at a rate of $e^{Nt/2}$ [Krasny(1986)]. It is important to note that this is a feature of the underlying system itself as opposed to an instability of the numerical method. For certain investigations a useful remedy is to introduce a Fourier filter that removes all grid-scale noise. This method has been implemented by Krasny (1986). A new development by Chorin and Benard (1973) rectified the problem of irregular motion by introducing desingularized point vortices. The desingularized point vortices are known as 'vortex blobs'. Krasny (1986) used a special type of vortex blob to study the growth of a free shear layer.

$$\frac{\mathrm{d}x_i}{\mathrm{d}t} = -\frac{\gamma}{2} \sum_{j=1, j\neq i}^{N} \frac{\sinh(2\pi(y_i - y_j))}{\cosh(2\pi(y_i - y_j)) - \cos(2\pi(x_i - x_j)) + \delta^2} \tag{1.15}$$

$$\frac{\mathrm{d}y_i}{\mathrm{d}t} = -\frac{\gamma}{2} \sum_{j=1, j\neq i}^{N} \frac{\sin(2\pi(y_i - y_j))}{\cosh(2\pi(y_i - y_j)) - \cos(2\pi(x_i - x_j)) + \delta^2} \tag{1.16}$$

This is an effective way to damp out high wavenumber instabilities. The quantity δ is known as the regularization parameter or the smoothing parameter. The smoothing operation prevents the velocity field from taking arbitrary large values and removes the infinite energy associated with a point vortex[4]. There are different regularization schemes for a point vortex system, for example, stabilizing the instability on the free shear layer by use of surface tension and approximating the sheet by a thin vortex patch.

A system of desingularized point vortices given in (1.15) and (1.16) cannot conserve the Hamiltonian function given in 1.14. However,

$$\frac{\gamma^2}{8\pi} \sum_{i\neq j} \log \frac{\cosh 2\pi(y_i - y_j) - \cos 2\pi(x_i - x_j) + \delta^2}{2} \tag{1.17}$$

---

[4] A point vortex has infinitely large speeds near at the centre of the vortex. There is also an infinite amount of energy in the vicinity of a point vortex.

is conserved. The vortex blob approximation gives a convergent solution: the solution is obtained by taking a finite value of the regularization parameter δ and taking the limit as δ go to zero. For a vortex blob approximation of a free shear layer the solution converges to a spiral. The uniqueness of limiting spiral for different types of regularization is an outstanding problem. Discussion of different regularization techniques can be found in Holm, Nitsche and Putkaradze (2006). Potential applications of vortex blob systems include vortex shedding from the trailing edge of aircraft wings and separation at a sharp edge.
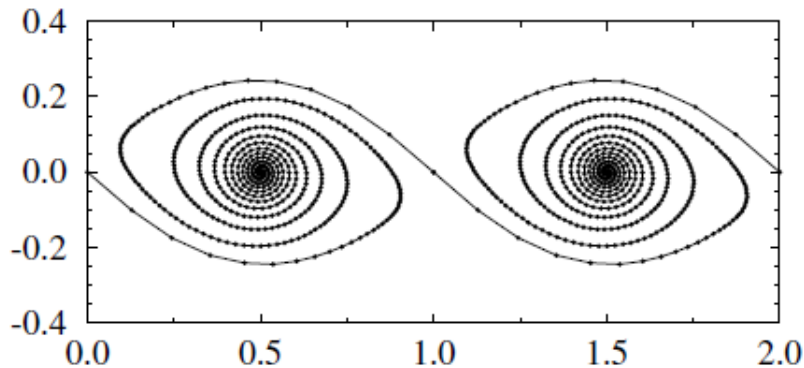
Figure 1.3: Smooth roll-up of point vortices by means of Krasny δ-regularization. The smoothing parameter is $\delta = 0.25$ and 512 points are used in the calculation. Note the convergence to a double branched spiral [Bertozzi and Majda (2002)].

The important step to note here is the order of the limits: δ goes to zero and h goes to zero, where h is the grid resolution. If N points are placed initially in a domain of size 1, then h is $1/N$. For a fixed finite value of δ, we get a smooth spiral solution as h goes to zero. Taking the limit δ goes to zero after h goes to zero adds more turns to the spiral. The effect of singularity formation on a point vortex approximation is further discussed in Chapter 3.

1.7 Adaptive Approximations

The numerical instabilities found in the point vortex approximation are found to be reduced if the point vortices are spaced equally on a curve. Fink and Soh (1974) readjusted the position and circulation of the point vortices so that the new equispaced vortices give a good representation of the vorticity distribution. Evidently, this method cannot be applied at the centre of the vortex spiral. Furthermore, the redistribution involves many interpolations, which leads to accumulation of errors.

Bromilow and Clements (1982) amalgamated clusters of vortices into a single equivalent vortex. They also used an extension of the rediscretization method to prevent points getting too close or too distant. Recent studies by Sohn (2005,2010) vary the number of points and the strength in an adaptive fashion in order to achieve better resolution.

Chapter 2

The Vortex Sheet Approximation

Discrete approximation of a vortex sheet by point vortices has been a success in many physical and engineering applications, but growing randomness in the location of points makes interpolation difficult after a stage. That is, we cannot join the point vortices at a later time in the same sequence as in the initial state. The resultant curve would cross itself and can no longer represent a vortex sheet. The onset of chaos can be delayed significantly by using desingularized point vortices, see Suryanarayanan, Narasimha and Dass (2014), but it does prevent the vortex sheet from getting entangled eventually. However, a turbulent flow is inherently chaotic and therefore a chaotic cloud of point vortices can represent a free shear layer. Even an intersecting vortex sheet can be made to free shear layer as the studies of Basu, Prabhu and Narasimha (1995) have shown. In the current simulations, however, the vortex sheet does not get entangled. The vortex sheet approximation for a spatial free shear layer is revisited in 2.2. The objective is to modify it so that it can represent a temporal shear layer with periodic boundaries. The modification is not a simple procedure as it requires a large number of changes.

In a vortex sheet representation, the motion is determined from the discretization of the Birkhoff-Rott intergral,

$$\frac{\partial z^*}{\partial t} = -\frac{i}{2\pi} \int\limits_{-\infty}^{\infty} \frac{\gamma(s',t)\mathrm{d}s'}{z(s,t) - z(s',t)} \tag{2.1}$$

introduced in Section 0.3. This is an integro-differential equation. The operator $\frac{\partial}{\partial t}$ denotes a usual partial-derivative, while $\frac{\mathrm{d}}{\mathrm{d}t}$ denotes material derivative. The two derivatives are usually not the same. The advantage of this formulation is that it is a purely kinematical equation. This method is termed as 'vortex sheet element' in order to distinguish it from point vortex methods described in Chapter 1. A vortex sheet element model can be used to generate shear flows. It is an expensive procedure compared to modelling with point vortices. However, with the development of powerful computers, computational cost becomes a less serious factor. A major motivation for continuous approximations is that the outcome of the method would not depend on factors like inter-vortex spacing.

2.1 Birkhoff-Rott Integral

The background mathematical theory of equation (7) or equation (2.1) is summarized in this section. The velocity field is denoted by $\boldsymbol{u}$ and the vorticity field is denoted by $\boldsymbol{\omega}$. In a two-

dimensional flow it is more economical to describe the motion in terms of vorticity field than in terms of the velocity field. The velocity field in an incompressible fluid is solenoidal, that is, $\nabla \cdot \boldsymbol{u} = 0$ and its *Helmholtz decomposition* is given by

$$\boldsymbol{u} = \nabla \times \boldsymbol{A} + \nabla\Phi$$

The scalar potential Φ satisfies $\nabla^2\Phi = 0$ and $\Phi = 0$ on the boundary of the domain. If there are no boundary surfaces, $\Phi = 0$ everywhere. To guarantee uniqueness of the vector potential $\boldsymbol{A}$, it is required to have $\nabla \cdot \boldsymbol{A} = 0$. Then $\boldsymbol{A}$ satisfies the Poisson equation,

$$\nabla^2\boldsymbol{A} = -\boldsymbol{\omega} \tag{2.2}$$

Thus, the decomposition of the velocity field produces a solenoidal field and a potential field. The proof of this theorem is available in the textbook by Aris (1962). Equation 2.2 is known as the Poisson equation.

In two dimensions the Poisson equation has a fundamental solution which satisfies the following inhomogeneous equation,

$$\nabla^2\left(-\frac{1}{2\pi}\log\left(\frac{1}{r}\right)\right) = \delta(\boldsymbol{r})$$

The solution of $\boldsymbol{A}$ can be found by the principle of superposition using a Green's function. There are various iterative methods for numerical solution. Since $\boldsymbol{\omega}(\boldsymbol{r}) = \int \boldsymbol{\omega}(\boldsymbol{\xi})\delta(\boldsymbol{r} - \boldsymbol{\xi})\mathrm{d}\boldsymbol{\xi}$, it follows that

$$\begin{aligned}
\boldsymbol{\omega}(\boldsymbol{r}) &= -\frac{1}{2\pi}\int \boldsymbol{\omega}(\boldsymbol{\xi})\nabla^2\log\left(\frac{1}{|\boldsymbol{r} - \boldsymbol{\xi}|}\right)\mathrm{d}\boldsymbol{\xi} \\
&= \nabla^2\left[-\frac{1}{2\pi}\int \boldsymbol{\omega}(\boldsymbol{\xi})\log\left(\frac{1}{|\boldsymbol{r} - \boldsymbol{\xi}|}\right)\mathrm{d}\boldsymbol{\xi}\right]
\end{aligned}$$

Therefore,

$$\boldsymbol{A}(\boldsymbol{r}) = \frac{1}{2\pi}\int \boldsymbol{\omega}(\boldsymbol{\xi})\log\left(\frac{1}{|\boldsymbol{r} - \boldsymbol{\xi}|}\right)\mathrm{d}\boldsymbol{\xi} \tag{2.3}$$

It can be verified that the solution of $\boldsymbol{A}$ given in equation (2.3) is solenoidal. The velocity field $\boldsymbol{u}$ can be determined by taking the curl of $\boldsymbol{A}$. The contribution from the potential field Φ is not considered here, as there are no solid boundaries in a temporal free shear layer.

$$\begin{aligned}
\boldsymbol{u}(\boldsymbol{r}) &= \nabla \times \boldsymbol{A} \\
&= \frac{1}{2\pi}\int \nabla\log\left(\frac{1}{|\boldsymbol{r} - \boldsymbol{\xi}|}\right) \times \boldsymbol{\omega}(\boldsymbol{\xi})\mathrm{d}\boldsymbol{\xi} \\
&= -\frac{1}{2\pi}\int \frac{\boldsymbol{r} - \boldsymbol{\xi}}{|\boldsymbol{r} - \boldsymbol{\xi}|^2} \times \boldsymbol{\omega}(\boldsymbol{\xi})\mathrm{d}\boldsymbol{\xi} \\
&= \frac{1}{2\pi}\int \frac{\boldsymbol{\omega}(\boldsymbol{\xi}) \times (\boldsymbol{r} - \boldsymbol{\xi})}{|\boldsymbol{r} - \boldsymbol{\xi}|^2}\mathrm{d}\boldsymbol{\xi}
\end{aligned} \tag{2.4}$$

A vortex sheet in two dimensions is a singular distribution of $\boldsymbol{\omega}$ on a parametric curve $\boldsymbol{\xi}(s)$. Formally vorticity can be expressed as

$$\boldsymbol{\omega} = \boldsymbol{\gamma}(s)\delta(n) \tag{2.5}$$

where $\boldsymbol{\gamma} \cdot \boldsymbol{n} = 0$, $\gamma = |\boldsymbol{\gamma}|$, n is distance along the sheet normal $\boldsymbol{n}$ and s is distance along the sheet. $\boldsymbol{\gamma}(\mathrm{s})$ is called the sheet strength and has the same direction as $\boldsymbol{\omega}$. Substituting (2.5) into

(2.4), and using $\mathrm{d}\boldsymbol{\xi} = \mathrm{d}s\mathrm{d}n$ we obtain

$$
\begin{aligned}
\boldsymbol{u}(\boldsymbol{r}) &= \frac{1}{2\pi}\int\limits_{s}\int\limits_{n}\delta(n)\frac{\boldsymbol{\gamma}(s)\times(\boldsymbol{r}-\boldsymbol{\xi})}{|\boldsymbol{r}-\boldsymbol{\xi}|^2}\mathrm{d}n\mathrm{d}s \\
&= \frac{1}{2\pi}\int\limits_{s}\frac{\boldsymbol{\gamma}(s)\times(\boldsymbol{r}-\boldsymbol{\xi}(s))}{|\boldsymbol{r}-\boldsymbol{\xi}(s)|^2}\mathrm{d}s
\end{aligned}
$$

The velocity obtained above is finite when the point $\boldsymbol{r}$ is off the sheet $\boldsymbol{\xi}(s)$. If the position vector is on the sheet, the velocity at that point is taken as a principal value integral

$$
\boldsymbol{u}(\boldsymbol{s}) = \frac{1}{2\pi}\oint\limits_{s'}\frac{\boldsymbol{\gamma}(s')\times(\boldsymbol{\xi}(s)-\boldsymbol{\xi}(s'))}{|\boldsymbol{\xi}(s)-\boldsymbol{\xi}(s')|^2}\mathrm{d}s' \tag{2.6}
$$

Thus the velocity produced by a vortex sheet is finite but has a simple jump in tangential component on the sheet, the normal component being continuous. The jump in tangential component is

$$
[\boldsymbol{u}] = \boldsymbol{\gamma}\times\boldsymbol{n}
$$

A complex variable representation of equation (2.6) follows from the next change of variables, $\boldsymbol{\xi}(s)\mapsto z(s)$.

$$
\frac{\partial z(s)}{\partial t} = \frac{1}{2\pi}\oint\limits_{s}\frac{i\gamma(s')(z(s)-z(s'))}{|z(s)-z(s')|^2}\mathrm{d}s'
$$

or,

$$
\frac{\partial z^*(s)}{\partial t} = -\frac{i}{2\pi}\oint\limits_{s}\frac{\gamma(s')}{z(s)-z(s')}\mathrm{d}s' \tag{2.7}
$$

This kinematical equation determines the self-induced motion of the vortex sheet. The material derivative of z is identical to the partial derivative[1]. Therefore, the left hand side of equation (2.7) can be equated to $\frac{\mathrm{d}z^*(s)}{\mathrm{d}t}$. This is true for an inviscid vortex sheet model. For vortex sheet models with viscous smoothing, the material derivative differs from the partial derivative. See Chapter 4 for a continuation of this topic.

2.2 Vortex Sheet Approximation for a Spatial Free Shear Layer

The basic reference for this work is the vortex panel or sheet element model for a spatial free shear layer by Basu, Prabhu and Narasimha (1992). This model splits the vortex sheet into a finite number of linear segments called vortex sheet elements or vortex panels. Earlier studies on continuous models include Fink and Soh (1978) that introduces a vortex sheet element method, and Higdon and Pozrikidis (1985) for implementation of higher order discretization of a vortex sheet. The concept of dynamic update of sheet elements by Basu, Prabhu and Narasimha (1992) is reused in this thesis.

A plane canonical mixing layer is a mixing layer in the limit of infinite Reynolds number that forms downstream of a semi-infinite splitter plate and extends to infinity far downstream. The flow is assumed incompressible and two dimensional with no body forces. In the limit considered

---

[1]This is due to the fact that there is no dissipation in the equation. In the presence of dissipation the two derivatives are different. See Section 4.2 for the derivation.

(Reynolds number infinity), the only role of viscosity is to generate vorticity; thereafter it does not affect the flow.
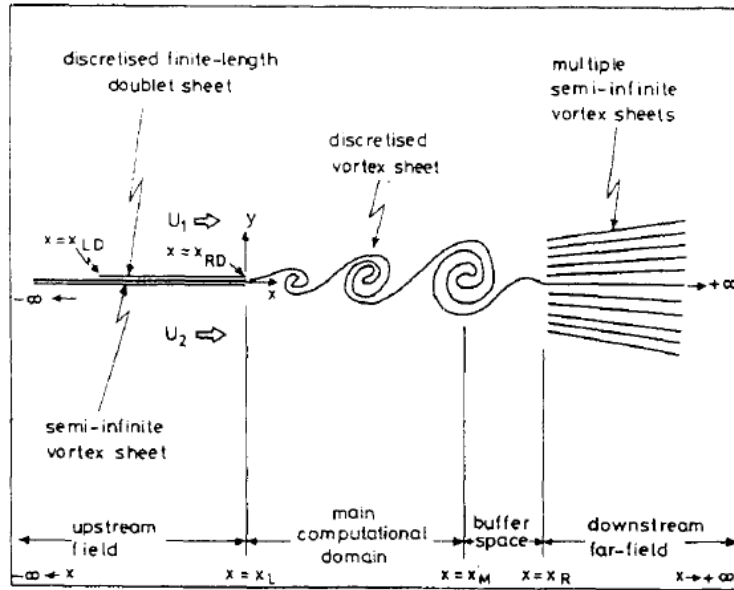
Figure 2.1: A vortex sheet model of a spatial mixing layer with appropriate inflow and outflow boundaries. This schematic diagram is taken from the works of Basu, Prabhu and Narasimha (1992).

Figure 2.1 shows the vortex sheet model of a canonical mixing layer. The flow field is divided into four parts: upstream of the trailing edge of the splitter plate, the main computational domain, a buffer space and downstream far field region. The model simulates a spatial free shear layer with appropriate inflow and outflow boundaries. At each time step the circulation density gets readjusted and the vortex sheet segment splits into two equal parts if it gets stretched beyond a certain prescribed amount. Note that this scheme is different than the methods mentioned in Section 1.7. Some features of a spatial free shear layer simulation which will be lacking in a temporal case, are the semi-infinite downstream sheets, the doublet sheet and the buffer vortex. A doublet is necessary to ensure the physically realistic zero normal velocity at the splitter plate. The downstream buffer vortex was added to conserve global circulation.
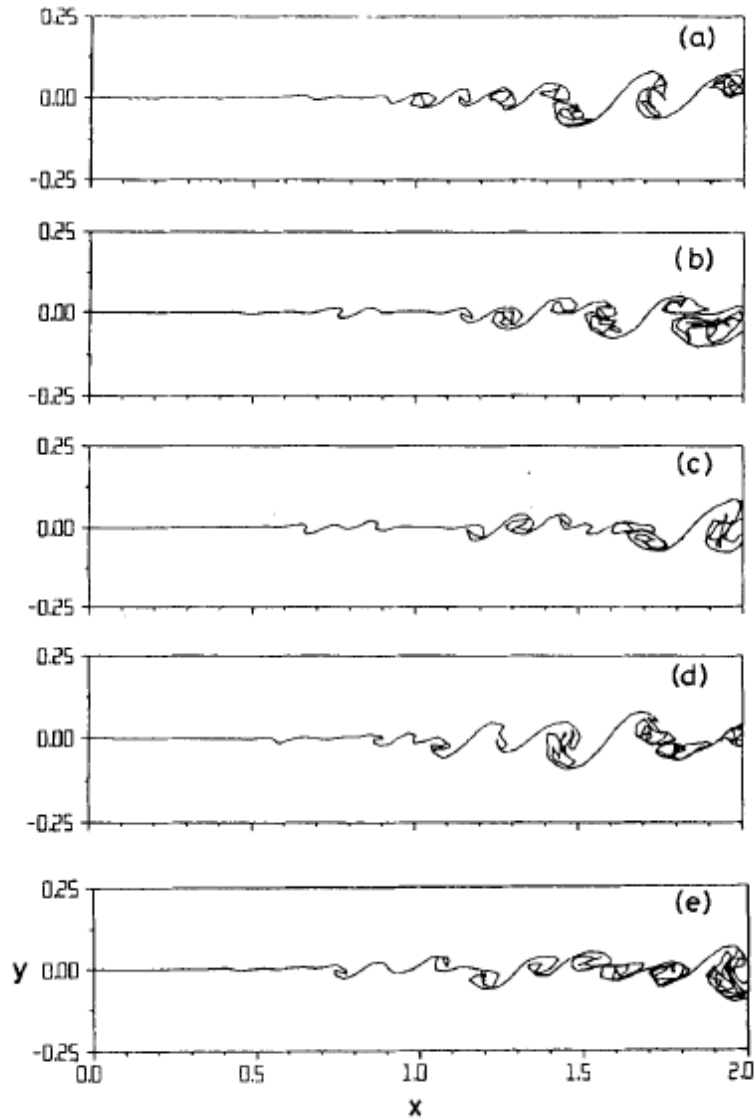
Figure 2.2: Various stages of evolution of the vortex sheet inside the main computational domain. Reproduced from the works of Basu, Prabhu and Narasimha (1994). Shedding of coherent structures from the trailing edge of the splitter plate is seen.

The vortex sheet element method was found to be better than the point vortex method, see Figure 2.2. The vortex sheet crosses itself at places. This is a violation of the principles of vortex dynamics. The situation does not improve if we use smaller time steps or shorter elements. However, the picture obtained is still meaningful. This method was found to be half as fast the point vortex scheme, while computed stresses and moments converged twice as fast. The moments are also closer to values obtained experimentally.

The main difficulty with this model developed in the 1990s was the lack of computational power. The vortex sheet is extremely sensitive to small numerical errors, which leads to spurious intersections. There is an additional problem of singularity formation that did not appear here due to the finite size of vortex panels. We shall attempt to rectify both issues in the following sections and chapters.

2.3 Vortex Sheet Approximation for a Temporal Free Shear Layer

The vortex sheet approximation consists of approximating the temporal free shear layer by a vortex sheet. The sheet is periodic in the x-direction. An introduction to vortex sheets was given in Section 0.3. The objective of what follows in this section is to find a closed form function that will give the induced velocity (due to the temporal vortex sheet) at any point in the domain. The infinite span of the vortex sheet must be accounted for mathematically. It is not advisable to take a numerical approach as the vortex sheet is extremely sensitive to computer round-off errors. If the sheet was of a finite size none of this would be required. In Section 2.2 where a spatial free shear layer is studied, the effects of the semi-infinite downstream region is taken care of by downstream sheets and a buffer vortex.

The vortex sheet is broken into linear segments or panels. This technique is borrowed from vortex sheet model for a spatial free shear layer in Section 2.2. As a first approximation we divide the sheet into equal (or almost equal) parts. There is no constraint on the number of segments. Division into equal parts is problematic when the vortex sheet has regions of high curvature. This leads to loss of resolution. But, at the start i.e. $t = 0$ the vortex sheet is almost flat, and therefore can be approximated by panels of equal size. The vortex sheet element method decomposes a vortex sheet into a system of panels. It is not necessary to have nonlinear panels. In Figure 2.3 we show a portion of a schematic vortex sheet and its segmentation. The variables marked in the inset are for the particular vortex panel k.
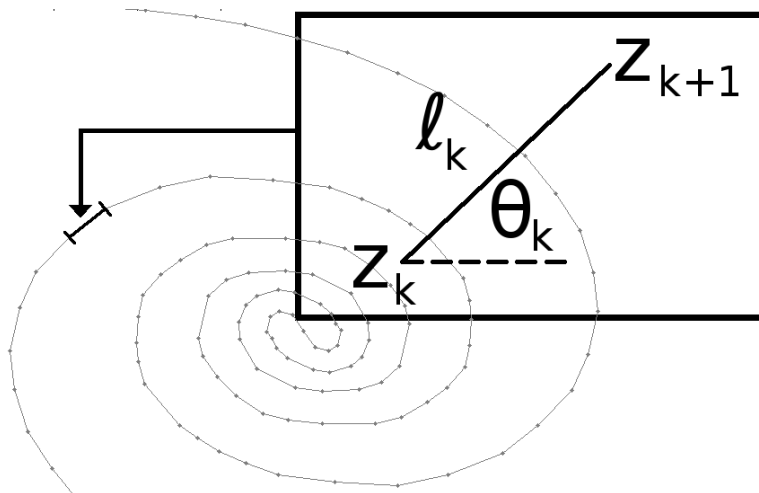
Figure 2.3: A vortex sheet model for a temporal mixing layer. The vortex sheet has rolled up due to self-induced motion. The start and end of the segments or panels are marked by grey dots. A typical segment is highlighted in black. (Inset) Shows the variables needed to describe the marked segment.

Since the domain is periodic, it is sufficient to analyze the strip $[0, 1) \times (-\infty, +\infty)$. The strip is unbounded in the $\pm$ y-directions. The vortex sheet within this domain is split into N segments. The segments of the vortex sheet are marked 1 to N, where N is finite. The vortex segments should approximate the vortex sheet sufficiently well, otherwise it leads to a distortion. The kth vortex segment has length ℓ_k, tilt θ_k with respect to the x-direction, circuation density γ_k, starting at z_k and ending at z_{k+1} in a complex plane. The complex plane representation $z_k = x_k + \imath y_k$ simplifies the writing of the equations that appear towards the end of this section.

We assume that the circulation density is uniform over a segment. Note that the variable γ is used here to denote circulation density and not circulation. The variable for circulation is Γ. This gives a complete description of the vortex sheet segmentation.

Each segment generates a velocity field and the velocity field induced by the vortex sheet will be the vector sum of the components induced by each segment. The segments themselves will be advected by the resultant velocity field, but self-induction cannot take place as it leads to an infinite velocity. Consider the subset of vortex segments whose length is ℓ and inclination is θ, across the entire domain $(-\infty, +\infty) \times (-\infty, +\infty)$. The strength of each segment in the subset is γ. We assume that each segment in $[0, 1) \times (-\infty, +\infty)$ is unique, so that no two of them can have exactly equal length and inclination. But it is possible for them to have an indentical circulation density.

If the starting point of a vortex segment is at (x_1, y_1) and an arbitrary point in the plane is at (x, y) or (x', y') in the reference frame of the segment, then the relation between (x, y) and (x', y') is given by

$$x' = (x - x_1) \cos \theta + (y - y_1) \sin \theta \tag{2.8a}$$

$$y' = -(x - x_1) \sin \theta + (y - y_1) \cos \theta \tag{2.8b}$$

where θ is the angle between the unprimed and primed frames of reference. See Figure 2.4, which shows the respective positions of the two frames of reference. The reason for considering a frame of reference attached to a panel is that computation of induced velocities is easier in this frame. To get back to induced velocities in the unprimed frame of reference, we apply the reverse transformation.
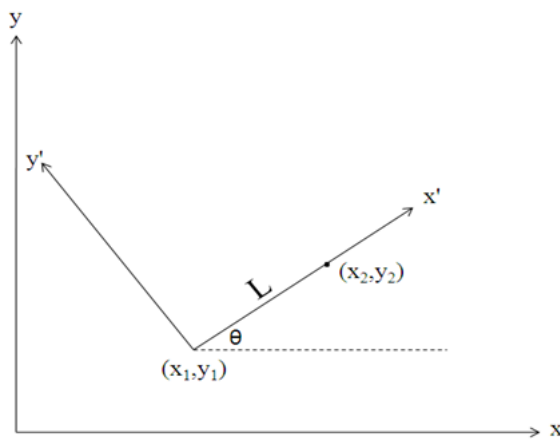
Figure 2.4: The primed and the unprimed frames of reference. xy is the normal laboratory frame. $x'y'$ is the frame attached to the vortex segment.

The induced velocities u' and v' in the reference frame of the segment are computed by using the Biot-Savart formula. The detailed derivation can be found in Basu, Prabhu and Narasimha (1990), and the final forms of u' and v' are written down directly,

$$u' = \frac{\gamma}{2\pi} \left[\arctan \left(\frac{x'}{y'} \right) - \arctan \left(\frac{x' - \ell}{y'} \right) \right] \tag{2.9a}$$

$$v' = -\frac{\gamma}{4\pi} \left[\log \frac{x'^2 + y'^2}{(x' - \ell)^2 + y'^2} \right] \tag{2.9b}$$

The induced velocities u and v in the laboratory frame are then obtained by another coordinate transformation.

$$u = u' \cos\theta - v' \sin\theta \tag{2.10a}$$

$$v = u' \sin\theta + v' \cos\theta \tag{2.10b}$$

We now return to the subset of all vortex segments whose length is ℓ and inclination is θ. Let the segment in the domain $[n, n+1)$ be labelled as the nth segment. If the coordinates of a point wrt the 0th segment is (x', y'), then its coordinates wrt the nth segment will be

$$x'_n = x' - n \cos\theta \tag{2.11a}$$

$$y'_n = y' + n \sin\theta \tag{2.11b}$$

Note that x' and y' is the same as x'_0 and y'_0 respectively. The schematic diagram shown in Figure 2.5 depicts the periodic repetition of vortex segments.
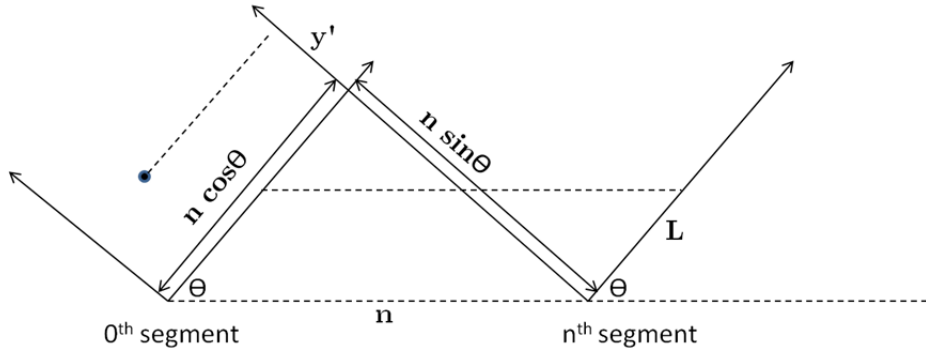
Figure 2.5: Representation of the nth segment with respect to the 0th segment. They have identical length, tilt and circulation density.

The velocities induced at a point in the reference frame of the nth segment are obtained directly from (2.9).

$$u'_n = \frac{\gamma}{2\pi} \left[\arctan\left(\frac{x'_n}{y'_n}\right) - \arctan\left(\frac{x'_n - \ell}{y'_n}\right) \right] \tag{2.12a}$$

$$v'_n = -\frac{\gamma}{4\pi} \left[\log \frac{x'^2_n + y'^2_n}{(x'_n - \ell)^2 + y'^2_n} \right] \tag{2.12b}$$

The unprimed induced velocities will be

$$u_n = u'_n \cos\theta - v'_n \sin\theta \tag{2.13a}$$

$$v_n = u'_n \sin\theta + v'_n \cos\theta \tag{2.13b}$$

and the unprimed velocities induced by the entire infinite row of segments will be

$$u = \sum_{n=-\infty}^{\infty} u'_n \cos\theta - \sum_{n=-\infty}^{\infty} v'_n \sin\theta \tag{2.14a}$$

$$v = \sum_{n=-\infty}^{\infty} u'_n \sin\theta + \sum_{n=-\infty}^{\infty} v'_n \cos\theta \tag{2.14b}$$

Therefore we need to evaluate the following quantities:

$$u' = \sum_{n=-\infty}^{\infty} u'_n \qquad \text{and} \qquad v' = \sum_{n=-\infty}^{\infty} v'_n$$

Since u' and v' are infinite sums they cannot be manipulated as ordinary expressions unless we can show they are convergent quantities. The convergence of u' and v' are established in Lemma 1 and 2 respectively.

Lemma 1. $u' = \sum_{n=-\infty}^{\infty} u'_n$ *is a convergent quantity.*

Proof. The expansion of u' in terms of x'_n and y'_n is given in equation (2.12). Let us express $\frac{x'_n}{y'_n}$ as numbers in a complex plane.

$$\arctan \frac{x'_n}{y'_n} = \frac{1}{2i} \log \frac{i - \frac{x'_n}{y'_n}}{i + \frac{x'_n}{y'_n}} = \frac{1}{2i} \log \frac{iy'_n - x'_n}{iy'_n + x'_n} = \frac{1}{2i} \log \frac{z_n^*}{z_n} \tag{2.15}$$

where $z_n = iy'_n + x'_n$. Similarly

$$\arctan \frac{x'_n - \ell}{y'_n} = \frac{1}{2i} \log \frac{w_n^*}{w_n} \tag{2.16}$$

where $w_n = iy'_n + (x'_n - \ell)$. Therefore

$$\sum_{n=-\infty}^{\infty} u'_n = \frac{\gamma}{2\pi} \sum_{n=-\infty}^{\infty} \left[\frac{1}{2i} \log \frac{z_n^*}{z_n} - \frac{1}{2i} \log \frac{w_n^*}{w_n} \right]$$

$$= \frac{\gamma}{4\pi i} \sum_{n=-\infty}^{\infty} \left[\log \left(\frac{z_n}{w_n} \right)^* - \log \left(\frac{z_n}{w_n} \right) \right] \tag{2.17}$$

In the expression for u' the real part of $\log \left(\frac{z_n}{w_n} \right)$ cancels out with the real part of $\log \left(\frac{z_n}{w_n} \right)^*$. Thus u' turns out to be real as expected.

$$z_n = iy'_n + x_n = i(y' + n \sin \theta) + (x' - n \cos \theta) = i(y' + x') - ne^{-i\theta}$$
$$= z - ne^{-i\theta} \tag{2.18}$$

$$w_n = iy'_n + (x_n - \ell) = i(y' + n \sin \theta) + (x' - \ell - n \cos \theta) = i(y' + x' - \ell) - ne^{-i\theta}$$
$$= w - ne^{-i\theta} \tag{2.19}$$

It is sufficient to show that $\sum_{n=-\infty}^{\infty} \log \frac{z_n}{w_n}$ is convergent.

$$\sum_{n=-\infty}^{\infty} \log \frac{z_n}{w_n} = \log \frac{z}{w} + \sum_{n=1}^{\infty} \left[\log \frac{z_n}{w_n} + \log \frac{z_{-n}}{w_{-n}} \right]$$

$$= \log \frac{z}{w} + \sum_{n=1}^{\infty} \left[\log \left(1 + \frac{\ell}{w - ne^{-i\theta}} \right) + \log \left(1 + \frac{\ell}{w + ne^{-i\theta}} \right) \right]$$

$$= \log \frac{z}{w} + \sum_{n=1}^{\infty} \left[\frac{\ell}{w - ne^{-i\theta}} + \frac{\ell}{w + ne^{-i\theta}} + O\left(\frac{1}{n^2} \right) \right]$$

$$= \log \frac{z}{w} + \sum_{n=1}^{\infty} \left[\frac{2\ell w}{w^2 - n^2 e^{-i\theta}} + O\left(\frac{1}{n^2} \right) \right] \tag{2.20}$$

The above series is convergent. □

It must be noted that $\sum_{n=-\infty}^{\infty} u'_n$ is conditionally convergent. Therefore we adopt the convention of using a principal value:

$$\sum_{n=-\infty}^{\infty} u'_n = \lim_{m\to\infty} \sum_{n=-m}^{m} u'_n \tag{2.21}$$

Lemma 2. $v' = \sum_{n=-\infty}^{\infty} v'_n$ *is a convergent quantity.*

Proof. The argument given here is similar to that given in Lemma 1. The expansion of v' in terms of x'_n and y'_n is taken from equation (2.12).

$$\sum_{n=-\infty}^{\infty} v'_n = -\frac{\gamma}{4\pi} \sum_{n=-\infty}^{\infty} \left[\log \frac{x'^2_n + y'^2_n}{(x'_n - \ell)^2 + y'^2_n} \right] \tag{2.22}$$

Since

$$\log \frac{x'^2_n + y'^2_n}{(x'_n - \ell)^2 + y'^2_n} = \log \frac{(iy'_n + x'_n)(-iy'_n + x'_n)}{(iy'_n + x'_n - \ell)(-iy'_n + x'_n - \ell)} = \log \frac{z_n{}^* z_n}{w_n{}^* w_n} \tag{2.23}$$

z_n and w_n are defined in equations (2.18) and (2.19) respectively. Therefore,

$$\sum_{n=-\infty}^{\infty} v'_n = -\frac{\gamma}{4\pi} \sum_{n=-\infty}^{\infty} \log \frac{z_n{}^* z_n}{w_n{}^* w_n} = -\frac{\gamma}{4\pi} \sum_{n=-\infty}^{\infty} \left[\log \left(\frac{z_n}{w_n} \right)^* + \log \frac{z_n}{w_n} \right] \tag{2.24}$$

Here the imaginary part of $\log \left(\frac{z_n}{w_n} \right)$ cancels out with the imaginary part of $\log \left(\frac{z_n}{w_n} \right)^*$. The convergence of $\log \left(\frac{z_n}{w_n} \right)$ has already been proved in Lemma 1. Therefore $\sum_{n=-\infty}^{\infty} v'_n$ has a finite limit. $\qquad\square$

So far, we have proved the general requirement that u' and v' are well defined. Clearly, this is not enough as there is no way to obtain the values of u' and v' yet. The remainder of this section formulates a way to obtain explicit equations for the infinite sums $u' = \sum_{n=-\infty}^{\infty} u'_n$ and $v' = \sum_{n=-\infty}^{\infty} v'_n$. Another approach would be to sum the series numerically. Due to the alternating nature of the series, the convergence is painfully slow. In principle, a computer can find the summation values to any degree of accuracy. The number of terms required to attain a precision of 6 significant digits is of the order of 1 million or higher. This is a complete waste of computer resources. Numerical summation converges very fast for a few trivial configurations: the flat vortex sheet. Other approximations are not reliable, given that numerical errors might have catastrophic effects later. We shall use the following closed form expressions for u' and v' respectively,

$$u' = \sum_{n=-\infty}^{\infty} u'_n = \frac{\gamma}{2\pi}\mathrm{Im} \left[\log \frac{\sin \pi(z' - \ell)\mathrm{e}^{i\theta}}{\sin \pi z'\mathrm{e}^{i\theta}} \right] \tag{2.25a}$$

$$v' = \sum_{n=-\infty}^{\infty} v'_n = \frac{\gamma}{2\pi}\mathrm{Re} \left[\log \frac{\sin \pi(z' - \ell)\mathrm{e}^{i\theta}}{\sin \pi z'\mathrm{e}^{i\theta}} \right] \tag{2.25b}$$

These values can be otained from a computer quite easily. The proof of equation (2.25a) uses the same approach as was used in Lemma 1. The proof of equation (2.25b) will be identical and therefore not given. We begin by writing u' from equation (2.17),

$$u' = \frac{\gamma}{4\pi i} \sum_{n=-\infty}^{\infty} \left[\log\left(\frac{z_n}{w_n}\right)^* - \log\left(\frac{z_n}{w_n}\right) \right]$$

Let us consider the series

$$\sum_{n=-\infty}^{\infty} \log\left(\frac{z_n}{w_n}\right)$$

The infinite sum is transformed into an infinite product and two functions f and g are defined for ease of manipulation.

$$\sum_{n=-\infty}^{\infty} \log\left(\frac{z_n}{w_n}\right) = \log \prod_{n=-\infty}^{\infty} \left(\frac{z_n}{w_n}\right) = \log \prod_{n=-\infty}^{\infty} \left(\frac{z - ne^{-i\theta}}{z - \ell - ne^{-i\theta}}\right) = \log \prod_{n=-\infty}^{\infty} f_n(z) \quad (2.26)$$

and

$$g(z) = \log \prod_{n=-\infty}^{\infty} f_n(z) \quad (2.27)$$

Taking the logarithm of the above expression and then differentiating we get

$$\frac{g'(z)}{g(z)} = \sum_{n=-\infty}^{\infty} \frac{f'(z)}{f(z)} \quad (2.28)$$

We evaluate the functions $f_n(z)$ and $f'_n(z)$, and substitute their values in (2.28).

$$f_n(z) = \frac{z - ne^{-i\theta}}{z - \ell - ne^{-i\theta}} = 1 + \frac{\ell}{z - \ell - ne^{-i\theta}}$$

$$f'_n(z) = \frac{-\ell}{(z - \ell - ne^{-i\theta})^2}$$

Therefore,

$$\frac{f'(z)}{f(z)} = \frac{\frac{-\ell}{(z-\ell-ne^{-i\theta})^2}}{\frac{z-ne^{-i\theta}}{z-\ell-ne^{-i\theta}}} = \frac{-\ell}{(z - ne^{-i\theta})(z - \ell - ne^{-i\theta})} = \frac{1}{z - ne^{-i\theta}} - \frac{1}{z - \ell - ne^{-i\theta}}$$

and

$$
\begin{aligned}
\frac{g'(z)}{g(z)} &= \sum_{n=-\infty}^{\infty} \frac{1}{z - ne^{-i\theta}} - \sum_{n=-\infty}^{\infty} \frac{1}{z - \ell - ne^{-i\theta}} \\
&= \frac{1}{z} + \sum_{n=1}^{\infty} \left[\frac{1}{z - ne^{-i\theta}} + \frac{1}{z + ne^{-i\theta}} \right] - \frac{1}{z - \ell} - \sum_{n=1}^{\infty} \left[\frac{1}{z - \ell - ne^{-i\theta}} + \frac{1}{z - \ell + ne^{-i\theta}} \right] \\
&= \frac{1}{z} + \sum_{n=1}^{\infty} \frac{2z}{z^2 - (ne^{-i\theta})^2} - \frac{1}{z - \ell} - \sum_{n=1}^{\infty} \frac{2(z - \ell)}{(z - \ell)^2 - (ne^{-i\theta})^2} \\
&= \frac{1}{z} + e^{i\theta} \sum_{n=1}^{\infty} \frac{2ze^{i\theta}}{(ze^{i\theta})^2 - n^2} - \frac{1}{z - \ell} - e^{i\theta} \sum_{n=1}^{\infty} \frac{2(z - \ell)e^{i\theta}}{((z - \ell)e^{i\theta})^2 - n^2} \\
&= e^{i\theta} \left[\frac{1}{ze^{i\theta}} + \sum_{n=1}^{\infty} \frac{2ze^{i\theta}}{(ze^{i\theta})^2 - n^2} \right] - e^{i\theta} \left[\frac{1}{(z - \ell)e^{i\theta}} + \sum_{n=1}^{\infty} \frac{2(z - \ell)e^{i\theta}}{((z - \ell)e^{i\theta})^2 - n^2} \right] \\
&= e^{i\theta} \pi \cot(\pi z e^{i\theta}) - e^{i\theta} \pi \cot(\pi(z - \ell)e^{i\theta})
\end{aligned}
$$

The last step is an identity: *Euler's partial fraction expansion of the cotangent.* The solution of function g is obtained by integration.

$$\log g(z) = \log \sin(\pi z e^{i\theta}) - \log \sin(\pi(z - \ell)e^{i\theta})$$

Therefore,

$$\sum_{n=-\infty}^{\infty} \log\left(\frac{z_n}{w_n}\right) = \log g(z) = \log \frac{\sin(\pi z e^{i\theta})}{\sin(\pi(z - \ell)e^{i\theta})} \tag{2.29}$$

which implies

$$u' = \sum_{n=-\infty}^{\infty} u'_n = \frac{\gamma}{4\pi i}\left[-2i\operatorname{Im}\left[\log \frac{\sin(\pi z e^{i\theta})}{\sin(\pi(z - \ell)e^{i\theta})}\right]\right] = \frac{\gamma}{2\pi}\operatorname{Im}\left[\log \frac{\sin(\pi(z - \ell)e^{i\theta})}{\sin(\pi z e^{i\theta})}\right]$$

This completes the proof of equation (2.25a). Once we have obtained u', it is easy to put v' in a similar form, as given in equation (2.25b). We recall a relation from Lemma 2:

$$v' = -\frac{\gamma}{4\pi}\sum_{n=-\infty}^{\infty}\left[\log\left(\frac{z_n}{w_n}\right)^* + \log\left(\frac{z_n}{w_n}\right)\right] \qquad [\text{see}(2.24)]$$

Since

$$\sum_{n=-\infty}^{\infty} \log\left(\frac{z_n}{w_n}\right) = \log \frac{\sin \pi z' e^{i\theta}}{\sin \pi(z' - \ell)e^{i\theta}}$$

it follows that

$$v' = \sum_{n=-\infty}^{\infty} v'_n = -\frac{\gamma}{4\pi}\left[2\operatorname{Re}\left[\log \frac{\sin \pi z' e^{i\theta}}{\sin \pi(z' - \ell)e^{i\theta}}\right]\right] = \frac{\gamma}{2\pi}\operatorname{Re}\left[\log \frac{\sin \pi(z' - \ell)e^{i\theta}}{\sin \pi z' e^{i\theta}}\right] \tag{2.30}$$

Once we know the exact functional values of u' and v', it becomes straight forward to find out the induced velocity due to an infinite row of vortex panels. There are N sets of such rows (of panels) that make up the vortex sheet. Let u'_k and v'_k be the velocities induced due to the kth row of segments where $k = 1, 2, \ldots, N$. It must be noted that u'_k and v'_k differs from the previously used quantities u'_n and v'_n and should not be confused.

$$u = \sum_{k=1}^{N} u_k = \sum_{k=1}^{N}(u'_k \cos\theta_k - v'_k \sin\theta_k) \tag{2.31a}$$

$$v = \sum_{k=1}^{N} v_k = \sum_{k=1}^{N}(u'_k \sin\theta_k + v'_k \cos\theta_k) \tag{2.31b}$$

Subscript k denotes the contribution from the kth row of segments. Let $z_k = x_k + iy_k$ be the origin of the 0th segment of the kth row. For self induced motion of the vortex sheet, we need to find the complex velocity only at specific locations. These points are the origin or starting

coordinates of each vortex panel. We are now in a position to obtain $\frac{dz_j^*}{dt}$.

$$
\begin{aligned}
\frac{\mathrm{d}z_j^*}{\mathrm{d}t} = u - iv &= \sum_{k=1}^{N}{}' \left(u_k'(\cos\theta_k - i\sin\theta_k) - iv_k'(\cos\theta_k - i\sin\theta_k) \right) \\
&= \sum_{k=1}^{N}{}'(u_k' - iv_k')(\cos\theta_k - i\sin\theta_k) \\
&= \sum_{k=1}^{N}{}'(u_k' - iv_k')\mathrm{e}^{-i\theta_k} \\
&= \sum_{k=1}^{N}{}' \left[\frac{\gamma_k}{2\pi}\mathrm{Im}\left[\log\frac{\sin\pi(z_k'-\ell_k)e^{i\theta_k}}{\sin\pi z_k' e^{i\theta_k}}\right] - \frac{i\gamma_k}{2\pi}\mathrm{Re}\left[\log\frac{\sin\pi(z_k'-\ell_k)e^{i\theta_k}}{\sin\pi z_k' e^{i\theta_k}}\right] \right]\mathrm{e}^{-i\theta_k} \\
&= -\sum_{k=1}^{N}{}'\frac{i\gamma_k}{2\pi}\left[i\mathrm{Im}\left[\log\frac{\sin\pi(z_k'-\ell_k)e^{i\theta_k}}{\sin\pi z_k' e^{i\theta_k}}\right] + \mathrm{Re}\left[\log\frac{\sin\pi(z_k'-\ell_k)e^{i\theta_k}}{\sin\pi z_k' e^{i\theta_k}}\right] \right]\mathrm{e}^{-i\theta_k} \\
&= -\sum_{k=1}^{N}{}'\frac{i\gamma_k}{2\pi}\left[\log\frac{\sin\pi(z_k'-\ell_k)e^{i\theta_k}}{\sin\pi z_k' e^{i\theta_k}}\right]\mathrm{e}^{-i\theta_k} \qquad (2.32)
\end{aligned}
$$

z_k' is the relative position of the jth segment wrt the origin of the 0th segment of the kth row. It is related to z_j as

$$
z_j = z_k + z_k'\mathrm{e}^{i\theta_k} \qquad (2.33)
$$

Substituting the value of z_k' from equation (2.33) in equation (2.32) we obtain

$$
\frac{\mathrm{d}z_j^*}{\mathrm{d}t} = -\sum_{k=1}^{N}{}'\frac{i\gamma_k}{2\pi}\left[\log\frac{\sin\pi(z_j - z_k - \ell_k e^{i\theta_k})}{\sin\pi(z_j - z_k)}\right]\mathrm{e}^{-i\theta_k} \qquad j = 1, 2, \ldots, N \qquad (2.34)
$$

This is a closed form expression that gives the complex velocity field as a function of the state variables of the vortex sheet: z, ℓ, θ and γ. Since this is a finite sum no approximations are required. For self-induced motion of the vortex sheet it is necessary to eliminate the singular term in the summation. However, if the point at which the complex velocity is evaluated is not located on the vortex sheet, then equation (2.34) simply becomes

$$
\frac{\mathrm{d}z_p^*}{\mathrm{d}t} = -\sum_{k=1}^{N}\frac{i\gamma_k}{2\pi}\left[\log\frac{\sin\pi(z_p - z_k - \ell_k e^{i\theta_k})}{\sin\pi(z_p - z_k)}\right]\mathrm{e}^{-i\theta_k} \qquad (2.35)
$$

In Chapter (3) we use equations (2.34) and 2.35 to simulate a vortex sheet motion. The equations are first-order ordinary differential, that can be solved by standard methods of integration. This approach, however, leads to a finite time singularity in curvature and circulation density. A mathematical interpretation of this phenomenon is: neglect of physically important effects like viscosity and surface tension leads to highly unrealistic solutions, see Chapter 4 for more details.

Chapter 3

Finite-time Singularities

The problem of the finite time singularity in vortex sheets with analytic initial data was discussed briefly in Section 0.5. Asymptotic analysis and numerical studies of the Birkhoff-Rott equation by Meiron, Baker and Orszag (1982) have shown that a vortex sheet loses analyticity in finite time. A first-order estimate of the time $t_c < \infty$ (known as the critical time) at which the vortex sheet solution becomes singular is given by

$$1 + \pi t_c + \log 2\pi t_c = \log\left(\frac{4}{2\pi\epsilon}\right) \tag{3.1}$$

where ϵ is the amplitude of the periodic displacement on the vortex sheet. This equation appears in the paper by Moore (1979). It is assumed that the magnitude of ϵ is small compared to the size of the domain. The ratio of amplitude ϵ to wavelength of the disturbance should be small, preferably less than 0.05 for small ϵ analysis to be valid. Equation (3.1) may be solved by Newton's method to obtain values of t_c. It should be noted that equation (3.1) gives an estimate of t_c and not an exact solution. However, it is certain that the vortex sheet becomes singular at t_c, or at some time prior to t_c [Moore(1979)].

The roll-up of a temporal vortex sheet before the time of singularity is investigated in Section 3.2. The vortex sheet evolution is slow at first, then rapid afterward. In qualitative terms, the sheet takes a considerable time for the spiral to appear compared to the expansion of the spiral (refer to Section 3.2 and Section 3.5 for a quantitative treatment). No smoothing parameter, like the desingularization parameter of point vortex systems mentioned in Section 1.6, is inserted before the vortex sheet becomes singular: since the numerical vortex sheet solution developed in this chapter (without regularization) is a smooth and well-defined curve before t_c. Only when the vortex sheet does becomes nearly singular, does it become necessary to take smoothing operations into consideration. See Chapter 4 for 'viscosity switch' smoothing of vortex sheets.

Numerical computation of the vortex sheet beyond critical time is practically quite difficult, since direct integration methods blow up in finite time and desingularized methods generate 'solutions' that are dependent on extraneous parameters. It is also not possible to choose a path in the complex-time plane and obtain a smooth spiral solution by analytic continuation. This is due to the distribution of complex singularities, and their limiting behaviour near t_c is given in Sakajo (2003). It is conjectured that the solution beyond t_c is a double branched spiral with an infinite number of turns. While it is not possible to get an infinite number of turns in numerics, it means that the number of turns in the spiral increases without bound as the parameter used to

regularize the vortex sheet vanishes. The problem of vortex sheet solution after t_c is considered in Chapter 4 and Chapter 5.

3.1 Numerical Procedure

The analysis of Section 2.3 provides an efficient method for evaluating induced velocities on the vortex sheet. Since we know the induced velocities, the displacement of the vortex sheet with time can be programed on a computer. The outline of the program is enlisted at the end of this paragraph. The code starts with $N = 100$ vortex segments or panels. We can choose a higher or lower number of segments at the start, but it makes no difference in the end and therefore modifications are unwarranted. The RESEGMENT subroutine in the code adds vortex segments when required to maintain smoothness of the vortex sheet. The adjustment is an one step procedure and the value of N relaxes to the minimum number needed. However, if N is too low to resolve the initial vortex sheet[1], then that one step error before resegmentation will affect the vortex sheet. Another ad-hoc parameter is the time integration step size Δt (written as dt in the code). It will be necessary to specify a reasonable starting value. The start values used are 0.05 or 0.04: based on multiple runs of the code. It is not mandatory to start with these values. Subsequent values of Δt are generated by the code itself, and further specifications are not necessary.

Pseudocode for vortex sheet motion

---

1. input $N, dt, z_j, \gamma_j \; \forall j$

2. for $j = 1, 2, \ldots, N$

$\ell_j = |z_{j+1} - z_j|; \; \theta_j = \text{atan2}(z_{j+1} - z_j);$

end

3. TIMESCALE FUNCTION

4. for $j = 1, 2, \ldots, N$

$m_j = (z_j + z_{j+1})/2;$

$dm_j = \sum\limits_{k=1, k \neq j}^{N} \frac{i\gamma_k}{2\pi} \left[\log \frac{\sin \pi(z_j - z_k - \ell_k e^{i\theta_k})}{\sin \pi(z_j - z_k)} \right] e^{-i\theta_k} dt$

$m_j = m_j + dm_j$

INTERPOLATE FUNCTION

end

5. for $j = 1, 2, \ldots, N$

$\gamma_j = \gamma_j \ell_j / (z_{j+1} - z_j);$

$\phi_j = \text{atan2}(z_{j+1} - z_j);$

end

6. for $j = 1, 2, \ldots, N$

if $(z_{j+1} - z_j) > 2\ell_j | \max(|\phi_{j-1} - \phi j|, |\phi_{j+1} - \phi j|) < \pi/9$

RESEGMENT FUNCTION

---

[1]A minimum of 5 panels are necessary to represent the initially flat vortex sheet. If one takes $N = 2$, the representation becomes so stiff that the computed induced velocities are wrong.

   end

end

7. output $N, z_j, \gamma_j \ \forall j;$

The above algorithm is implemented in MATLAB[2]. The input variables are N, Δt and the initial configuration of the vortex sheet. The lengths and inclination of each vortex segment are obtained in step 2. The TIMESCALE subroutine in step 3 adjusts time steps automatically and removes the chance of vortex segments intersecting each other. In actual running of the program, some intersections do occur due to faulty initialization of N and Δt, and one would need to retract and correct the panel number and step size. The TIMESCALE function is presented in Section 3.5. The time integration in step 4 is performed by using fourth order Runge Kutta. Self-induction is eliminated. The velocities are calculated at the mid-point of each segment. The INTERPOLATE subroutine interpolates the velocities at the end points of a segment. In two dimensions, in the absence of viscosity, vorticity is transported along with material points. The vortex segments therefore transport vorticity. The length of the segments will change after time integration. The strength of each segment is then readjusted in step 5, so that total circulation of each segment is conserved. The circulation of the vortex sheet also remains constant. Step 6 involves the RESEGMENT subroutine. If a segment is stretched too much (the cut-off value used is 1.5 times the initial length for nearly flat sections), it is divided into two equal halves. If the angle between two segments is too big, both the arms are divided into two equal halves. The 'if' condition displayed in the algorithm is not rigid. In another instance, the conditions can be changed, as the geometry of a vortex sheet can be very complicated. It is not effective to use one universal condition.

The output of this code gives the state of the vortex sheet after a small time interval Δt. For long time intervals, the code is iterated. Note that since the boundaries of the computational domain are periodic, we substitute $z_{N+1} = z_1$, $z_{N+2} = z_2$ and so on, whenever required. There is no subroutine for merging of vortex segments in this code. The merging operation is difficult to control, and is rarely used in numerical simulation. However, if the number of segments becomes prohibitively large, the merging operation can be utilized. Merging of segments will be explicitly mentioned whenever such an operation takes place.

3.2 The Roll-up of a Periodic Vortex Sheet

In this section we consider a periodic vortex sheet, set into motion by a small ϵ amplitude disturbance, and investigate its singular properties. Our calculation starts with $N = 100$ segments. The segments have uniform and identical circulation density. The length of each segment is approximately equal to 0.01. The order of variation of the length of a segment is 1 part 100. It is not necessary to start with exactly equal segments. The sheet is highly unstable, as mentioned earlier in Section 0.2. In fact, the periodic vortex sheet is so unstable that it is an ill-posed problem (Kelvin-Helmholtz instability) i.e. an initially smooth vortex sheet loses all differentiable

---

[2]MATLAB stores all numbers in the long format of the floating point representation. This means that real numbers have a finite precision of roughly sixteen significant digits, and a range of definition roughly varying between 10^{-308} and 10^{+308} in absolute value. All computations are performed in double precision.

properties at a finite time. Because the problem is not well-posed, the numerical procedure given in Section 3.1 needs to modified, by the addition of some suitable parameter like viscosity. For a short period of time, the shape of the vortex sheet can be predicted by a linearized theory. The vortex sheet $z(\Gamma, t) = \Gamma$ is a stationary solution of equation (10) as it is valid for all t, where Γ is the proxy for arclength s along the sheet:

$$\Gamma = \int_0^s \gamma(s')\mathrm{d}s' \tag{3.2}$$

As long as $z(\Gamma, t)$ remains an analytic function of Γ, it will have a Fourier series expansion. Adding a disturbance to the stationary solution gives

$$z(\Gamma, t) = \Gamma + \sum_{n=-\infty}^{\infty} A_n(t)\mathrm{e}^{i2n\pi\Gamma} \tag{3.3}$$

where the $A_n(t)$ are time-dependent Fourier coefficients. The growth of A_n is obtained from the equation:

$$\frac{\mathrm{d}^2 A_n}{\mathrm{d}t^2} = \pi^2 n^2 A_n \tag{3.4}$$

via a series expansion solution. Some steps leading to equation (3.4) are given in the text box below.

Substituting the Fourier expansion of $z(\Gamma, t)$ given in equation (3.3) into equation (10), we have

$$\sum_{n=-\infty}^{\infty} A_n^*(t)\mathrm{e}^{-in2\pi\Gamma} = -\frac{i}{2\pi} \int_{-\infty}^{\infty} \frac{\mathrm{d}\Gamma'}{(\Gamma - \Gamma') + \sum_{n=-\infty}^{\infty} A_n(t)\left(\mathrm{e}^{in2\pi\Gamma} - \mathrm{e}^{in2\pi\Gamma'}\right)}$$

$$\text{put} \quad \phi = \Gamma' - \Gamma$$

$$= -\frac{i}{2\pi} \int_{-\infty}^{\infty} \frac{\mathrm{d}\phi}{-\phi + \sum_{n=-\infty}^{\infty} A_n\mathrm{e}^{in2\pi\Gamma}\left(1 - \mathrm{e}^{in2\pi\phi}\right)}$$

$$= \frac{i}{2\pi} \int_{-\infty}^{\infty} \frac{\mathrm{d}\phi/\phi}{1 - \sum_{n=-\infty}^{\infty} A_n\mathrm{e}^{in2\pi\Gamma}\left(\frac{1-\mathrm{e}^{in2\pi\phi}}{\phi}\right)}$$

$$= \frac{i}{2\pi} \int_{-\infty}^{\infty} \frac{\mathrm{d}\phi}{\phi}\left(1 + \sum_{n=-\infty}^{\infty} A_n\mathrm{e}^{in2\pi\Gamma}\left(\frac{1 - \mathrm{e}^{in2\pi\phi}}{\phi}\right) + O(A_n^2)\right)$$

The principal value integral refers to both $\phi = 0$ and $\phi = \infty$, so $\int_{-\infty}^{\infty} \frac{\mathrm{d}\phi}{\phi} = 0$. Further, $\int_{-\infty}^{\infty} \left(\frac{1-\mathrm{e}^{in2\pi\phi}}{\phi^2}\right)\mathrm{d}\phi = 2\pi^2|n|$. Hence to the first order in the amplitude of the disturbance,

$$\sum_{n=-\infty}^{\infty} \frac{\mathrm{d}A_n^*}{\mathrm{d}t}\mathrm{e}^{-in2\pi\Gamma} = \frac{i}{2\pi} \sum_{n=-\infty}^{\infty} 2\pi^2|n|A_n\mathrm{e}^{in2\pi\Gamma}$$

Equating the coefficients of $\mathrm{e}^{-in2\pi\Gamma}$, we have

$$\frac{\mathrm{d}A_n^*}{\mathrm{d}t} = i\pi|n|A_{-n} \qquad n = 0, \pm 1, \pm 2, \ldots \tag{3.5}$$

Taking complex conjugate of equation (3.5) and differentiating wrt time, we obtain

$$\frac{\mathrm{d}^2 A_n}{\mathrm{d}t^2} = \pi^2 n^2 A_n$$

This is a straightforward derivation but it is useful, and a similar application in Section 4.2 helps us to extend formally to a vortex sheet with viscosity switch.

The Fourier coefficient $A_n(t)$ at $t = 0$ is obtained directly from equation (13) and equation (3.3).

$$A_1(0) = \epsilon/2, \quad A_{-1}(0) = -\epsilon/2, \quad A_n(0) = 0 \quad \forall n \neq \pm 1$$

Starting from the above initial state, the Fourier coefficients, A_1 and A_{-1}, therefore grow like

$$A_1(t) = \frac{\epsilon}{4}(1 + i)\mathrm{e}^{\pi t} + \frac{\epsilon}{4}(1 - i)\mathrm{e}^{-\pi t}, \qquad A_{-1}(t) = \frac{\epsilon}{4}(-1 - i)\mathrm{e}^{\pi t} + \frac{\epsilon}{4}(-1 + i)\mathrm{e}^{-\pi t}$$

Higher order Fourier coefficients remain at zero according to this linearized theory. But initial conditions may differ from equation (13), and then a positive growth rate is obtained for all Fourier modes:

$$A_n(t) = \frac{A_n(0) - iA_{-n}(0)^*}{2}\mathrm{e}^{\pi n t} + \frac{A_n(0) + iA_{-n}(0)^*}{2}\mathrm{e}^{-\pi n t}$$

The above expression shows that the growth of $A_n(t)$ is exponential with time t. Furthermore, the higher the wavenumber of a Fourier mode, the faster is grows. If the Fourier coefficients of the vortex sheet do not decay exponentially with increasing wavenumber, then the sheet can no longer be analytic. This led Birkhoff (1962) to speculate that a finite time singularity occurs in vortex sheet.

However, a linear theory cannot be extended much beyond the initial state, since the assumptions we make are no longer valid. If the nonlinear interactions are also taken into account, loss of analyticity can no longer be guaranteed. In Section 3.4 we briefly mention the analytical reasoning for the appearance of singularity at a finite time. Asymptotic analysis shows that for a finite value of t, the vortex sheet Fourier modes will have coefficients decaying at an algebraic rate with increasing wavenumber. The sheet can, therefore, no longer be analytic at this time. The appearance of a finite-time singularity in a periodic vortex sheet terminates (unregularized) numerical simulations presented in this section.

At the start of numerical simulation the profile of the vortex sheet is a sine wave. The sheet takes a considerable amount of time (compared to later stages) to change its shape initially (See Figure 3.6. The vortex sheet does not undergo any rapid change until $t = 0.6$). Eventually it rolls over the centre point and a spiral structure begins to emerge. The process accelerates as it proceeds. The centre of the sheet rotates and decreases in size. Because of rapid decrease of timescale and lengthscale, only the centre portion of the sheet undergoes change. Outside the centre the vortex sheet remains unchanged. For example, the shape of the sheet at $t = 0.67715$ is same as the shape of the sheet at $t = 0.67732$, if we are unable to see the extremely small details at the centre. In other words, we can superimpose one on another perfectly after rotation and affine transformation.

The shape of the vortex sheet at the centre is that of an exponential spiral of the form $r \sim \mathrm{e}^{-a\theta}$ where r and θ are the polar coordinates, and a is a constant. This can be seen in Figure 3.2. The spiral has two branches. Therefore the plot of $\log r$ versus θ should be a straight line. The

pattern is remarkably self-similar: it is a characteristic of an exponential spiral. In other words, the shape of the vortex sheet is identical at any magnification.
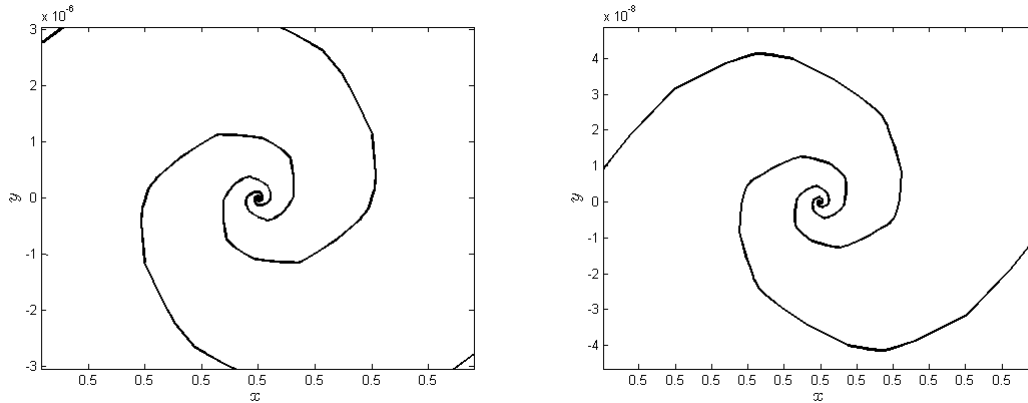
Figure 3.1: The centre of the vortex sheet at magnification level 10^{-6} and 10^{-8} respectively. The double-branched spirals can be superimposed on one another after rotation and scaling transform.

The functional form of the double-branched exponential spiral is given in Figure 3.2. This is calculated on the basis of a fully developed spiral structure at $t_c = 0.67732+$. If the spiral structure is not complete, as at earlier times, the black squares would move away from the dashed line in Figure 3.2, at the centre of the vortex sheet.
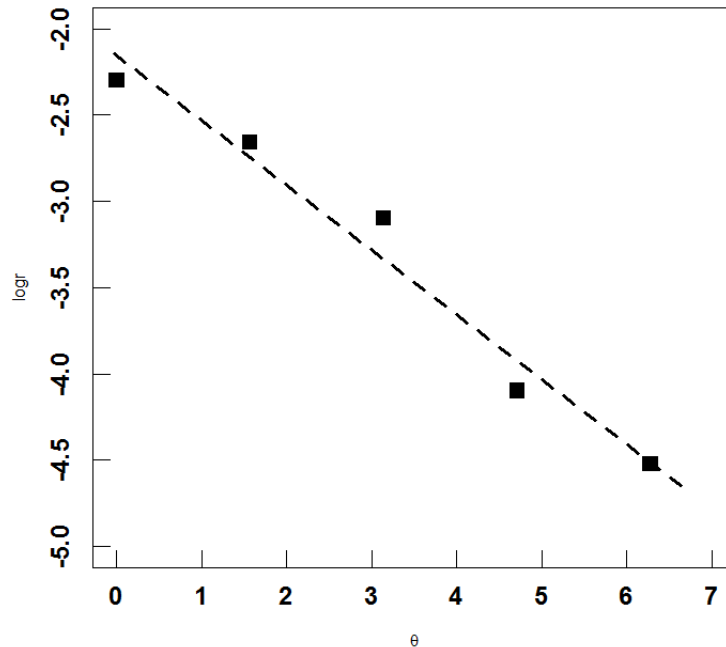
Figure 3.2: Plot of $\log r$ versus θ. The dashed line $\log r = -0.3747\theta - 2.1585$ is fitted to the actual datapoints marked as black squares. The deviations are numerical errors due to improper resolution.

The onset of singularity is marked by a blow up in the curvature of the vortex sheet while the tangent to the sheet remains continuous. The circulation density also peaks at this instant.

Between $t = 0.66855$ and $t_c = 0.67732+$ extremely fine scale structures appear at the centre of the vortex sheet. This has been shown in Figure 3.1. A fully developed exponential spiral emerges within this short duration of time. Ideally, a fully developed spiral should have an infinite number of turns and infinite curvature, but a numerically generated vortex sheet will be finite. The rate at which the spiral emerges gives us an estimate of the critical time. This is measured by the blow up of the maximum curvature or the decay of minimum the radius of curvature.
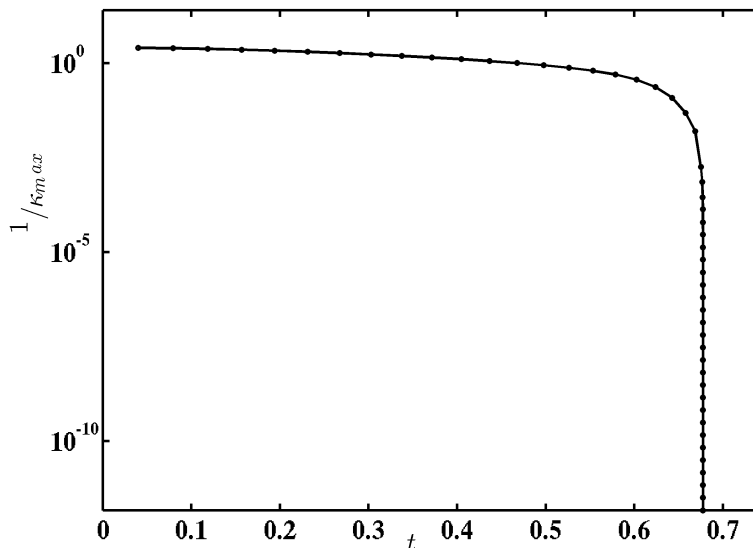
Figure 3.3: Semilog plot of $1/\kappa_{max}$ versus t. κ_{max} is the maximum curvature of the vortex sheet, which occurs at the centre of the spiral; t is the non-dimensional time. Notice how fast the vortex sheet spirals down as the singularity is approached. The tangent to the vortex sheet, however, remains continuous.

To determine if and when the maximum curvature becomes infinitely large, we plot the inverse of the maximum curvature with time in Figure 3.3. It is clear that this quantity approaches zero at a finite critical time, which is estimated as $t = 0.67732+$ approximately. This value is obtained by extrapolation of the graph in Figure 3.3. At this time the vortex sheet will have an infinite number of turns and the radius of curvature goes to zero. Similarly, circulation density peaks at the same time, while its derivative blows up. Since the two estimates are independent and they match, it can be concluded that the critical time is $t_c = 0.67732+$.
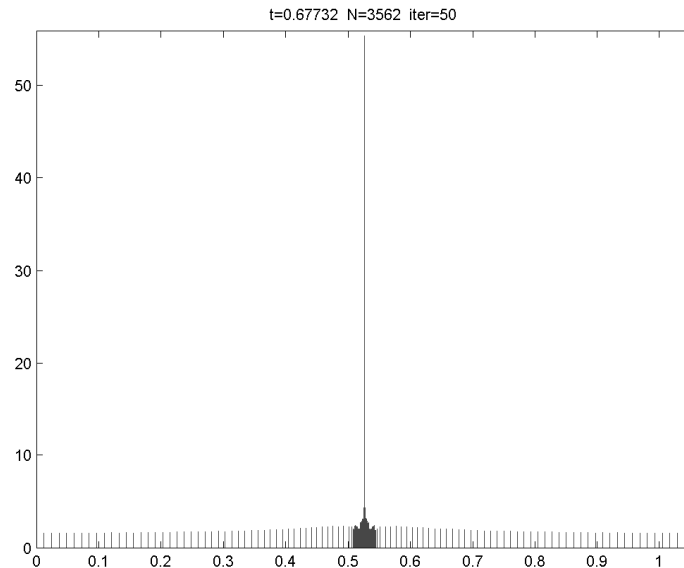
Figure 3.4: The time at which this peak appears is $t_c = 0.67732$. The circulation density (y-axis) is plotted as a function of arclength (x-axis). This value of critical time is almost the same as the value of t_c obtained in Figure 3.3. Notice the density of vortex panels at the centre of the spiral.

The peak of the circulation density that occurs at the centre of the vortex sheet is shown in Figure 3.4. Since circulation is a conserved quantity, compression of segments leads to an increase of circulation density, while expansion of segments leads to a decrease of circulation density. It can be inferred that the centre of the vortex sheet is a region of high compression. In Figure 3.4 notice that the number of segments is 40 times as large as at the centre of the spiral: there are 3474 segments in the centre region and 88 in the arms. The simultaneous appearance of singularities in curvature and in circulation density can be viewed as a consequence of the rapidly diminishing length and timescales to be further discussed in Section 3.5.

3.3 Effects of Amplitude

All numerical simulations presented in Section 3.2 have used $\epsilon = 0.01$. This was not mentioned explicitly, since we do not alter it anywhere other than to find the effects of amplitude. With smaller values of ϵ the critical time is larger, as the vortex sheet motion is reduced initially. For larger or finite initial amplitudes, the singularity formation occurs at two distinct points. Since equation (3.1) is derived for small values of ϵ, a theoretical estimate cannot be given here. Numerical solutions do not indicate any singular behaviour at $\Gamma = 0.5$ for large values of ϵ. By large values of epsilon we mean ϵ greater than 0.09. This is nine times the value of perturbation amplitude we normally use.
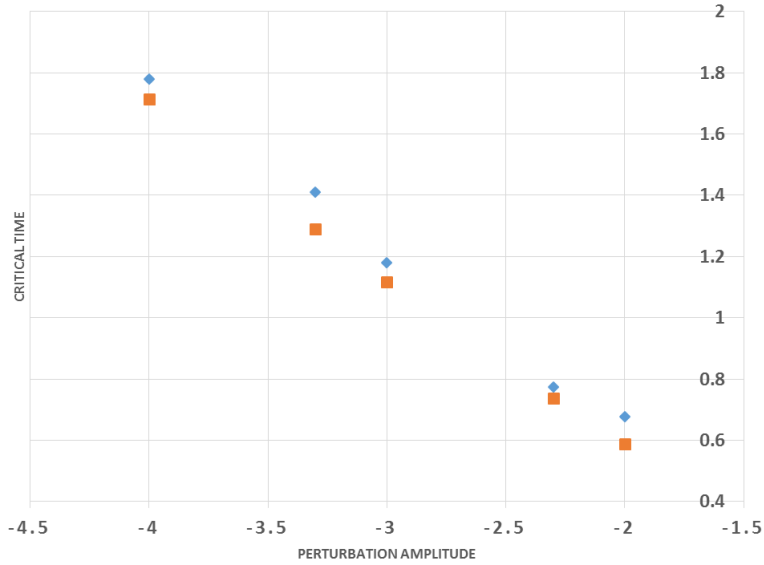
Figure 3.5: Plot of critical time t_c versus log of perturbation amplitude ϵ. Shows the delayed appearance of singularity at smaller values of ϵ. The numerical values (blue) consistently over-estimate the theoretical values (red). The numerical values are obtained by extrapolation, so they are always slight over-estimates.

Figure 3.5 shows the plot of t_c versus amplitude ϵ. The asymptotic predictions are marked in red squares. The numerical values are marked in blue squares. The results are broadly consistent. Assuming that the asymptotic predictions estimate the growth rate of higher wavenumbers more accurately than a numerical simulation, the over-estimation is not more than 18% in any case. The average over-estimation rate is 10%. Note that all comparisons are made for very small values of ϵ. There is no effect of discretization i.e., the initial number of vortex segments and the initial time step do not affect the final state as the numerical simulations are adaptive.

3.4 The Critical Time

At the initial time, $A_{\pm 1}(t)$ is of $O(\epsilon)$ and $A_n(t) = 0$ if $n \neq \pm 1$. But nonlinear interactions quickly give rise to nonzero values of $A_n(t)$, $n \neq \pm 1$. It can be verified that the Fourier coefficients satisfy the symmetry conditions $A_0(t) = 0$ and $A_{-n}(t) = -A_n(t)$. The proof is omitted. In Section 3.2 we did not consider any interaction or nonlinear term. If nonlinear terms are also taken into account, the vortex sheet becomes singular at a finite time. The following is the generalized equation:

$$
\frac{\mathrm{d}A^*_{-n}}{\mathrm{d}t} = \frac{i}{2\pi}\left[2\pi^2 |n| A_n + \sum_{m_1 + m_2 = n} I(m_1, m_2) A_{m_1} A_{m_2} \right.
$$
$$
\left. + \sum_{m_1 + m_2 + m_3 = n} I(m_1, m_2, m_3) A_{m_1} A_{m_2} A_{m_3} + \dots \right] \tag{3.6}
$$

where $I(m_1, m_2)$ and $I(m_1, m_2, m_3)$ are the following principal value integrals:

$$
I(m_1, m_2) = \fint_{\mathbb{R}} \frac{1}{\phi}\left(\frac{1 - \mathrm{e}^{im_1 2\pi\phi}}{\phi} \right)\left(\frac{1 - \mathrm{e}^{im_2 2\pi\phi}}{\phi} \right) \mathrm{d}\phi
$$

$$I(m_1, m_2, m_3) = \oint_{\mathbb{R}} \frac{1}{\phi} \left(\frac{1 - e^{im_1 2\pi\phi}}{\phi} \right) \left(\frac{1 - e^{im_2 2\pi\phi}}{\phi} \right) \left(\frac{1 - e^{im_3 2\pi\phi}}{\phi} \right) d\phi$$

When t is small, the dominant term in the RHS of (3.6) is proportional to A_1^n, and therefore A_n is $O(\epsilon^{|n|})$. This dependence of A_n on ϵ cannot be generalized, since for large values of t values of A_n are no longer negligible compared to A_1. However, if we assume that A_n is $O(\epsilon^{|n|})$ then no term in (3.6) can be larger than $O(\epsilon^{|n|})$. Therefore, it possible to write A_n in the form

$$A_n(t) = \epsilon^{|n|} A_{n0}(t) + \epsilon^{|n+2|} A_{n2}(t) + \epsilon^{|n+4|} A_{n4}(t) + \dots \tag{3.7}$$

for a small amplitude ϵ. The sums $\sum_{m_1+m_2=n}$, $\sum_{m_1+m_2+m_3=n}$ etc in equation (3.6) is over all positive and negative integers so that each term has an infinite number of contributions.

Order analysis following Moore (1980) and Meiron, Baker and Orszag (1982) shows that the evolution equation of A_{n0} contains only terms like A_{k0} where $k \leq n$. For a large value of n, the asymptotic equation of A_{n0} is given by

$$\epsilon^n A_{n0}(t) \approx (2\pi)^{-\frac{3}{2}}(1+i)n^{-\frac{5}{2}}(2\pi t)^{-1}e^{n\left[\log\left(\frac{\epsilon t}{4}\right)+1+\pi t+2\log(2\pi)\right]}$$

If the vortex sheet is well described by this lead order behaviour, then $A_n(t) = \epsilon^n A_{n0}(t)$. The coefficient $A_n(t)$ has exponential decay with increasing wavenumber when $\log\left(\frac{\epsilon t}{4}\right) + 1 + \pi t + 2\log(2\pi) < 0$. But, at the critical time t_c given by

$$1 + \pi t_c + \log 2\pi t_c = \log\left(\frac{4}{2\pi\epsilon}\right) \tag{3.8}$$

the decay is algebraic as $n^{-5/2}$. This is when the sheet is expected to lose analyticity. With initial condition $\epsilon = 0.01$, $L = 1$ and $U = \pm 1$, the vortex sheet stops being analytic at the critical time $t_c = 0.5879$, due to the formation of singularity at $\Gamma = 0.5$ (the point $z = 0.5$).

If more higher order corrections are made, the general form of $A_n(t)$ for sufficiently large n is assumed to be

$$A_n(t) = C(t) \, n^{-\beta(t)} e^{-n\alpha(t)} \tag{3.9}$$

The above equation cannot be proved mathematically, but Meiron, Baker and Orszag (1982) obtained an empirical value of $\beta(t) = 2.7 \pm 0.2$, which Moore (1980) reported as $\beta = 2.5$ independent of time. The current numerical simulations could not obtain a value of $\beta(t)$ independent of time or not being affected by the amplitude ϵ.

3.5   Length and Time Scales

It was mentioned in Section 3.2 that the appearance of singularity in a vortex sheet leads to rapidly diminishing length and time scales at the centre of the spiral. A computer program for vortex sheet motion exhibits a similar nature. The step size and length of vortex panels are set by the user at $t = 0$. But after that, there is no user control on these parameters. The automatic selection of timescale was introduced in the numerical procedure in Section 3.1. The TIMESCALE subroutine forces the following selection:

$$\Delta t^{(n)} = \Delta t^{(1)} \times \frac{\min_j \left[\ell_j^{(n)}/\gamma_j^{(n)}\right]}{\min_j \left[\ell_j^{(1)}/\gamma_j^{(1)}\right]} \qquad j = 2, 3, \dots N \tag{3.10}$$

The nth timestep is, therefore, derived from the latest vortex sheet profile. This prevents inconsistency in numerical solutions like self-intersection of vortex segments. This is a type of error which incidentally prevents a singularity from appearing in the vortex sheet.

The number of segments N increases drastically if there is a singularity in the simulation. From a starting value of 100, it reaches 3562 near critical time. Significantly, it rises from 1096 to 3652 in a span of 7.5×10^{-9} units of non-dimensional time. On the other hand, there is no significant rise of the arc length of the vortex sheet in Figrure 3.6. The decay of lengthscale affects the time steps. Exact values of Δt are listed in the columns below:

0.040000000000000	0.031014858623355	0.000512946603711
0.039460419315483	0.029851638623877	0.000222664340045
0.038844285358096	0.028564102858880	0.000093165380337
0.038224000133990	0.027126262467626	0.000040919469298
0.037590787263112	0.025500937225262	0.000017644929679
0.036936142792155	0.023631089126948	0.000007705882238
0.036251674911217	0.021423038185782	0.000003340626058
0.035528939184565	0.018716007877975	0.000001455206425
0.034759256423979	0.015251421290615	0.000000632168133
0.033933494707117	0.010829862815207	0.000000275068742
0.033041787303005	0.006371003826707	0.000000119575657
0.032073141069967	0.001490536989196	0.000000052010715

and so on. This is decrease by a factor of $\sim 10^{-6}$. The rise of arclength is shown in Figure 3.6. The arclength appears to diverge near the singularity. In fact, the arclength is bounded above. The jump in arclength is due to the first turnover of the vortex sheet. Thereafter, the increments are small. Since, the arclength of an exponential spiral is bounded, the arclength of the vortex sheet also remains finite.
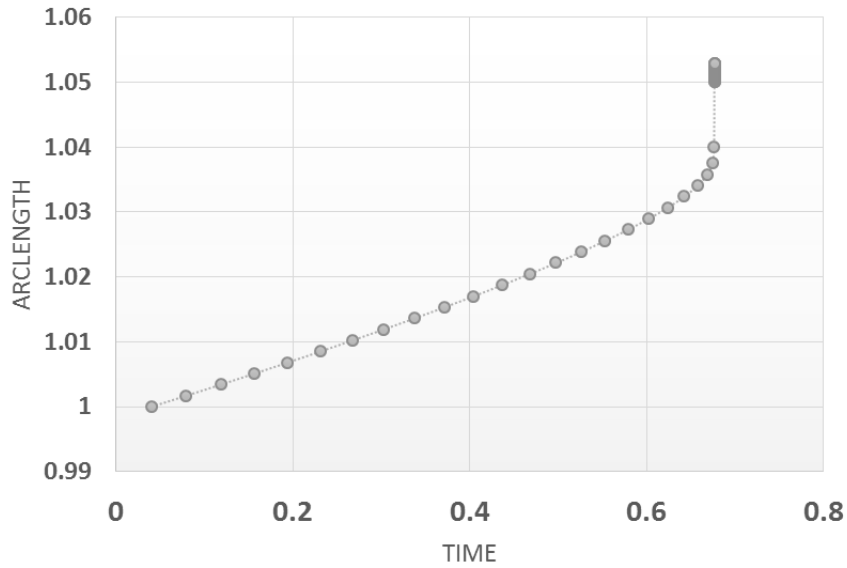
Figure 3.6: The plot of arclength of the vortex sheet versus time. There is no significant rise: the initial value is close to 1 and the final value is slightly more than 1.05. But most of the increase takes place near the singular time.

The combination of very small lengthscales and high curvature at the centre of the vortex sheet gives rise to a point vortex like object. As the time steps decay away to zero, the numerical solution of the vortex sheet does not go beyond the critical time. One artificial technique to overcome this problem would be to fix a minimum lengthscale in the code. However, this is only an ad hoc solution as opposed to a regularization. A minimum lengthscale selection acts as an inefficient local smoothing operation. The centre of the vortex spiral rotates like a rigid object once its dimension becomes comparable to the minimum lengthscale. But, it is unable to prevent vortex segments from intersecting. Despite this shortcoming, it might still be useful when used together with a regularization procedure.

Chapter 4

Viscous Regularization

The Birkhoff-Rott equation and, by extension equation (2.34), can be used for computation before critical time t_c is reached. For computing the vortex sheet past the critical time, a desingularization is needed. A natural procedure, motivated by other numerical methods, is to smooth the equations of motion of an ill-posed vortex sheet by means of some extraneous parameter, and thence to construct a sequence of smooth solutions. The convergence of this sequence of solutions is verified mathematically, but it would also be necessary for the limit solution to satisfy certain physical conditions: in this case the equation of motion of an ideal fluid. Because of singularity formation there is no smooth or differentiable solution to this problem. The hope or objective in mind is that in the limit of vanishing regularization, the limit solution will be a weak solution to the Euler equation. A weak solution differs from a strong solution in the sense that it satisfies the equation in an integral formulation. A formal notion of weak solutions to second order partial differential equations is given in the review by Grandall, Ishii and Lions (1992) and Beale, Kato and Majda (1984).

4.1 Viscosity as a Regularization Parameter

The regularization used by Krasny (1986) for computing the vortex sheet beyond t_c used a 'radial' or 'length' parameter δ to smooth the equations. This is numerically convenient, but difficult to interpret as a physical process. Empirically its effect is similar to spreading a singular point vortex over a finite region. The true physical regularization in fluids is due to viscosity. Computation of a vortex sheet with a small amount of viscosity is equivalent to solving the Navier-Stokes equations at high Reynolds number. Such a solution is not attempted, as a limited setup makes the problem computationally intractable. It should be noted that for Reynolds numbers encountered in most industrial applications, the computational resources required by a DNS would exceed the capacity of the most powerful computers currently available. Approximate solutions may, however, be obtained, exhibiting a roll-up, similar to that of Krasny (1986). It is known that for viscous regularization, in the limit of zero viscosity, a weak solution to the Euler equation is obtained, provided the initial vorticity is of one sign. The proof of this statement is given in Delort (1991), and also in the textbook by Majda and Bertozzi (2002). However, it is not known whether this weak solution is unique or whether it depends on the regularization.

Viscosity dissipation has been used in the past to capture shock wave discontinuities. A shock wave is not a true physical discontinuity, but a very narrow transition zone whose thickness is on the order of a few molecular mean-free paths. Numerical solutions to shock waves are observed to develop oscillations behind the discontinuity. The artificial viscosity technique introduces a very large value of viscosity around the discontinuity (but negligible otherwise) to damp out unwanted oscillations. Physically, the effect of artificial viscosity is like viscous dissipation. Artificial viscosity is different from numerical viscosity, which is an artefact of certain types of numerical approximations. Numerical viscosity arises from discrete approximations to the momentum advection terms in the Euler equations. Computer simulations seek to reduce numerical viscosity to maximize fidelity of solutions. Numerical diffusion does not behave like true viscous diffusion because it depends on the choice of computational grid and does not possess the correct stress-versus-strain-rate dependency.

In the case of point vortex approximation to a vortex sheet, irregular motion can be suppressed by introduction of an 'artificial viscosity'. This irregular motion is not an undesired effect as it may be a manifestation of two-dimensional turbulence. In real fluids, the velocity field is weak compared to that of an ideal fluid. By 'weak' we mean that the velocity gradients do not change very fast and the absolute velocities are bounded. The introduction of artificial viscosity in point vortex systems reduces irregular motion and suppresses the associated singularity. But, it also reduces circulation and dissipates kinetic energy. However, if the reduction in circulation is negligible and the loss of kinetic energy is not great, then the introduction of artificial viscosity may prove useful to study such systems.

4.2 Viscosity Switch

A smoothing parameter like viscosity may be used intermittently in a vortex sheet evolution. In real fluids with viscosity, the 'ill-posedness' of the vortex sheet problem is automatically taken care of by viscous forces. Viscosity also acts to thicken the vortex sheet into a vortex layer. However, if vorticity is allowed to diffuse tangentially only, following the standard diffusion model

$$\frac{\mathrm{d}\gamma}{\mathrm{d}t} = \nu \frac{\partial^2 \gamma}{\partial s^2} \tag{4.1}$$

then its effect is to smoothen the vortex sheet equation without actually thickening the vortex sheet. The parameter ν represents viscous smoothing, s is arcwise distance and γ is the circulation density. The typical values of ν are small, otherwise vorticity gradients will be destroyed completely affecting the dynamics of the vortex sheet. This is mentioned in Section 4.3 where the optimal values of ν are given. Diffusion is a slow process compared to advection, therefore transport of vorticity would still dominate the dynamics of the vortex sheet, except in regions of high curvature where smoothing occurs due to the viscosity switch. The term viscosity switch is used to indicate that the viscosity parameter ν is set to zero unless the vorticity gradient crosses a high cut-off value. As mentioned in Chapter 3, a rising vorticity gradient is indicative of impending singularity formation. The effect of viscosity switch is therefore entirely localized in the sense that it affects only a small portion of the vortex sheet directly. This is the feature which makes computer coding of the model straightforward and concise. The indirect effect is

however widespread, as the vortex sheet would never roll-up in its absence. We introduced the circulation coordinate

$$\Gamma = \int_0^s \gamma(s')\mathrm{d}s' \tag{4.2}$$

in Section 0.3. Then $z(\Gamma, t)$ is the position on the vortex sheet which has net vorticity Γ between it and an arbitrary but specified origin.

When no viscous forces are present, the circulation parameter along the sheet is conserved i.e. $\mathrm{d}\Gamma/\mathrm{d}t = 0$. The circulation of a vortex segment therefore remains constant with time. For viscous fluids with tangential diffusion only, Γ does not transport intact along with vortex segments. The change in circulation of a vortex segment can be updated as follows:

$$\mathrm{d}\Gamma_i = \nu \frac{2\beta\Gamma_{i+1} - 2\beta(1+\beta)\Gamma_i + 2\beta^2\Gamma_{i-1}}{\beta(1+\beta)h_{i-1}{}^2}\mathrm{d}t \tag{4.3}$$

where γ_i is the strength of the ith segment, ℓ_i is the length of the ith segment, $h_i = \frac{\ell_i + \ell_{i+1}}{2}$ and $\beta = \frac{h_i}{h_{i-1}}$. This follows from a derived form of equation (4.3) or (4.1)

$$\frac{\mathrm{d}\Gamma}{\mathrm{d}t} = \nu \frac{\partial^2\Gamma}{\partial s^2} \tag{4.4}$$

Because of viscosity, the dynamics of the sheet is altered by the addition of a viscous term. The viscosity parameter ν is local: it is non-zero only in singular regions. The motion of the vortex sheet is obtained as follows:

$$\frac{\mathrm{d}z}{\mathrm{d}t} = \frac{\partial z}{\partial t} + \frac{\partial z}{\partial \Gamma}\frac{\mathrm{d}\Gamma}{\mathrm{d}t} \tag{4.5}$$

The first term on the right in equation (4.5) can be substituted from equation (7) directly. The second term in equation (4.5) can be written as

$$\frac{\partial z}{\partial \Gamma} \nu \frac{\partial^2\Gamma}{\partial s^2} \tag{4.6}$$

due to the tangential diffusion given in equation (4.4). Furthermore, we convert $\frac{\partial^2\Gamma}{\partial s^2}$ into circulation coordinates

$$\frac{\partial^2\Gamma}{\partial s^2} = \frac{\partial}{\partial s}\left(\frac{\partial\Gamma}{\partial s}\right) \tag{4.7}$$

$$= \frac{\partial\gamma}{\partial s} \tag{4.8}$$

$$= \gamma\frac{\partial\gamma}{\partial \Gamma} \tag{4.9}$$

In the last step, we have used the change of variable relation $\frac{\partial}{\partial s} = \gamma\frac{\partial}{\partial \Gamma}$. Therefore, the adjusted form of equation (4.5) is

$$\frac{\mathrm{d}z^*}{\mathrm{d}t} = -\frac{i}{2\pi}\int_{-\infty}^{\infty}\frac{\mathrm{d}\Gamma'}{z(\Gamma, t) - z(\Gamma', t)} + \nu\gamma\frac{\partial\gamma}{\partial\Gamma}\frac{\partial z^*}{\partial\Gamma} \tag{4.10}$$

This is a type of advection-diffusion equation. When $\nu = 0$ we recover the un-modified vortex sheet equation given in (2.1). The flat vortex sheet is unstable to perturbations: let the sheet be disturbed to assume the instantaneous shape:

$$z(\Gamma, t) = \Gamma + \sum_{n=-\infty}^{\infty} A_n(t)\mathrm{e}^{i2\pi n\Gamma} \tag{4.11}$$

On replacing $z(\Gamma, t)$ in equation (4.10) by the Fourier expansion in equation (4.11), the coefficients of the Fourier modes can be equated to give

$$\frac{\mathrm{d}A_n^*}{\mathrm{d}t} = \imath\pi n A_{-n} + 2\imath\pi\nu n(A_n + A_{-n}) \tag{4.12}$$

This shows that the Fourier coefficient A_n has an exponential growth with rate

$$\frac{-4\pi^2\nu n^2 + \sqrt{16\pi^4\nu^2 n^4 + 4\pi^2 n^2}}{2} \tag{4.13}$$

The growth rate converges to a factor of ν^{-1} as n tends to infinity. The smoothened vortex sheet is therefore linearly well-posed with analytic initial data. Note that for vanishing ν the growth rate for the Fourier modes is unbounded as in the case of an unsmoothed vortex sheet.

4.3 The Effect of Variable Viscosity

The viscosity parameter introduced in Section 4.2 is written as ν, like the kinematic viscosity. However, this is not a physical property of the medium. The value of ν is non-zero at some space subsets and also time varying. It is zero when there is no singularity formation. There can only be a countable number of singularities on the vortex sheet, as a singular point leads to a jump in cumulative circulation and the total circulation must remain conserved. This follows from the fact, that any monotonic right or left continuous function can have only a countable number of discontinuities[1]. Usually, this theorem is presented in literature without a name, but a variant appears for the first time in the thesis of Froda (1929). If there were an uncountable number of singularities, the theoretical setup of vortex sheet computation would breakdown. Therefore, the following statement is an important property:

There can only be a countable number of singularities on a vortex sheet. The measure of the set of singularities is zero.

So ν is zero almost everywhere. Where it is not zero, a constant value of ν would delay the singular time, but will not eliminate the effects of singularity or singularities, as shown in the following sections of this chapter. The growth rate obtained for high wavenumbers is a factor of ν^{-1}, which does not decay to 0 as n tends to ∞. This will lead to a finite but large growth rate of short wave disturbances in numerical computations. The only 'advantage' is that the vortex sheet is more evolved when the singularity appears. Theoretically an infinitely large value of ν will cause this instability to get damped, but this leads to the destruction of vorticity gradients and such a vortex sheet is degenerate. The Reynolds number is defined as

$$\mathrm{Re} = \frac{1}{\nu} \tag{4.14}$$

This is not the standard definition for Reynolds number, as ν is not the kinematic viscosity. It is to be used exclusively in the context of vortex sheet regularization. The Re represents the degree of 'roughness' in the model. The objective is to run the model at different levels of roughness. The development of a singularity in a vortex sheet with $\mathrm{Re} = 800$ at $\Gamma = 0.5$ is shown in Figure

---

[1]The projection of discontinuities onto the y-axis forms a set of non-intersecting intervals. Each interval contains a rational number. The set of rational numbers is countable.

4.1. The formation of a singularity is delayed due to viscous diffusion and the evolution of the vortex sheet is slowed down. This is not the solution to the problem we are looking for, since the growth of the vortex sheet is obstructed and a singularity appears by extrapolation. When $\mathrm{Re} = 400$, we obtain similar profiles for circulation density but at later times. Compare the times t in Figure 4.1 and Figure 4.2.
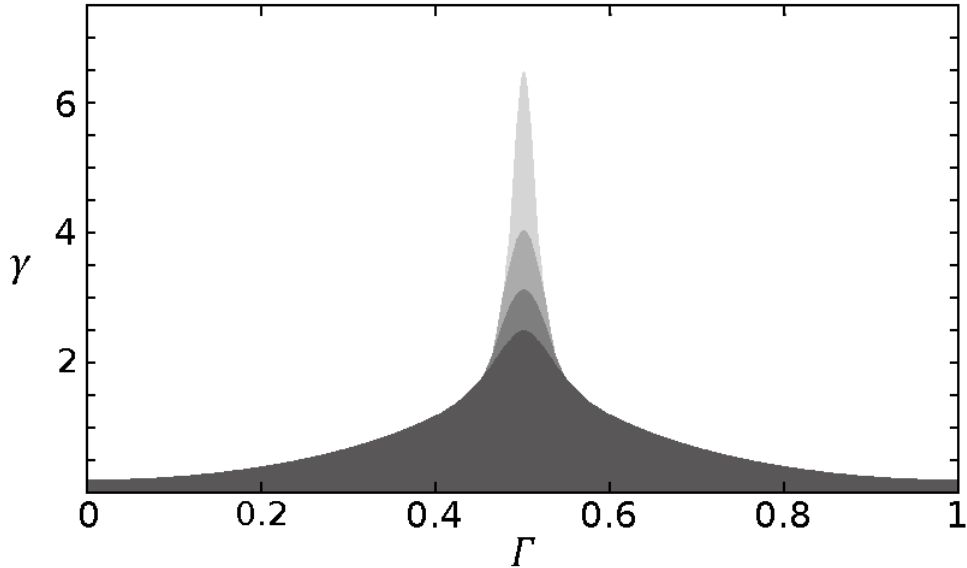
Figure 4.1: The distribution of circulation density γ at $\mathrm{Re} = 800$ for a vortex sheet at times $t = 0.20, 0.40, 0.60$ and 0.80 respectively. The colour codes change from dark to light gray respectively. The peak is not as high as in the inviscid vortex sheet due to viscous diffusion.

The comparison of Figure 3.4 with Figure 4.1 shows that the gradient of γ differs in quality. The steep rise (almost like a delta function) is absent in the latter. The peak circulation near critical time is 50 times as large as the initial value if there is no viscosity. In the presence of viscosity the peak is 5 times as large at approximately the same time[2].

There is indication that the circulation in the outer arms of the vortex sheet continues to drop with time. The growth of peak γ is accelerated with time. Concentration of vorticity occurs in the central 'core' region. This is evident at $t = 0.8$ in Figure 4.1 where depletion of γ from 0 to 0.4 and 0.6 to 1 has added density to 0.4 to 0.6. The singularity would form at $\Gamma = 0.5$ if the parameter ν is taken off. On the other hand, dynamically decreasing the value of ν can prevent the vortex sheet from becoming singular before a pre-fixed time without obstructing the vortex sheet roll-up.

[2]The curvature of a viscous vortex sheet is also less sharp than that of an inviscid vortex sheet.
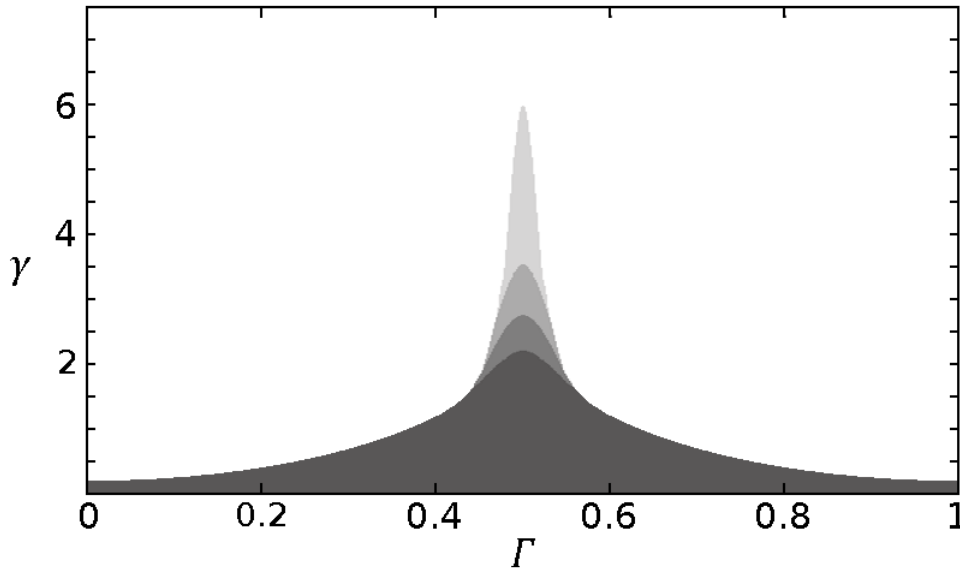
Figure 4.2: The distribution of circulation density γ at Re = 400 for a vortex sheet at times $t = 0.43, 0.71, 0.89$ and 0.99 respectively. The growth of the singularity makes significant progess after an initial delay. The depicted times t have been chosen to match the qualitative nature of Figure 4.1 approximately.

It is observed that the circulation density of the vortex sheet tends to have a high peak, like in the inviscid case, but the 'peakiness' is smaller for lower Re at a given time. The amplitudes of the Fourier modes of the periodic vortex sheet show growth at high modes with time. This is not very evident in the beginning, but at later times the higher modes are clearly present. Consider the Γ-periodic function

$$f(\Gamma, t) = z(\Gamma, t) - \Gamma \tag{4.15}$$

The exponential Fourier series decomposition of f is given by

$$f(\Gamma, t) = \sum_{k=-\infty}^{\infty} F_k(t) \mathrm{e}^{\imath 2\pi k \Gamma} \tag{4.16}$$

where the $F_k(t)$ are the Fourier coefficients. Since $\mathrm{e}^{i 2\pi k \Gamma}, k = 0, 1, 2, \ldots$ are a basis of orthogonal functions,

$$F_k(t) = \int_{\Gamma=[0,1)} \mathrm{e}^{-\imath 2\pi k \Gamma} f(\Gamma, t) \, \mathrm{d}\Gamma \tag{4.17}$$

The discrete analogue of the integral in equation (4.17) is required for numerical computation of $F_k(t)$. Let us sample the vortex sheet in $[0, 1)$ at n points. The number of samples n should be at least twice as large as the maximum frequency k we need to capture without error i.e. $|k| \leq n/2$ by the Nyquist frequency criterion.

$$F_k(t) = \frac{1}{N} \sum_{j=1}^{n} f(\Gamma_j, t) \mathrm{e}^{-\imath 2\pi k \Gamma_j} \tag{4.18}$$

The Fourier coefficients can be obtained by fast Fourier transform. We take $n = 400$ as the number of equally spaced sampling points. The plot of twice the Fourier amplitudes $|F_k(t)|$, $k =$

$1, 2, \ldots 200$ for $\mathrm{Re} = 800$ is shown in Figure 4.3. Note that $F_0(t) = 0$ identically from equation (4.18).
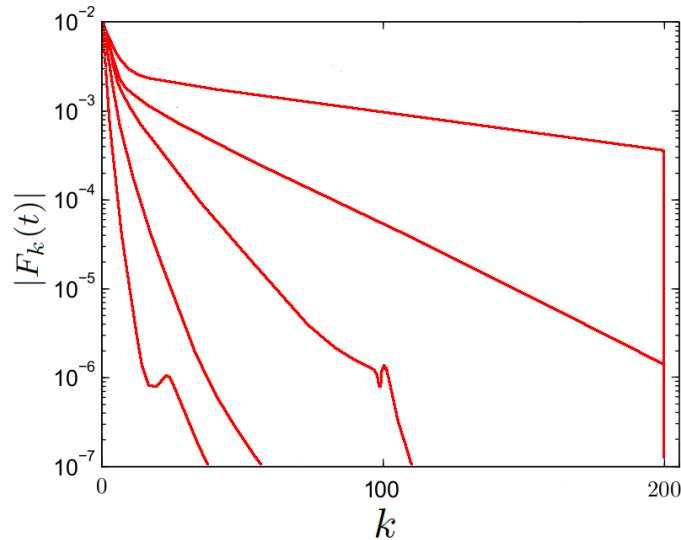
Figure 4.3: Plot of adjusted Fourier amplitudes $|F_k(t)|$, $k = 1, 2, \ldots 200$ at $\mathrm{Re} = 800$ truncated at $k = 200$ and at times $t = 0.60, 0.70, 0.80, 0.90$ and 0.99 respectively. The linear decrease in the figure indicates exponential decay. There are, however, anomalies in the graphs of $t = 0.60$ and $t = 0.80$ that creeps in due to improper spatial resolution.

The growth of Fourier amplitudes at high modes is also seen in the inviscid vortex sheet. Note that twice the absolute magnitude of the Fourier amplitudes are shown in Figure 4.3. The modes are truncated at $k = 200$. The decay of Fourier amplitudes is exponential until the graphs hit machine precision. After that, the amplitude obtained for a particular mode is spurious. There are isolated jitters on the graphs of $t = 0.60$ and $t = 0.80$. This occurs due to improper subdivision of vortex sheet panels during the run of the code. The effect is however only transient. Such anomalies should not occur when the split of vortex panels is perfect.

A single non-zero value of ν is unable to solve the vortex sheet problem. The computations in this section show that vortex sheet roll-up (increase in winding number) is largely dependent on the spontaneous appearance of singularity, but the growth of the vortex layer is stunted by singularity formation. Addition of a smoothing parameter contributes to a faster growth of the vortex layer, but the vortex sheet roll-up is slowed down. This leads us to the conclusion that partial preservation of the singularity is essential, along with dynamic smoothing of the vortex sheet circulation density by using a non-zero value of ν. The general idea is to allow the singularity to develop to a point by using high Re and then restrict the 'peak' of circulation density by lowering Re. This would allow the vortex sheet to wind up and increase in layer thickness simultaneously.

4.4 The Roll-up of a Periodic Vortex Sheet

The numerical simulation of a vortex sheet uses the following initial conditions: $N = 100$, $U = \pm 1$, $\epsilon = 0.01$ and $\lambda = 1$. This type of simulation incorporates the added effects of ν-smoothing. Since we know the location and time of appearance of the singularity, a large value

of Re is used in the beginning. This allows the viscous vortex sheet to begin the roll-up like an inviscid vortex sheet. Once the winding number has increased we reduce Re at the centre to suppress further rise of the singularity. The variation of Re at the centre of the spiral with time t is shown ib Figure 4.4. The trajectories shown are the envelopes which give successful roll-ups of a vortex sheet. Any variation or $\Re$ which lies within these limits can be used. The vortex sheet evolves into a double branched spiral. A vortex core is formed by regular windings of the vortex sheet and irrotational fluid in between the layers. Using a larger value of N would not change the shape of the vortex sheet. Markers in the fluid show that fluid particles follow a concentric circular trajectory similar to that of an irrotational vortex. The motion is shown in Figure 4.5.
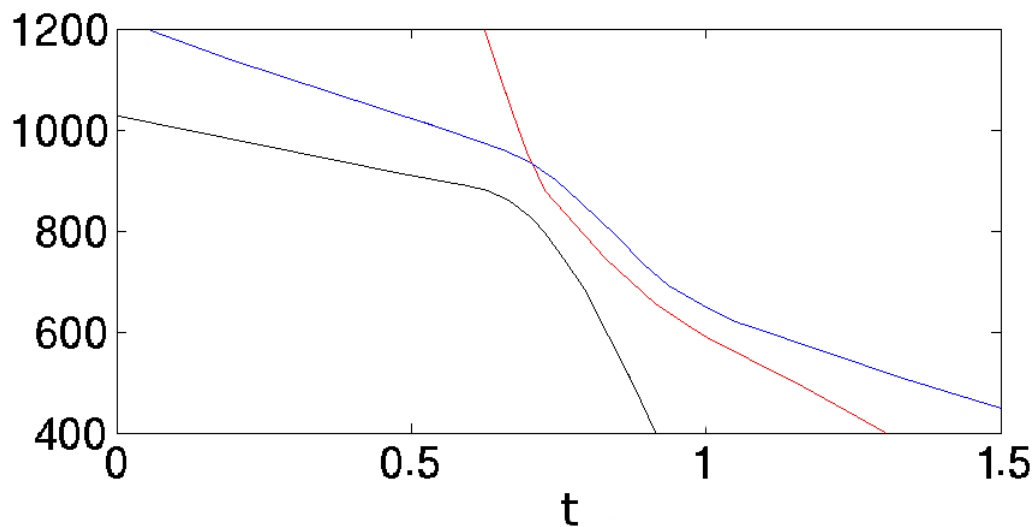
Figure 4.4: The envelopes of Reynolds number Re variation as a function of time t. The ν-smoothing is applied only at the centre of the spiral. Even though it acts locally, the effect is global due to viscous diffusion.
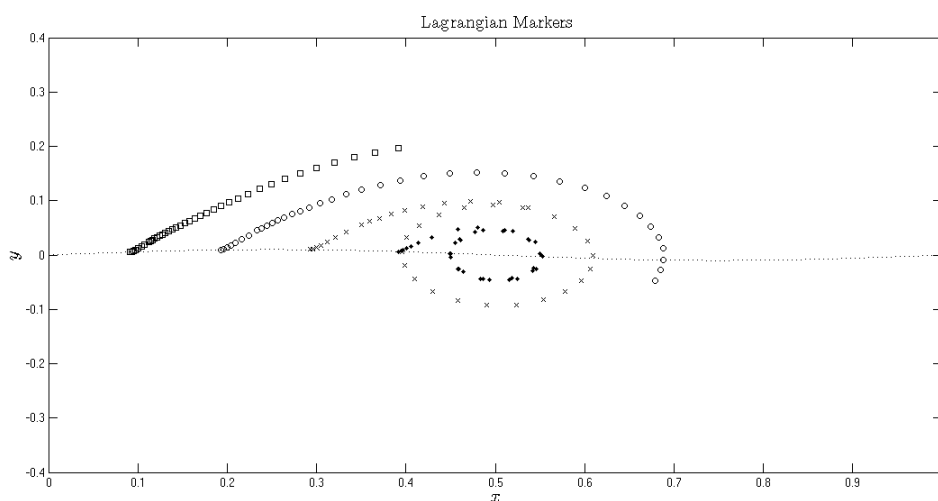
Figure 4.5: Formation of a vortex and the motion of fluid markers $p = 0.1(\square)$, $p = 0.2(\circ)$, $p = 0.3(\times)$ and $p = 0.4(\cdot)$. Also shown in dotted line is the vortex sheet at $t = 0$.

For a given smooth velocity field $\boldsymbol{u}(\boldsymbol{x}, t)$ the material trajectories $\boldsymbol{X}(\boldsymbol{\alpha}, t)$ satisfy

$$\frac{\mathrm{d}\boldsymbol{X}}{\mathrm{d}t} = \boldsymbol{u}(\boldsymbol{X}, t), \; \boldsymbol{X}(\boldsymbol{\alpha}, 0) = \boldsymbol{\alpha} \tag{4.19}$$

The parameter $\boldsymbol{\alpha} \in \mathbb{R}^2$ marks the position of the fluid particle at $t = 0$. Since the vortex sheet is flat, all markers on it can be parameterized by a scalar coordinate.

The centre of the vortex sheet becomes vertical at $t = 0.81$. Note that this is well beyond the critical time of the vortex sheet. After this, it is no longer possible to parameterize the vortex sheet as a single valued function of x. For $t > 2$ the inner region or core consists of multiple turns, and the winding number count increases with time. The outer region does not change significantly until boundary effects distorts it. Since, the core is a region of high curvature, majority of the vortex segments lie here.
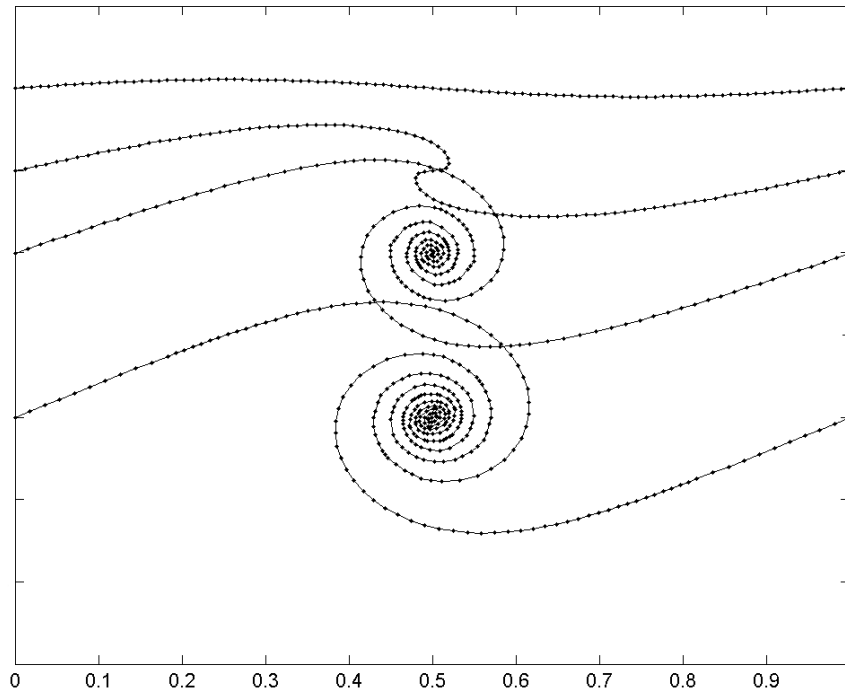
Figure 4.6: The roll-up of a periodic vortex sheet into a double-branched spiral. The end of a segment is a black dot. The number of segments are 100, 100, 206 and 284 respectively. Note that there is no intersection of segments, although the in the above diagram there is spatial overlap of vortex sheets at different times. This can be remedied by allotting more space during computation.

In Figure 4.6 the end of the vortex segments are marked with black circles. The development of the vortex is shown. It is evident that even with regularization, the majority of the vortex segments (roughly four-fifth) lie at the centre, but the vortex sheet never becomes singular. The present simulation is stopped at $t = 1.45$. The vortex sheet will continue to evolve beyond this time without difficulty. It is expected that domain effects will become important at later times, and this issue is presented in section 4.7.

Various statistical quantities like the growth rate and mean velocity profiles are also computed along with the evolution of the vortex sheet. The growth of vortex layer is discussed in the

following Section 4.5. A measure of dissipation due to regularization is given by relative loss of Hamiltonian. The drop in Hamiltonian during the simulation is 0.0184 of the initial value. The effect of regularization, therefore, leads to minor losses at this stage. The viscosity switch affects only one spot at the centre of the vortex sheet and the rest of the sheet is not altered in any way. The conservation of other integrals is discussed in Appendix A.

4.5 Growth of Vortex Layer Thickness

The growth of a mixing layer is due to entrainment of free-stream fluid and amalgamation of vortices. A vortex layer generated by a periodic vortex sheet presents a different image, as true mixing is not possible nor is actual vortex merger observed as time progresses (see Brown and Roshko, 1974, 2012). However, it will be seen that a simple vortex sheet model preserves some major features of a mixing layer and the growth rate is close to that observed in experiments.

A widely used measure of mixing layer growth is increase in momentum thickness. The momentum thickness has the dimension of length and is defined as

$$\theta = \int\limits_{y=-\infty}^{\infty} \left(\frac{1}{4} - \left(\frac{\langle u \rangle}{2U} \right)^2 \right) \mathrm{d}y \tag{4.20}$$

where $\langle u \rangle = \frac{1}{L} \int_0^L u(x,y,t)dx$. The non-dimensional momentum thickness is $\theta_{ND} = \theta/L$. Although, a periodic vortex sheet cannot lead to any true mixing of the top and bottom layers of fluid, the above definition can be used without any change. Another type of measure is (simply) the diameter or vertical extent of the vortex sheet, denoted by δ. In a mixing layer there is no sharp boundary between the mixing region and the free-stream region. Usually the mixing region or diameter is defined as the stretch where the x-averaged velocity profile deviates by more than 5% from the free-stream velocity. For a vortex sheet the x-averaged velocity profile has a sharp jump from the free-stream value within the 'mixing' region and therefore the delineation is automatic. Computer simulations suggest that the vortex layer growth is not linear with time[3]. It is convex during the initial phase and concave during the later phase. However, there is a point of inflection in the non-dimensional vortex diameter versus non-dimensional time curve. The second derivative (curvature) is momentarily zero at this time. The growth rate is defined as

$$r_1 = \frac{\mathrm{d}\delta_{ND}}{\mathrm{d}t_{ND}} = \frac{\mathrm{d}\left(\frac{\delta}{L}\right)}{\mathrm{d}\left(\frac{t2U}{L}\right)} = \frac{\mathrm{d}\delta/\mathrm{d}t}{2U} \tag{4.21}$$

where $\delta_{ND} = \delta/L$ is called the non-dimensional vortex diameter and $t_{ND} = t2U/L$ is called the non-dimensional time. The value of r_1 at inflection point is 0.2285. This value is remarkably close to the rate at which a free shear layer grows as we shall see in Chapter 5.

[3]The vortex layer growth is approximately linear over short distances, but this property holds for all smooth curves. Growth rates for vortex sheets with unpredictable perturbations are given in Chapter 5
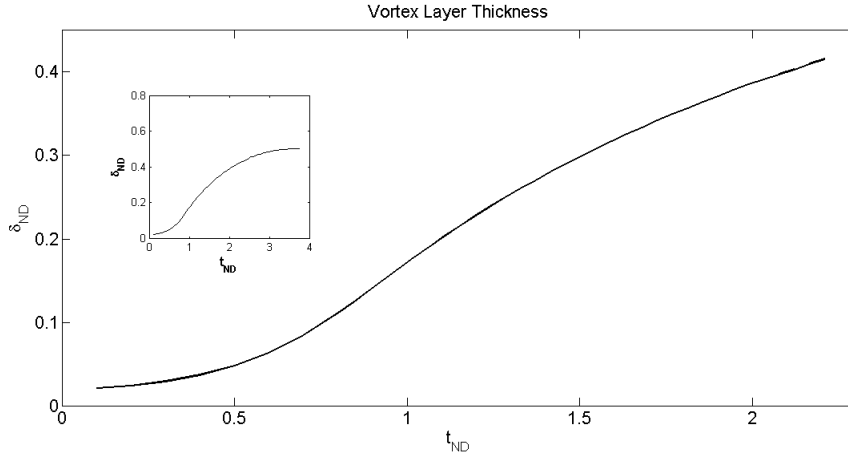
Figure 4.7: Vortex layer growth with $\epsilon = 0.01$ and $L = 1$. The slope r_1 at inflection point is 0.2285. Inset figure shows the decay in growth rate.

The finite size a periodic domain puts a restriction on the continued growth of a vortex sheet. When the size of the vortex spiral becomes comparable to the domain size, the gradient of the growth curve starts declining. Beyond $t_{ND} = 3.25$ the rate of increase is negligible. As will be seen in Chapter 5, a temporal shear layer stops expanding at approximately $t_{ND} = 3.15$ on an average. But, this does not imply that the vortex sheet motion has stopped. The vortex sheet continues to evolve in x-direction. The integration can be performed much longer. We, however, do not continue the integration here and long time integration is performed in the next Chapter.

The growth rate defined with vortex diameter as a measure can be extended to momentum thickness. The thickening rate r_2, based on momentum thickness, is similar to r_1 and is defined as

$$r_2 = \frac{\mathrm{d}\theta/\mathrm{d}t}{2U} \tag{4.22}$$

In this experiment r_2 has a minimum of 0.011 and a maximum of 0.029 in the range $1.3 < t_{ND} < 2.3$. In free shear layer experiments, the growth in the initial phase is dominated by initial conditions and towards the end by boundary conditions. Between these two regimes is a short regime in which it is expected that the momentum thickness θ grows linearly with time and the thickening rate r_2 should be a universal number. Reported values of r_2 in computer simulations range from 0.014 (Roger and Moser, 1994) to 0.0194 (Suryanarayanan and Narasimha, 2014). In the past a number of experiments have been performed on a spatial mixing layer. Let U_1 and U_2 be the free stream velocities on two sides of the spatial mixing layer. The transcription from temporal to spatial downstream evolution gives

$$\frac{\mathrm{d}\theta}{\mathrm{d}x} = 2r_2\Lambda \tag{4.23}$$

for the thickening rate, where $\Lambda = \frac{U_1 - U_2}{U_1 + U_2}$ is the non-dimensional velocity difference. Growth rate from experimental shear layers show that equation (4.23) is approximately satisfied. An estimate of r_2 based on various sources is 0.018. The self-similar behaviour in spatial shear layers is typically achieved at some distance from the splitter plate.

The universality of r_2 is based on dimensional analysis, which shows that the mean velocity

must be of the form

$$\frac{\langle u \rangle}{2U} = f\left(\frac{y}{x}, \Lambda\right) \tag{4.24}$$

and then there must be a constant c such that

$$\frac{\mathrm{d}\theta}{\mathrm{d}x} = c\Lambda \tag{4.25}$$

This is true only if Λ tends to zero and we assume that a spatial shear layer evolves asymptotically to a state independent of the any detailed initial conditions. Since viscosity is neglected, the flow has no lengthscale except for distance from the origin.

4.6 Effects of Amplitude ϵ

Unless mentioned explicitly, the vortex sheet is given a perturbation displacement amplitude $\epsilon = 0.01$, which is $1/100$ times the domain size. This is a large value, considering that the actual disturbances that offset a shear layer are much smaller in magnitude. However, the effects of 'largeness' or 'smallness' of the perturbation amplitude is not an important factor, once the vortex sheet motion begins. The usefulness of using a value of ϵ close to 0.01 is that we enter the evolution phase with little delay. However, if the value of ϵ is so large that it is no longer small compared to the domain size, then the qualitative properties of the vortex sheet roll-up change entirely. For example, with $\epsilon = 0.1$ there is no singularity formation at the centre of the vortex sheet, but two singularities appear symmetrically at some distance from it. The vortex sheet also does not roll-up into a single structure. Instead, it rolls-up into two identical asymmetrical vortices. This is very different from what we expect in a free shear layer.
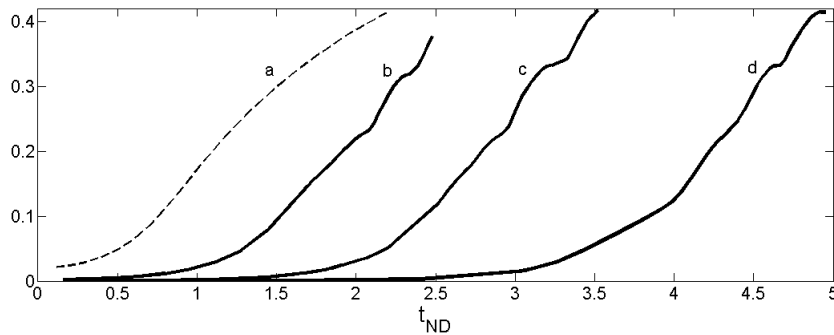
Figure 4.8: The growth of a vortex layer based on vortex diameter for different initial amplitudes: a. $\epsilon = 10^{-2}$ b. $\epsilon = 10^{-3}$ c. $\epsilon = 10^{-4}$ d. $\epsilon = 10^{-5}$. It is observed that for small amplitudes, the vortex sheet takes time to destabilize from its initial state.

On the other hand, the qualitative behaviour of the vortex sheet roll-up is not affected by variation of ϵ as long as its value is less than 0.05. Some of the values of ϵ chosen to study the roll-up of a vortex sheet are 10^{-3}, 10^{-4} and 10^{-5}. The growth curves for different initial conditions are shown in Figure 4.8. The values of ϵ are chosen somewhat arbitrarily, and the general conclusion is that the vortex sheet spends large amounts of time in the initial configuration state, if the value of ϵ is small. The difference is quite significant, considering that with $\epsilon = 0.01$ we achieve a complete roll-up at $t_{ND} = 2$, but with $\epsilon = 0.0001$ the vortex sheet is still flat at $t_{ND} = 2$. The vortex sheet is eventually destabilized, and once the roll-up occurs, the growth

is observed to be steady and the slope of growth is roughly the same across different initial conditions. The average growth rate based on vortex diameter lies in the interval $[0.2056, 0.2340]$ in all cases. This is before the size of the vortex becomes so large that its growth rate begins to slow down de to domain size effect. The smallest ϵ that was considered was 10^{-7}.

4.7 Asymptotic State

The growth of a vortex in the y-direction stops after some time, but evolution continues in the x-direction. The outer regions of the vortex sheet become elongated. If the scales of the axes are equal, the vortex is elliptical in shape and the ellipse's major axes develop a slight tilt (anticlockwise rotation) for $t_{ND} > 2.9$ and stretched in the free stream direction. The outer turns of the vortex sheet are advected by the freestream velocity into the adjacent domains.

We restart the simulation of a periodic vortex sheet with a wavenumber equal to 4 and amplitude $\epsilon = 0.01$. This allows us to get four vortices in a domain. The growth curve flattens for $t_{ND} \geq 0.8$. Compare this value with the time to flatten in Figure 4.5.
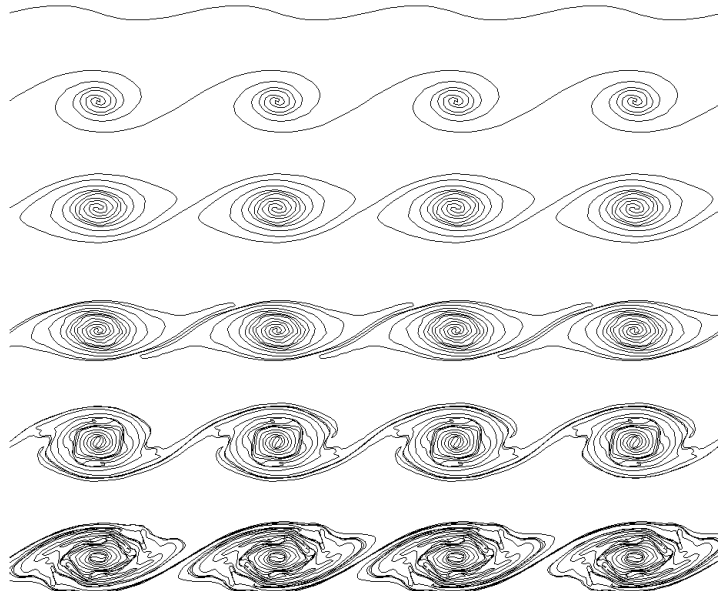
Figure 4.9:   Snapshots of a vortex sheet at $t_{ND} = 0.060933, 0.46715, 0.86225, 1.2, 1.5002$ and 1.8 respectively. The later timesteps have been inflated by manual intervention. This modification increases the chance of self-intersection of vortex segments, but allows us to progress quickly. The simulation is stopped when self-intersection occurs. The corresponding number of vortex segments are 120, 560, 1240, 2112, 3192 and 5040.

The 'long' time evolution of this periodic vortex sheet shows a tendency to cross over into the adjacent domains. This process is irreversible: once a portion of the sheet moves into the adjacent domains, it never returns. The circular or elliptical topology of the vortices gets distorted, although the cores are somewhat protected from the effect of neighbouring vortices by the outer layers. It may be conjectured that the inner turns successively cross the initial period's boundary at later times and that the sheet becomes highly elongated as $t \to \infty$.

Chapter 5

The Temporal Free Shear Layer

Much attention has been given to the temporal evolution of a vortex sheet where the initial perturbation is a small amplitude sine wave. The next generalization involves using an initial perturbation that is composed of several sine waves. In theory, we can decompose any continuous periodic function into sines and cosines. We shall however consider perturbations which are continuous in the first derivative. The evolution of a vortex sheet due to a non-sine wave perturbation displays features in experiments that have not been observed until now. Instead of a single vortex or multiple identical vortices, the vortex sheet rolls-up into multiple non-identical vortices that are rarely of circular or elliptical topology. At each inflection point, the sheet generates a vortex, which then morph into complex structures. The number of vortices or coherent structures decreases with time as some of them are absorbed or amalgamated with their neighbours. The size of the largest structure also increases with time. This is observed in the two-dimensional flows we consider in this Chapter.

5.1 The Temporal Free Shear Layer

The initial condition of the vortex sheet is chosen to be a combination of twenty sine waves with random intial amplitude. The wavelengths should not be integer multiples of one another, so that they do not have the same fixed points. The general form of the disturbance is

$$y = \sum_{k=1}^{20} \epsilon_k \sin\left(\frac{\lambda_k x}{2\pi}\right) \tag{5.1}$$

where λ_k is the wavelength of the kth component and ϵ_k is the amplitude of the kth component. All of the ϵs must be small in magnitude: they follow a uniform random distribution between 0 and 0.01. Any attempt to get an inviscid roll-up, as mentioned in Chapter 3, fails due to the lack of regularization. Since there are multiple vortices in the computational domain, the ν-smoothing used in Chapter 4 to smooth the centre of the spiral is needed now at several locations.
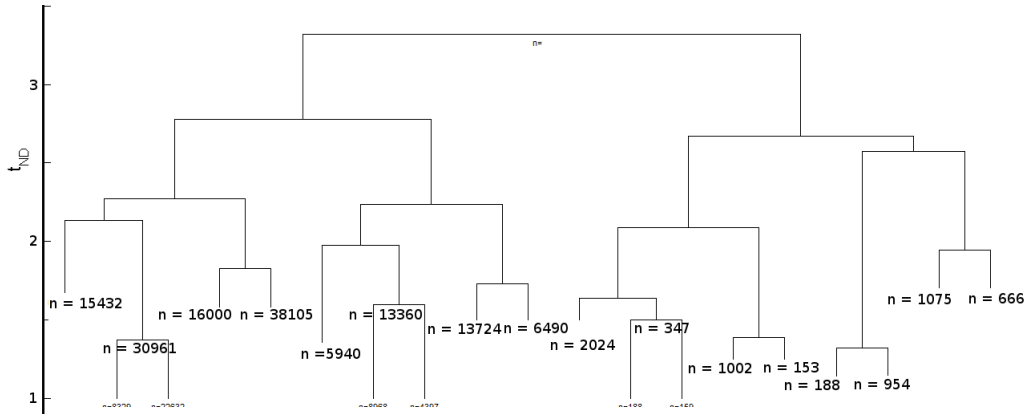
Figure 5.1: Binary tree type merger of vortex structures in a temporal shear layer after $t = 1.00$. This is a large computer simulation compared to the prototype models considered in Chapter 4. The number of panels in a structure is marked as n at each node. The total number of panels after $t = 1.00$ exceeds 100,000.

In Figure 5.3 a schematic diagram of the formation of vortices is shown. Then number of panels forming each cluster is marked. However, the clusters are 'soft' in the sense that their boundaries are subject to interpretation. In our analysis inflection points are taken as the end points. In Figure 5.3 merger of vortex structures are shown on the scale of time. However, it may not be evident from Figure 5.3 if it is a merger or an amalgamation. Usually, when two vortices with an unequal number of panels merge, the weaker vortex is annihilated completely. The identity of the weaker vortex is lost completely by elongation and filamentation.
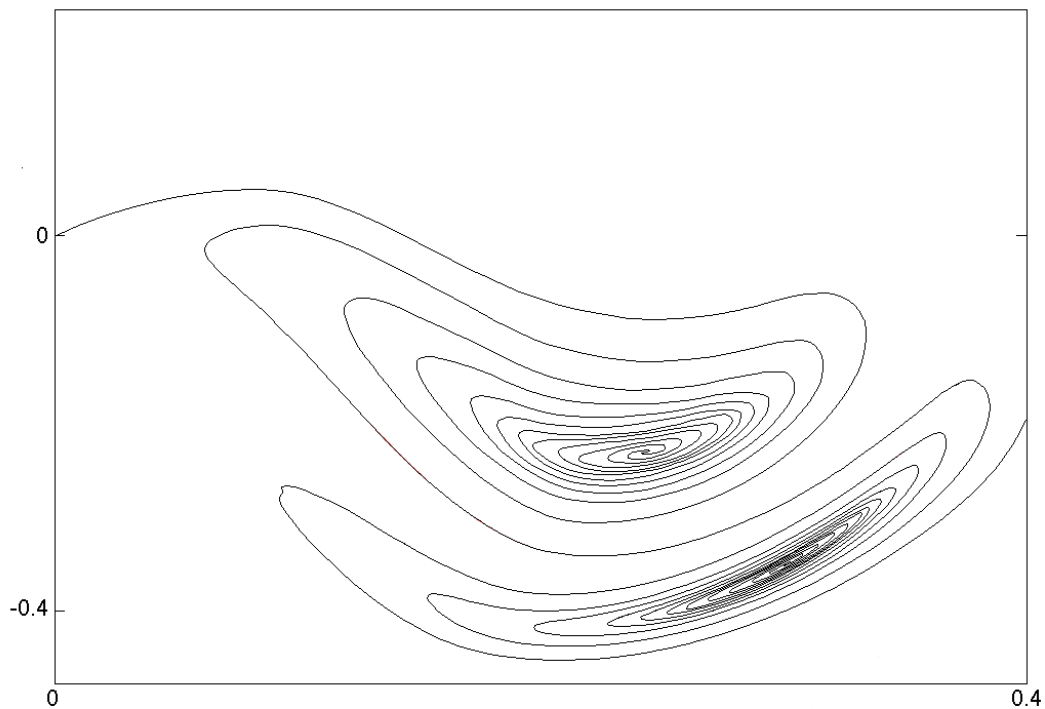
Figure 5.2: Interaction between two vortex structures in a temporal shear layer. Only a portion of the layer is visible. Vortex structures are not identical in a temporal shear layer. This leads to an unpredictable time-evolution. The x and y axes are not to the same scale.

Since the temporal shear layer gives rise to vortices of different shapes and sizes, a wide variety of phenomena is observable during its evolution. All vortex structures have a singular core. In Figure 5.2 we see one of the vortices being distorted by a neighbouring vortex. The singularities are located at approximately (0.27,-0.24) and (0.3,-0.38). The identification of coherent structures may be a nontrivial problem in some instances. The proper method to decompose the flow field into its components is given in Section 5.4. Otherwise, it suffices to track the singular spots that are associated with vortex structures. The number of panels in the above vortices is 1060 and 984 respectively. Since they are connected structures, the panel count will be affected by the changing boundary during evolution. Both of these points are at the centre of the vortex structure.

The exact shape of the vortex sheet in a temporal free shear layer will be dependent upon the initial conditions. As an alternate to a combination of small amplitude waves, one can also start with a completely randomized perturbation. This type of perturbation is generated by displacing the flat vortex sheet by a small random amount on a uniform grid. The displacement can follow a distribution like Gaussian with mean 0 and standard deviation 0.003. The important thing to note is that the sheet must be 'smooth' after being perturbed. The perturbed vortex sheet is constructed by a cubic spline interpolation. If the standard deviation of the Gaussian distribution is 0.001 or less a simple linear interpolation is done. The corresponding computer simulation is shown in Figure 5.3. The snapshots are taken at $t = 0.024, 0.036, 0.072, 0.9$ and 0.108 respsectively. The number of panels are 102, 256, 736, 2010 and 3060 respectively. This is an early phase for the temporal free shear layer where vortices are yet to merge, but singularities start to appear at $t = 0.04$. Once the vortices merge the memory of the initial condition gets lost in time. Integration for longer time periods are performed in Section 5.3. An approximate estimate of the number of panels at $t = 1$ would be 100,000. To reduce the computational cost for such large systems it may be useful to fix a lower bound for the length of a vortex panel. This will lead to the loss of microscopic details, but the macroscopic structures are not affected. We shall learn more about the mid and late stages of development of a temporal shear layer in Sections 5.2 and 5.3.
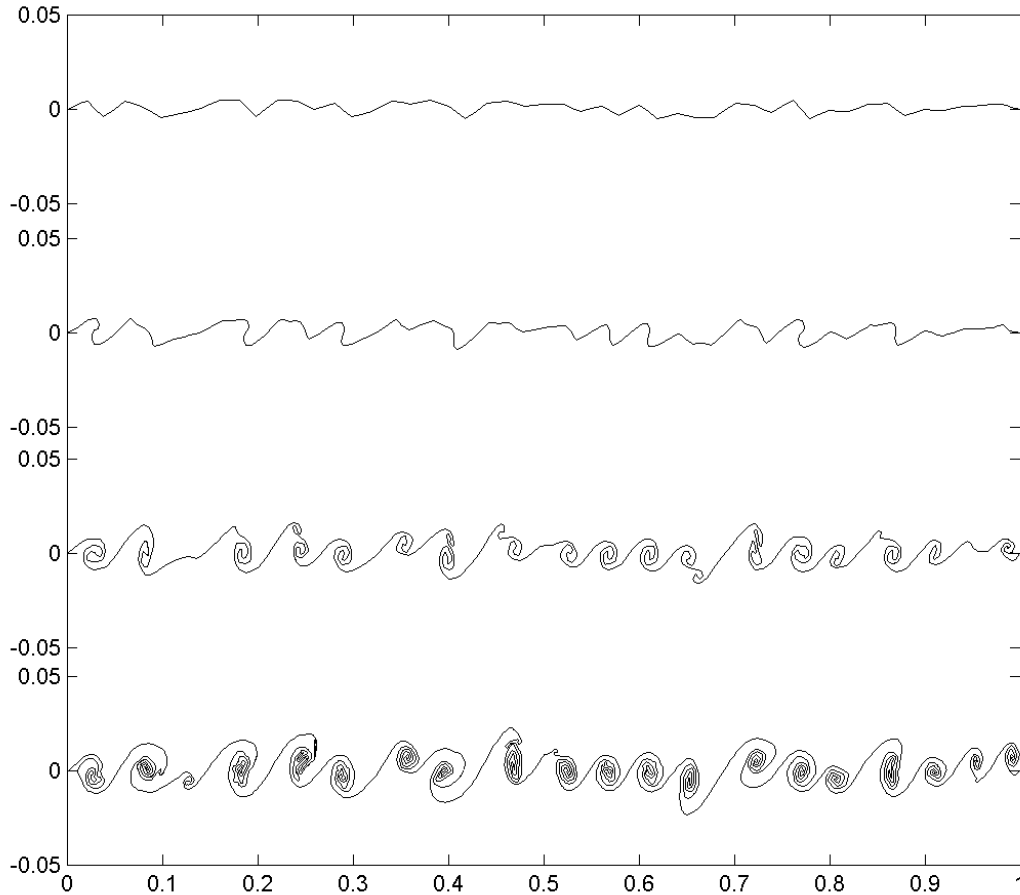
Figure 5.3: The vortex sheet with random Gaussian perturbations. The snapshots are taken at $t = 0.024, 0.036, 0.072, 0.9$ and 0.108 respectively. The y-axis is exaggerated for clarity. The temporal shear shear is still in the early phase where initial conditions play a dominant role. The number of vortices in the flow will depend on the type of perturbation given.

5.2 Coherent Structures

The use of randomized initial conditions in a temporal free shear layer gives rise to coherent structures. They are formed due to Kelvin–Helmholtz instabilities. We do not give a formal definition for coherent structures, but they can roughly described as long-lived objects in the vorticity field with a strong correlation pattern. A coherent structure can contain several sub-structures. There are also transient eddies in a temporal free shear layer. The boundary of a coherent structure is identified by the limits of coherent vorticity. Details can be found in the book by Monin and Yaglom (1965).

The merger of vortices leads to an asymptotic state where much of the shear layer, except the microscopic details, become free from the initial perturbation. In this regime the growth rate of the shear layer is statistically a constant number. More on this topic is given in Section 5.3. The number of singularities grows with time, but the number of coherent structures rises and then falls with time. In Figure 5.4 we can track the merger of vortices. This is a continuation of the vortex sheet evolution shown in Figure 5.3. The vortex sheet gets convoluted as a result of roll-up. Transient vortices would often arise in the shear layer, but then they disappear without

a trace. Non-transient vortices can still be identified after being absorbed into another vortex. Compare for example Figures 5.3 and 5.4 where we see smaller number of vortices at a larger time.
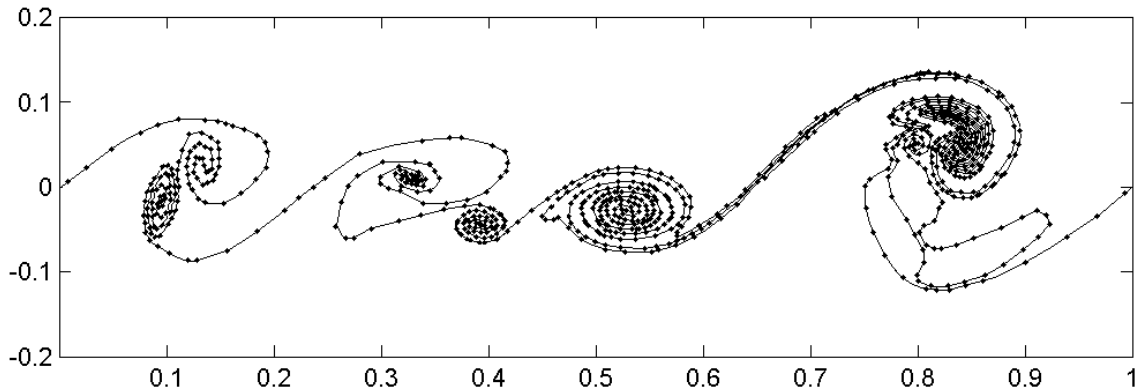
Figure 5.4:   The temporal free shear layer at time $t = 2.1$. The layer consists of four major coherent structures. The billowing pattern is a typical feature of a temporal free shear layer.

The chaotic nature of a vortex sheet roll-up can be seen in Figure 5.5. The outer layer of the main vortex suffers from Kelvin-Helmholtz instabilities at several locations, giving rise to many smaller vortices. This is what is likely to happen in a physical simulation where the exact nature of disturbance cannot be given. The secondary vortices in turn suffer from more instability giving rise to tertiary vortices. The location where these vortices pop up are random in the sense that even the slightest change in initial condition would move the vortices to a new and different set.
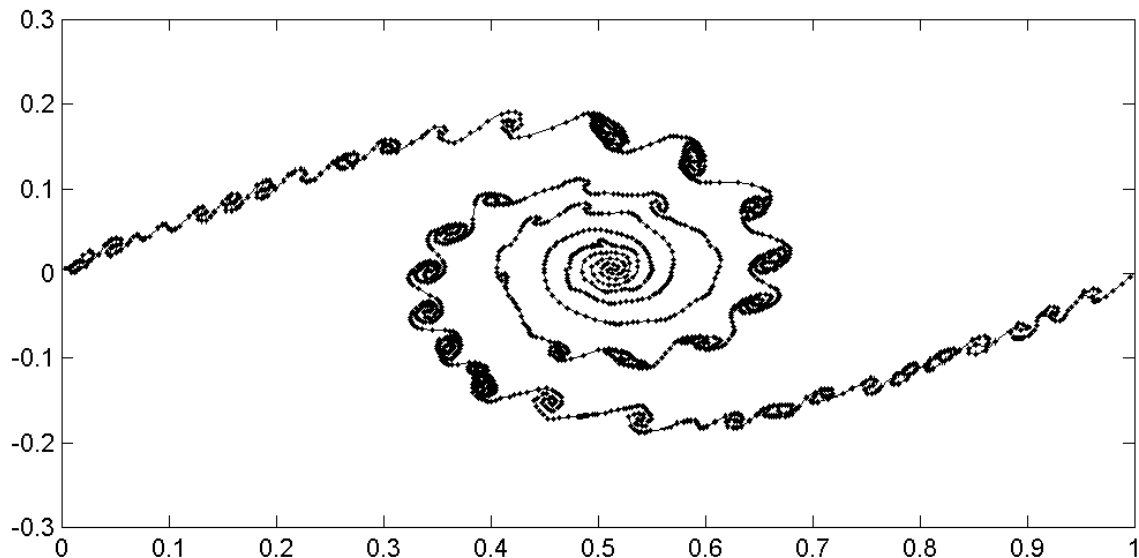
Figure 5.5:   The breakdown of a vortex due to a randomized high wavenumber disturbance. There are several smaller vortices that appear within the larger vortex. Although they do not grow much due to the lack of space, they resemble the original vortex in shape.

In the initial phase no distinction is made between a vortex and a coherent structure. The identification and count of coherent structures is not a straight-forward problem. The difficulty

lies in the fact that the outer layer of two vortices may merge, while their cores remain separated. The method of identification of coherent structures from the vorticity field is given in Section 5.4. The distribution of turbulent kinetic energy is not appropriate to count vortices, as shown in Figure 5.6.
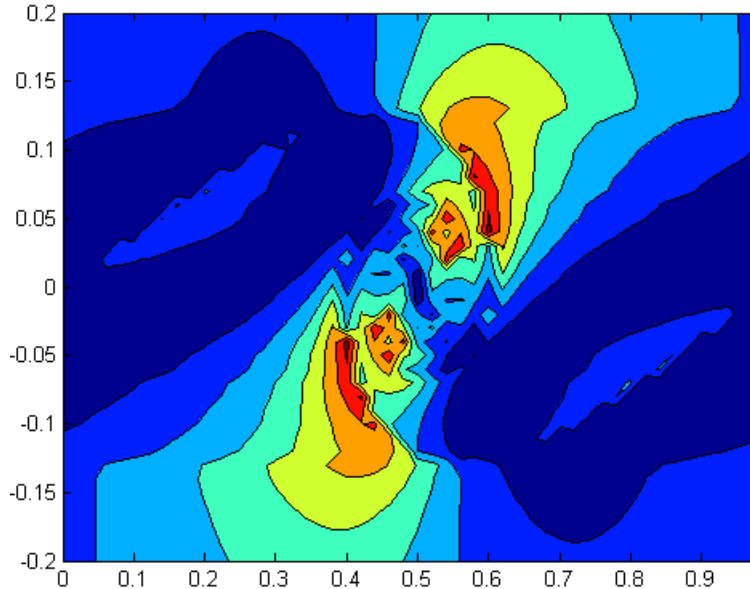
Figure 5.6: The turbulent kinetic energy distribution generated by a single vortex or a coherent structure. The red regions indicate higher concentration of energy compared to the blue regions. The fragmented high energy region actually lies within a single structure.

The distribution of the kinetic energy is fragmented even though it is confined to a single vortex.

5.3 Shear Layer Growth Curves

There have been numerous studies on the growth of a spatially evolving shear layer in the laboratory. A temporal shear layer is difficult to get in the laboratory, but easy to study on a computer. The growth of a temporal shear layer has been studied by Delcourt and Brown (1979), Aref and Siggia (1980) and Suryanarayanan and Narasimha (2013) by modelling the shear layer with point vortices. The vortex sheet model was used to study the growth of a spatial shear layer by Basu and Narasimha (1992).

Except for the initial phase, the growth of a shear layer is driven by the formation of coherent structures. For point vortices a coherent structure may be thought of as an agglomeration or cluster of points. A vortex sheet, however, rolls up to form distinctive coherent structures. Since a vortex sheet is a non-intersecting continuous curve the limits of a coherent structure are noticeable even if surrounded by many neighbours. It is observed that coherent structures grow by wrapping the vortex sheet and absorption of vortices weaker than themselves.

A natural measure for shear layer thickness is the maximum extent of the vortex sheet in the vertical direction or the region where y-velocity deviates significantly from the free stream velocity. This would give us an approximate measure of the shear layer thickness. This is however

difficult to evaluate on a computer, with the output not guaranteed to be symmetric about the horizontal $y = 0$ centerline. This would require us to measure both upside and downside. The measure for shear layer thickness used here is the momentum thickness. For the definition of momentum thickness refer to Section 4.5. Apart from momentum thickness, another possible measure of shear layer thickness can be vorticity thickness.

It is found that the growth of momentum thickness $\theta(t)$ with time t for a single realization is arbitrary apart from its generally increasing trend. No other substantial information is obtained. The growth curves are not monotonic and they vary widely from experiment to experiment i.e. when the initial conditions are changed. There is a general lack of stationary behaviour. The effect of shocks (random displacements) linger until boundary conditions are reached. However, the average growth curve obtained from an ensemble of vortex sheet experiments displays lesser variations and greater monotonicity. This is expected to occur and is of prime importance in the field of free shear flows.

Computer simulation of a vortex sheet model requires greater number of operations and memory than a point vortex model[1], but is less involved than solving the momentum and continuity equations[2]. Since the velocities are obtained from a summation operation, parallelization of this operation can reduce the computation time. For an ensemble of vortex sheets the realizations can be computed independently of one another. If there are N vortex segments in the sheet the cost of computation is $O(N^2)$. However, if the sheet is symmetric with repect to the streamwise axis computation on one-half of the sheet suffices[3]

---

[1]Additional operations include resegmentation to maintain resolution of the vortex sheet at every time step. There is a growth of in the number of computational panels with time in a standard vortex sheet model. The desingularization function, storage of circulation density and curvature requires additional memory.

[2]A direct global solution of Navier-Stokes equations often requires solving the Poisson equation for pressure.

[3] The following shows that vortex sheet model is not computationally intensive and a good resolution can be obtained to get desired output in reasonable time:

Ensemble Size	t=0.1	t=0.5	t=1.0	t=2.0	t=3.0	t=4.0
40	65 min	143 min	306 min	829 min	2008 min	3783 min
80	120 min	277 min	585 min	1600 min	3778 min	not performed
160	203 min	540 min	1165 min	3128 min	not performed	not performed

where usual Intel Xeon microprocessors (8 physical cores and 16 logical cores) and 4 GB memory per core are used on one single machine.
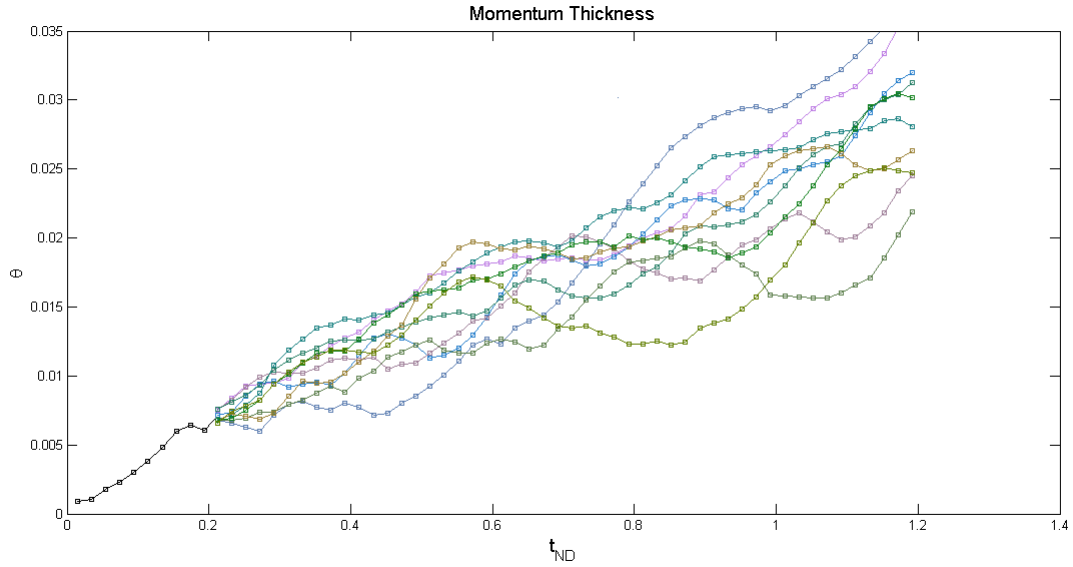
Figure 5.7: The effect of random shocks on the growth of a temporal free shear layer. The shock appears at $t_{ND} = 0.2$. The effect of the shock is permanent indicating a lack of stationary behaviour.
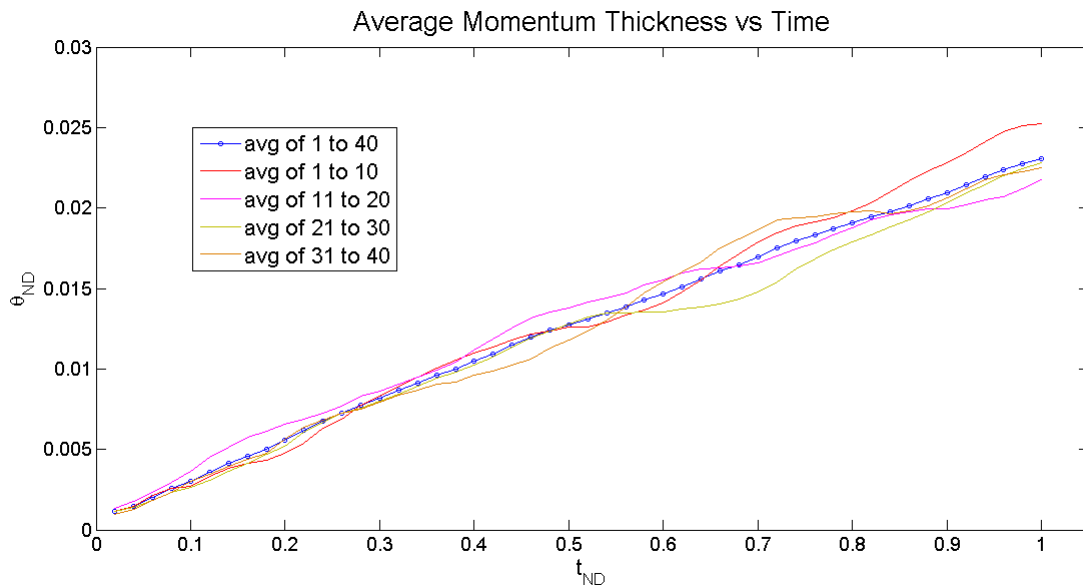
Figure 5.8: The effect of random shocks on a shear layer growth. There is no stationary behaviour as the growth curves gets displaced permanently. The average rate of growth of the shear layer is however not changed.

The shear layer stops growth saturates between $t = 3.5$ and $t = 4.0$, due to the effects of periodic boundaries. In the regime between $t = 0.1$ and $t = 3.0$, the growth rate is expected to be linear, but this has to be verified analytically. There is strong experimental evidence that the growth of shear layer is linear for a considerable period of time, after initial effects decay and before boundary effects grow. The details of growth are shown in Figure 5.7 and Figure 5.9.
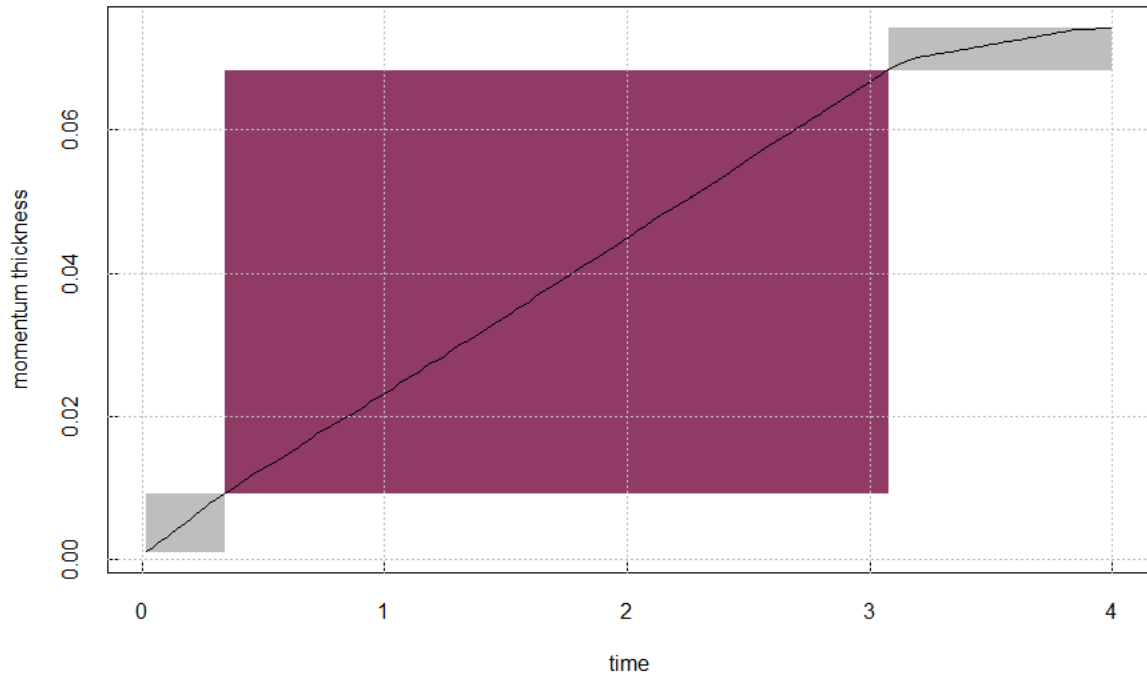
Figure 5.9: The black line is the growth of average momentum thickness of 120 realizations versus time, from $t = 0.1$ to $t = 4.0$. A transition occurs somewhat abruptly at $t = 3.15$. The black line levels-off due to the effect of boundary conditions.
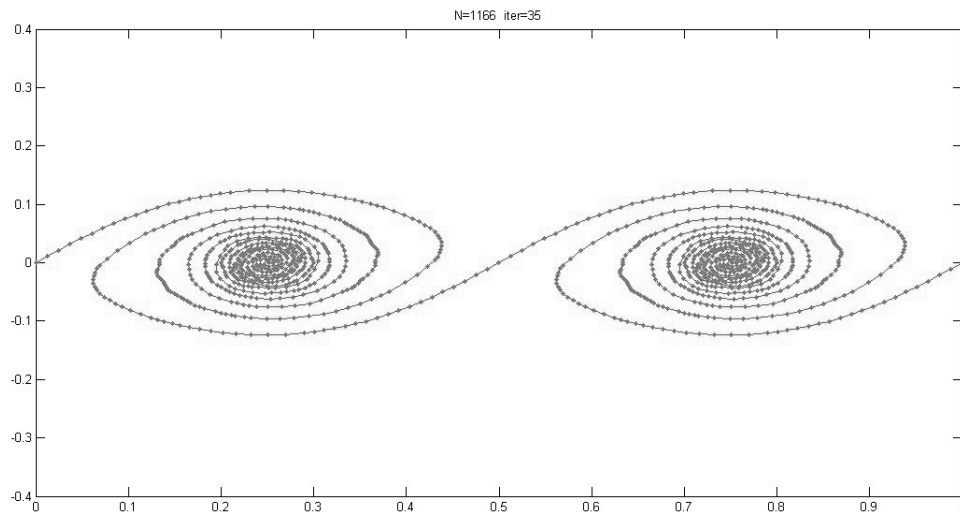
Figure 5.10: A vortex sheet where growth of momentum thickness is being slowed due to collision of vortices (regime III of vortex gas). The sheet cannot expand in the y-direction, but continues to expand in the x-direction. This, however, does not contribute to the growth of momentum thickness.

It is evident that the effect of periodic boundaries causes the growth to decay. But until that time is reached, it is expected that the average growth rate of a free shear layer is linear and

a universal number. This regime of growth has been studied in experiments, and growth rates ranging from 0.014 to 0.022 have been reported [Suryanarayanan and Narasimha (2013)]. Initial conditions may also affect the growth rate at the beginning, but such variations are transient in nature. If we assume that the growth rate becomes approximately linear, and independent of initial conditions when the ensemble size is large, then a linear fit can be used to find the average growth rate. For an ensemble of size 40 the average growth rate is 0.02234 and for an ensemble of size 120 the average growth rate is 0.02232. The later value is more stable i.e. fluctuations are less than 0.00002 in absolute magnitude if we repeat the numerical experiment again with a different set of initial configurations.

A generalized approach to find what a shear layer grows like would be to take a functional equation of the form

$$\theta = f(t) \tag{5.2}$$

where f is an unspecified smooth function. If f is linear or close to being linear, then there should be low curvature on the graph of f and hence the second derivative of the function should be low throughout its range.

We need not assume any adhoc parametric form of the function f, as we split it into a set of basis functions. Polynomial bases are not convenient because of the presence of higher order terms. A cubic spline basis is chosen and the knot selection problem is avoided by coinciding knots with datapoints. The complexity of the fit is controlled by regularization. One finds the penalized residual sum of squares

$$(\boldsymbol{y} - f(\boldsymbol{x}))^T(\boldsymbol{y} - f(\boldsymbol{x})) + \lambda \int_{x_1}^{x_n} f''(x)\mathrm{d}t, \tag{5.3}$$

where λ is a smoothing parameter. If $\lambda = 0$ then f can be any function that interpolates the datapoints. If $\lambda = \infty$, then no second derivative can be tolerated and the fit is a straight line. The intermediate values of λ index an interesting class of functions in between. For a general overview of such methods refer to Boyd (2001) and MacKay (2003).

It is possible to choose a maximal set of knots: at each unique value of t. This can make the model seem over-parametrized. However, the penalty coefficient λ translates to a penalty on the spline coefficients, which are shrunk some of the way to a linear fit. Remarkably it can be shown that there is an explicit, finite dimensional minimizer for f in (5.5) which is a natural cubic spline with knots at the unique values of time.

Since the solution is a natural spline, we can write it as

$$f(x) = \sum_{j=1}^{n} a_j N_j(x) \tag{5.4}$$

where the functions $N_j(x)$ are an n dimensional set of basis splines. The criterion thus reduces to

$$(\boldsymbol{y} - \boldsymbol{N}\boldsymbol{t})^T(\boldsymbol{y} - \boldsymbol{N}\boldsymbol{t}) + \lambda \boldsymbol{t}^T \boldsymbol{\Omega} \boldsymbol{t}, \tag{5.5}$$

where $N_{ij} = N_j(t_i)$ and $\Omega_{jk} = \int N_j''(t)N_k''(t)\mathrm{d}t$. The solution is easily seen to be

$$\hat{\boldsymbol{t}} = (\boldsymbol{N}^T\boldsymbol{N} + \lambda\boldsymbol{\Omega})^{-1}\boldsymbol{N}^T\boldsymbol{t} \tag{5.6}$$

The operator $\boldsymbol{N}^T\boldsymbol{N} + \lambda\boldsymbol{\Omega}$ is known as the smoother matrix and is denoted by $\boldsymbol{S}_\lambda$. The rank of $\boldsymbol{S}_\lambda$ is n. We shall define the effective dimension of the fit as the sum of the diagonal elements of the smoother matrix. An effective dimension value close to 1 implies that the fit is almost linear.

We have yet not discussed how the value of λ is chosen. The trace of $\boldsymbol{S}_\lambda$ is monotone in lambda and therefore it is possible to invert the relationship and specify λ by fixing the effective dimensions. In practice this can be achieved by simple numerical methods. Here we shall adopt the more traditional method of specifying the amount of smoothing instead of trying to optimize the fit by choosing λ based on GCV or AIC.

t	theta
0.02	0.001151267
0.04	0.001475856
0.06	0.002024048
0.08	0.002561791
0.1	0.002994422
0.12	0.003605196
0.14	0.004142852
0.16	0.004598748
0.18	0.004982338
0.2	0.005548533
0.22	0.006166292
0.24	0.006774561
0.26	0.007269074
0.28	0.007775658
0.3	0.008199794
0.32	0.008694752
0.34	0.009140405
0.36	0.009601541
0.38	0.009998445
0.4	0.010499068
0.42	0.010951167
0.44	0.011475339
0.46	0.011960887
0.48	0.012386766
0.5	0.012727656
0.52	0.013087302
0.54	0.013459252
0.56	0.013848761
0.58	0.014272964
0.6	0.014655818
0.62	0.015121867
0.64	0.015567459
0.66	0.016065476
0.68	0.016486445
0.7	0.016970981
0.72	0.017543459
0.74	0.017977911
0.76	0.018335016
0.78	0.01869477
0.8	0.019052178
0.82	0.019430947
0.84	0.019762517
0.86	0.020129428
0.88	0.020556847

There are 44 datapoints of time versus momentum thickness in the column to the left. We prefix the number of knots at 3 spread uniformly and use cubic splines as bases. They are penalized by integrated square second derivative cubic spline penalty. Assuming that the error distribution is Gaussian, and the growth depends continuously on time, we obtain a nonlinear fit with effective degrees of freedom 1.99 and a parametric intercept of 0.0126. However, the deviation from linearity is not systematic and the fit can be easily approximated by a straight line. See Figure 5.12 for a detailed analysis.
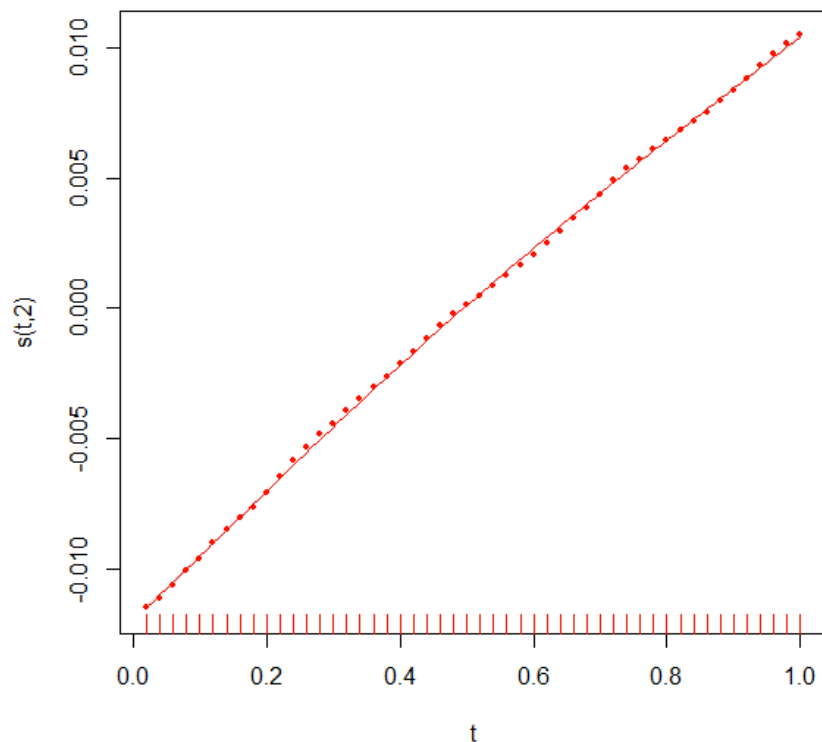
Figure 5.11: Spline interpolation of shear layer growth curve with 3 knots. The edf of the curve is 1.99, approximated to 2 in the above diagram.

Note that in the Figure 5.11 shown above, the datapoints are centered, so that there is no intercept term in the nonlinear part of the fit. Presence of a constant coefficient in the nonlinear function and an intercept outside will lead to collinearity.
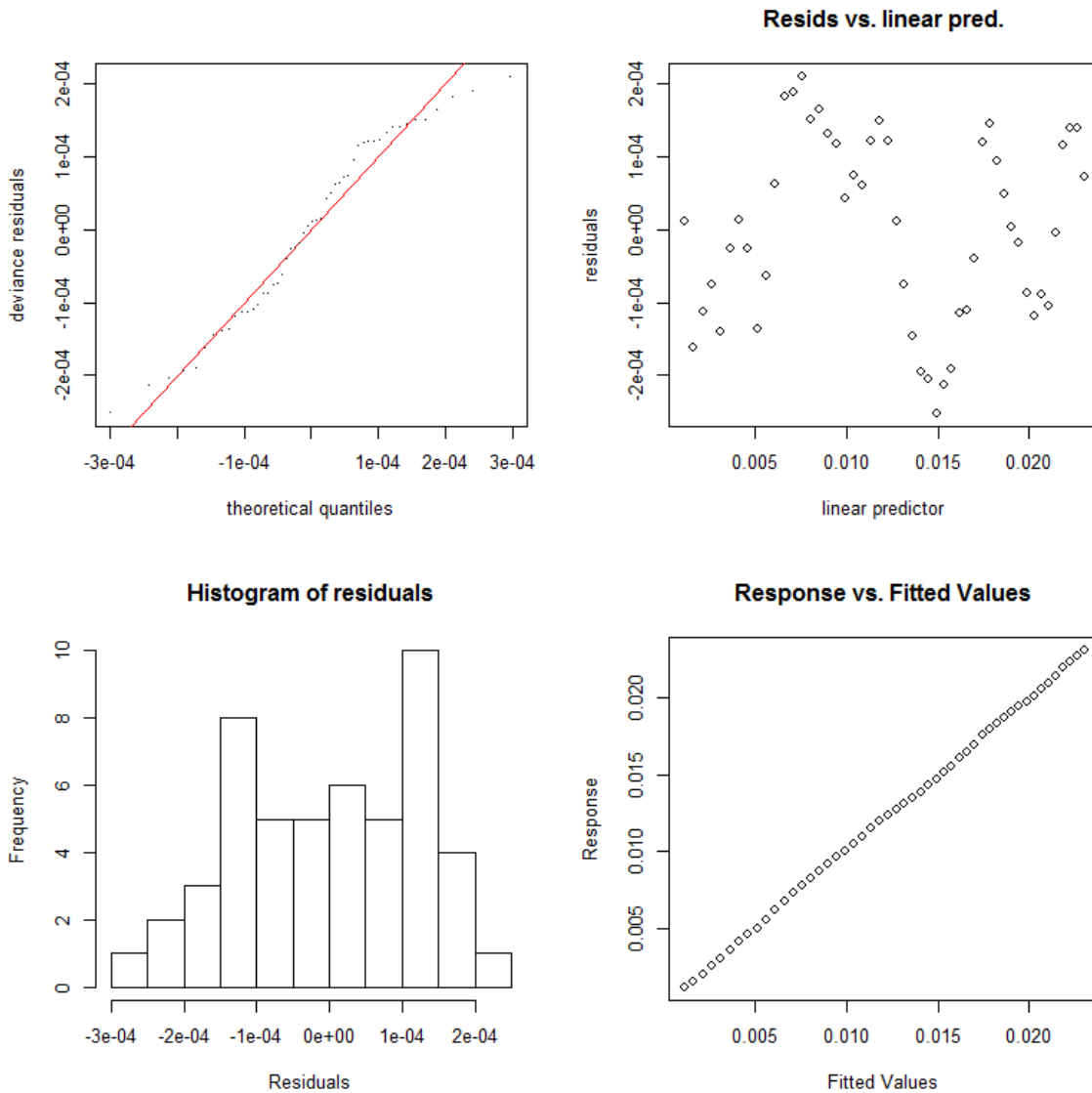
Figure 5.12: Top left: deviance versus theoritical quantiles. Top right: residuals versus linear predictor. Bottom left: distribution of errors. Bottom right: response versus fitted values.

We may conclude that the growth curve is strongly linear and that any nonlinear variations are entirely local. The largest size of the ensemble considered here consists of 160 realizations. On the restricted range between $t = 0$ and $t = 1$ the growth rate observed was 0.02120, which is a 5.01% decrease compared to the average growth rate of 0.02232. The former number can be considered as more stable as it is based on a larger number of realizations. Before we end this discussion, it must be noted that the growth rate becomes strongly linear even when there are only 40 realizations in the ensemble. However, the slope undergo slight variations with the size of an ensemble, and convergence is only observed when the simulation is run 120 to 160 times. The reason for running larger ensembles on a restricted range is due to limitations on computational resources.

5.4   Identification of Coherent Structures

In the later stages, identification of coherent structures may require some background analysis. We decompose a random field, preferably the vorticity field, into a mean and a time varying part:

$$\omega(\boldsymbol{x}, t) = \mu(\boldsymbol{x}) + \varepsilon(\boldsymbol{x}, t) \tag{5.7}$$

We get a number of snapshots at time $t = t_1, t_2, \ldots, t_N$. We find a basis function $\phi(\boldsymbol{x})$ that maximizes the average inner products between $\varepsilon_t(\boldsymbol{x})$ and $\phi(\boldsymbol{x})$:

$$\sum_{k=1}^{N} \left(\int_{\Omega} \varepsilon_k(\boldsymbol{x}) \phi(\boldsymbol{x}) \mathrm{d}\boldsymbol{x} \right)^2 \tag{5.8}$$

where $\varepsilon_k(\boldsymbol{x})$ is equal to $\varepsilon(\boldsymbol{x}, t_k)$ and Ω is the space $[0, 1] \times (-\infty, +\infty)$. We search for maximizers among the class of functions $\int_{\Omega} \phi^2(\boldsymbol{x}) \mathrm{d}\boldsymbol{x} = 1$. This is equivalent to maximizing the functional:

$$L(\phi) = \langle \varepsilon_k \phi \rangle^2 + \lambda(\langle \phi \phi \rangle - 1) \tag{5.9}$$

with respect to ϕ. For brevity, we have used the notation $\langle \cdot \rangle$ for inner product, and dropped the summation in equation (5.9). The maximizer must satisfy the Euler-Lagrange equation i.e. $\frac{\partial L}{\partial \phi} = 0$ which gives us

$$\int_{\Omega} \sum_{k=1}^{N} \varepsilon_k(\boldsymbol{x}) \varepsilon_k(\boldsymbol{x}') \phi(\boldsymbol{x}') \mathrm{d}\boldsymbol{x}' = \lambda \phi(\boldsymbol{x}) \tag{5.10}$$

This is a Fredholm equation of the second kind, the kernel of which is an autocorrelation function. The optimizer is not unique, but there are an infinity of solutions. For greater details refer to Berkooz, Holmes and Lumley (1993). The sequence of solutions ϕ_n are orthogonal eigenfunctions and we denote the corresponding eigenvalues as λ_n. The eigenvalues are positive and the eigenfunctions form a basis set. We index the eigenvectors such that the corresponding eigenvalues are in decreasing order. Every member of the ensemble $\boldsymbol{\varepsilon}_k$ can be reproduced by a linear combination of the eigenfunctions:

$$\varepsilon_k(\boldsymbol{x}, t) = \sum_{n=0}^{\infty} a_n(t) \phi_n(\boldsymbol{x}) \tag{5.11}$$

The first eigenvector ϕ_1 which has the largest eigenvalue, is the best to characterize the ensemble of ε. The second eigenvector ϕ_2 which has the second largest eigenvalue, is the best among all eigenvectors orthogonal to the first, and so on. Much of the flow field information, including the geometries of coherent structures, can be retrieved from the leading eigenfunctions.

Coherent structures identified by the preceding pattern recognition technique can further be collapsed into fewer groups by means of iterative descent clustering algorithms. The region of highest vorticity concentration within a coherent structure is taken as the location marker for the structure. Given the set of centres $\boldsymbol{x}_1, \boldsymbol{x}_2, \ldots \boldsymbol{x}_n$ we partition the n centres into k sets, such that the within-cluster sum of squares is minimized. The dissimilarity measure is taken as the squared Euclidean distance. The steps of the algorithm are:

1. For a given group C find the observation in the group minimizing total distance to other points in that group:

$$i_\ell = \operatorname*{argmin}_{i:C(i)=\ell} \sum_{C(j)=\ell} d\left(\boldsymbol{x}_i, \boldsymbol{x}_j\right) \tag{5.12}$$

where d is the dissimilarity measure. Then $\boldsymbol{m}_\ell = \boldsymbol{x}_{i_\ell}$, $\ell = 1, 2, \ldots, k$ are the current estimates of the group centres.

2. Given a current set of group centers $\boldsymbol{m}_1, \boldsymbol{m}_2, \ldots \boldsymbol{m}_k$, minimize the total error by assigning each structure centre to the closest (current) group centre:

$$C(i) = \underset{1 \leq \ell \leq k}{\operatorname{argmin}} \, d(\boldsymbol{x}_i, \boldsymbol{m}_\ell) \tag{5.13}$$

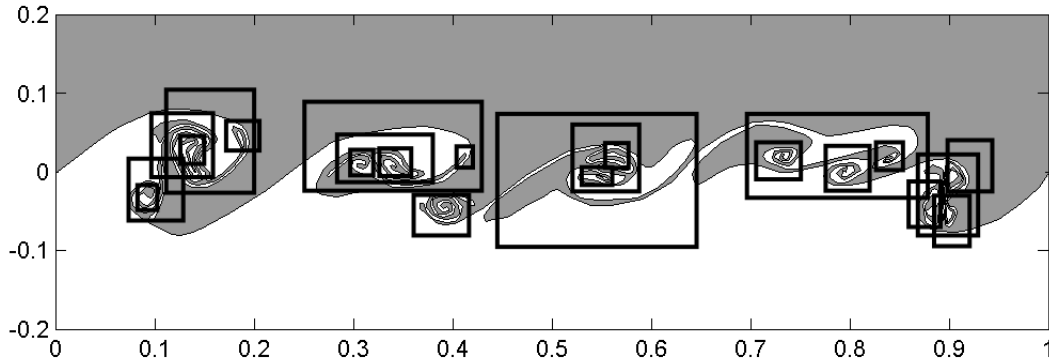3. Iterate steps 1 and 2 until the groupings do not change.

Figure 5.13: Schematic diagram for the identification of coherent structures in a free shear layer: marked by black boxes. The figure shows the occurrence of vortices inside a coherent structure.

This is a method may not give us the best groupings [4]. Each of steps 1 and 2 reduces the value of variance criterion, so that convergence is assured. However, the result may present a suboptimal local minimum. For this reason, we need to start the algorithm with many different initial conditions, and choose the solution with the smaller objective function. In step 1 or in equation (5.12), a k-means method would require an amount of computation proportional to the group size n_ℓ, whereas here we would require $O(n_\ell^2)$ computations. The second step or equation (5.13) requires computation proportional to kn. A method that gives the global minimum is not attempted here, because of slow convergence. But for a very small number of structure centres, finding the global optimum may be practical.

5.5   Notes

In a previous section (see Section 5.3) we have described how a temporal free shear layer expands with time. An experimental free shear layer can be related closely to the output of a computer simulation by the rate at which the shear layer grows with time. However, the average growth curve is an integral quantity and there are interior details that are not captured.

The initial conditions cannot be completely random. If the magnitude of the initial disturbance may be taken as small, then the vortex sheet remains static. Controlling factors in the initial period are amplitude and distribution of the initial perturbation. The magnitude of initial disturbance is the amplitude if the disturbance is a sine wave. If the disturbance is some non-standard function, then the magnitude of the disturbance is the rms value of the function. The

---

[4]The two stage process followed here is an instance of greedy algorithm. However, we need a solution in reasonable time, even if the solution is sub-optimal.

functional form of the disturbance is deterministic if it is a sine wave. For a non-deterministic function we take a mesh of Gaussian or uniform modes. The locations of the modes are uniformly distributed. A natural cubic spline is fitted. For obtaining discrete values, the range [0,1] is sampled at 100 points [5]. These points are spaced equally. The magnitude of disturbance should be less than or approximately 0.01 times the size of the domain.

In many figures the segments of the vortex sheet are marked with a line, and dots denote the start/end points. Since the core is a region of high curvature, the number of segments residing in core is always large. There can no discontinuities or self intersection of the vortex sheet. The problem of discontinuity can arise if the periodic boundary conditions are not enforced. The problem of self intersection in vortex sheets has been addressed in Basu and Narasimha (1992). While self intersection is a phenomenon which should not be seen, its effect is local and macroscopic predictions are not too out of line. It is possible to rectify self-intersection of vortex sheets by using more computer resources: to create a higher resolution.

It is possible to generate any number of vortices in [0,1] by adjusting the wavenumber of a deterministic sine wave perturbation. There is, however, no additional insight to be obtained. The generated vortices are smaller in magnitude when the wavenumber of the perturbation is larger, their geometries are self similar and they stop growing when they collide with their neighbours. The growth of the vortex layer can be measured by calculating the momentum thickness or by finding the vertical diameter of the vortex structures. Note that the average vorticity is zero anywhere outside the diameter.

---

[5]We take 100 sample points as a standard at the starting point of each simulation. One can as well take 200 sample points. Taking more sample points does not lead to different results as the density of segments increases. On the other hand, taking very few points, like less than 5, at the beginning of the simulation will lead to failure.

Chapter 6

Conclusion

6.1 Summary

The major focus of this work has been to get past the finite time singularity in a vortex sheet. An inviscid vortex sheet is unable to break the critical time limit. In the past, desingularization techniques have been applied to point vortex systems, and the vortex panel or sheet model (without desingularization) has been able to mimic major features of a spatially evolving free shear layer. These are powerful techniques with a scope for further research and development. The desingularized vortex sheet model has not been used in the past to study a free shear layer or otherwise. The equation of motion of a self induced temporal vortex sheet with periodic boundaries is derived from the basic kinematical principles and the Biot-Savart law. This equation has a singular solution. The circulation density and curvature blow up at a finite critical time. This is a consequence of unrealistic assumptions like the fluid has zero viscous diffusion and no surface tension. The method of viscosity switch proposed here shows that the vortex sheet solution exists beyond the critical time. For the first time it enables us to integrate past the Moore's singularity. The tangential smoothing of the circulation density can be interpreted physically, and therefore its inclusion does not alter framework of the Navier-Stokes equations. The smoothing by viscosity happens only in regions of high vorticity gradients. The smoothened equation converges to the Birkhoff-Rott equation in the limit of zero tangential viscous diffusion. The limiting solution, starting with a simple small amplitude single frequency perturbation, is a spiral with infinite number of turns. The rise of large scale coherent structures from smaller vortices is seen in the vortex sheet simulations. The coherent structures are stable and long-lived. The flow inside the free shear layer is chaotic in the sense that trajectories of fluid particles initially very close to each other in the phase space separate exponentially. The checks on the conservation of momentum and energy are provided in Appendix A.

6.2 Remarks

The vortex sheet model for a temporal free shear layer is more involved than a point vortex model (because of finite time singularity) but easier to compute than a direct Navier-Stokes solution at high Reynolds number. This makes it a compromise between the two methods. A major task is to interpret the output of the vortex sheet model obtained from a computer. This thesis covers the mathematical formulation, computer simulation and physical redundancy

checks.

1. Coherent structures in a free shear layer are long-lived. They sometimes continue to exist even when absorbed by other bigger coherent structures. However, for a computer to detect it requires a significant amount of programing effort. Principal order decomposition is one method to detect the presence of structures within structures.

2. Numerical errors in computation cannot be treated as random perturbations as they are systematic and lead to the non-conservation of Hamiltonian in the inviscid vortex sheet. Accumulation of numerical errors also leads to self-intersection of a vortex sheet.

3. A numerical integration scheme that is faster than the present one is one way to increase computational efficiency. The conservation of the Hamiltonian function is a rigorous check on the accuracy of integration. The other way to the increase computational efficiency is by using more powerful computers.

4. We are yet to comment on the applications and usefulness of the vortex sheet element model. While the model is important from a theoretical perspective, it is also of interest to find practical utility. It can be used to simulate free shear layers occurring in nature or in engineering. It reduces the flow to a mathematical problem that can be solved with the aid of computers. It is less complex than the solution of Navier-Stokes equations by DNS: the computations can be performed on a desktop computer. The model is however two-dimensional and cannot be used in three dimensions.

5. The role of surface tension has been ignored in this thesis. In free shear layers surface tension minimizes or reduces the interface between the fast and slow streams. This prevents the layer from developing extremely fine scale structures. Surface tension can provide a regularization to the equation of motion of a self-induced vortex sheet, only if the medium is liquid. For gases there is no surface tension.

<div align="center">THE END</div>

Appendix A

Evolution of the Flow Field u, v and p, and Conservation of Invariants

The vortex sheet model does not require explicit input of the velocity field $\boldsymbol{u} = (u, v)$ and the pressure field p to march forward in time. The velocity field can be obtained from the vortex sheet equation (2.35). All information of the velocity field is contained in the vortex sheet itself. However, in direct solution methods of the incompressible Navier-Stokes equations the velocity field is required as an input. Further, the momentum equation links velocity with pressure.

The role of pressure in incompressible Navier-Stokes equations is not as a thermodynamic variable related to density and temperature. It is a property of the flow which can be solved from the velocity field

$$\nabla^2 p = -\nabla \cdot (\boldsymbol{u} \cdot \nabla)\boldsymbol{u} \tag{A.1}$$

This is known as the *pressure Poisson equation*, and needs to solved in both implicit and explicit solutions of the Navier-Stokes equations. For a vortex sheet model, finding pressure is not required for time evolution, but the sheet itself does not formulate pressure unlike velocity. One needs to solve (A.1) along with appropriate bounary conditions. The general form of the the Poisson equation is $\nabla^2 p = f$ in a volume V with surface S. f is called the source term. If p is known on the surface S (Dirichlet boundary conditions) then the solution to p in V is unique. In two dimensions the source term of equation (A.1) reduces to

$$f = -(u_x u_x + v_x u_y + u_y v_x + v_y v_y) \tag{A.2}$$

Equation (A.1) can be solved by a finite difference scheme. Assume a uniform spatial discretization on a $m \times n$ grid:

$$(\nabla^2 p)_{ij} = \frac{p_{i+1,j} + p_{i-1,j} - 2p_{ij}}{h^2} + \frac{p_{i,j+1} + p_{i,j-1} - 2p_{ij}}{h^2} \tag{A.3}$$

$$= \frac{p_{i+1,j} + p_{i-1,j} + p_{i,j+1} + p_{i,j-1} - 4p_{ij}}{h^2} \tag{A.4}$$

for all $1 < i < m$ and $1 < j < n$. The boundary values are zero and therefore need not be included in the equation. Here we have assumed Dirichlet boundary conditions. The momentum equation requires only derivatives of pressure, so its absolute magnitude can include constant terms. We solve for a $(m-2) \times (n-2)$ linear system of equations. The derivatives of the u and v are also obtained by central differencing on a staggered grid with repect to the grid for p.

Note that solution obtained for p may be weakly singular (no singularity in p or its first or its second derivtaives) because of the presence of corners in the boundary.

The solution of the pressure field is used to update the velocity field in time in a direct solution of the Navier-Stokes equations. The updated velocity field is not divergence free in implicit or semi-implicit methods. The velocity and pressure fields are then iterated to obtain the correct values. The vortex sheet, however, is derived from kinematics and solution of Poisson equation is unnecessary other than to visualize the flow field.
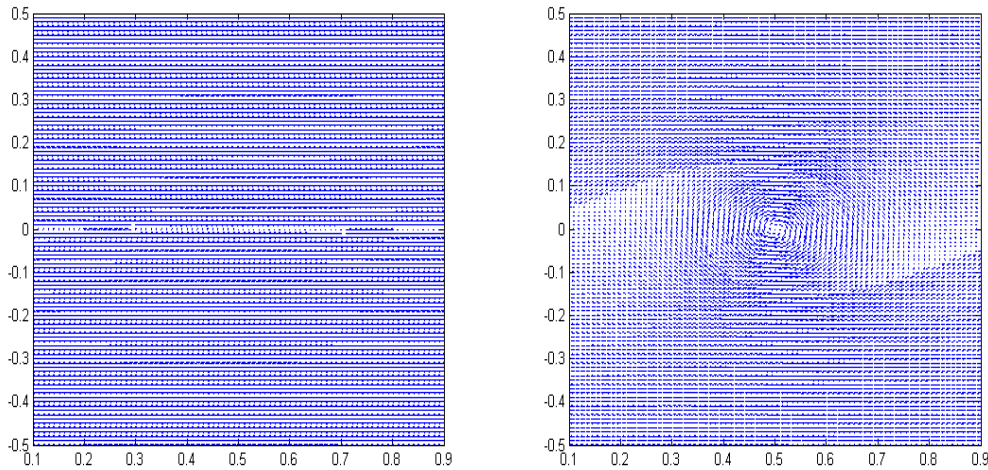

Figure A.1:   Velocity field obtained from model equations before and after the formation of vortex with centre at (0.5,0) respectively.
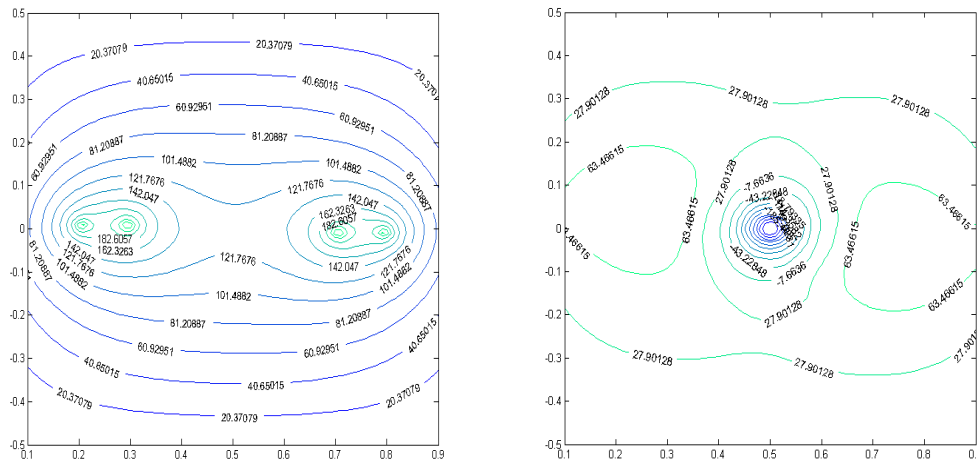
Figure A.2:   Pressure field obtained from velocity before and after the formation of vortex with centre at (0.5,0) respectively. The vortex core is a low pressure zone. The absolute values of the pressure are not important, since only gradients of pressure enter the momentum equation.

The physical variables: mass and momentum should be conserved in the flow generated by the vortex sheet. The Navier-Stokes equations automatically ensure the conservation of mass and momentum. Kinetic energy is also conserved in the absence of viscosity. For a temporal mixing layer associated with a periodic vortex sheet, the absolute magnitudes of all three variables are

infinite. However, the variation of these quantities from their respective initial values at $t = 0$ must be zero. All changes are to be measured in the domain $[0, 1) \times (-\infty, +\infty)$. The averaged quantity

$$\langle u_i \rangle (y, t) = \frac{1}{L} \int_0^L u_i(x, y, t) dx \tag{A.5}$$

is denoted as U_i. Note that $L = 1$ here, but the symbol is retained for nevertheless. The function $\langle u_i \rangle$ gives a velocity profile depending on t. One important consequence of the above definition is that

$$\left\langle \frac{\partial u_i}{\partial x} \right\rangle = \frac{1}{L} \int_0^L \frac{\partial u_i}{\partial x} dx = \frac{1}{L} u_i(x, y, t) \big|_{x=0}^L = 0 \tag{A.6}$$

This is a consequence of the periodic nature of u_i in x.

The conservation law for mass is reduced to the continuity equation, and in the absence of density term follows:

$$\frac{\partial u_i}{\partial x_i} = 0 \tag{A.7}$$

The momentum equation in the absence of viscous term reduces to

$$\frac{\partial u_i}{\partial t} + u_j \frac{\partial u_i}{\partial x_j} = -\frac{\partial p}{\partial x_i} \tag{A.8}$$

Note this is not a single equation, but a set of two equations. Multiplying both sides of (A.8) by u_i we get

$$u_i \frac{\partial u_i}{\partial t} + u_i u_j \frac{\partial u_i}{\partial x_j} = \frac{\partial}{\partial t} \left(\frac{1}{2} u_i u_i \right) + u_j \frac{\partial}{\partial x_j} \left(\frac{1}{2} u_i u_i \right) = -u_i \frac{\partial p}{\partial x_i} \tag{A.9}$$

Let $K(x, y, t) = \frac{1}{2} u_i u_i$ be the kinetic energy per unit mass of the fluid. The kinetic energy therefore follows the conservation equation

$$\frac{\partial K}{\partial t} + u_j \frac{\partial K}{\partial x_j} = -\frac{\partial}{\partial x_i} (p u_i) \tag{A.10}$$

A Reynolds type decomposition separates the flow variable u_i into the mean component and the fluctuating component.

$$u_i = \langle u_i \rangle + u_i' = U_i + u_i' \tag{A.11}$$

The mean value of the fluctuating component is zero. This follows from the previous equation.

$$\langle u_i' \rangle = 0 \tag{A.12}$$

The pressure p is also divided as a mean pressure plus a fluctuating component.

$$p = \langle p \rangle + p' = P + p' \tag{A.13}$$

The mean value of the pressure fluctuation is also zero.

$$\langle p' \rangle = 0 \tag{A.14}$$

Then taking the mean of the continuity equation (A.7) we get

$$\left\langle \frac{\partial u_i}{\partial x_i} \right\rangle = \left\langle \frac{\partial u_1}{\partial x_1} \right\rangle + \left\langle \frac{\partial u_2}{\partial x_2} \right\rangle = 0 + \frac{\partial \langle u_2 \rangle}{\partial x_2} = \frac{\partial (U_2 + \langle u_2' \rangle)}{\partial x_2} = \frac{\partial U_2}{\partial x_2} = 0 \tag{A.15}$$

Since U_1 and U_2 are not functions of x_1, the following derivatives are also zero:

$$\frac{\partial U_1}{\partial x_1} = 0, \quad \frac{\partial U_2}{\partial x_1} = 0 \tag{A.16}$$

Derivative of U_2 with respect to x_2 is zero. It follows that U_2 must be a constant function at each time t. The far field value of U_2 is always zero i.e. $U_2(\infty, t) = 0$. Therefore

$$U_2 = 0 \tag{A.17}$$

Equation (A.17) can be verified directly from the flow. The flow variables are computed over a discrete rectangular grid with spacing 0.001.

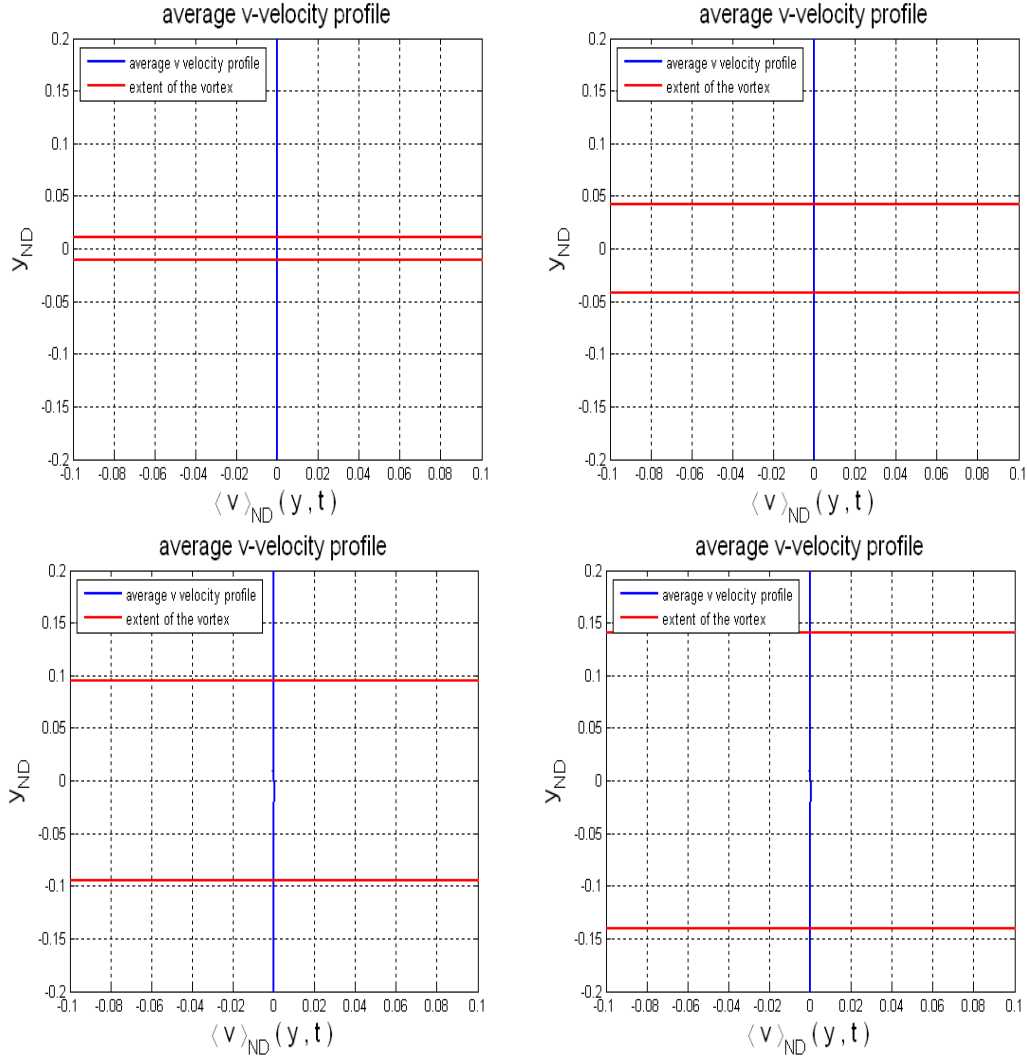Figure A.3: Velocity profiles for $\frac{U_2}{2U}$ at $t_{ND} = 0, 0.7, 1.1080$ and 1.4160 respectively. $U = 1$ and variations of U_2 from zero is of $O(10^{-4})$.

There is no vorticity in the fluid except on the vortex sheet. Outside the vortex layer, the magnitude of U_1 is constant and equal to $\pm U$. Therefore

$$\omega = \frac{\partial u_2}{\partial x_1} - \frac{\partial u_1}{\partial x_2} = 0 \tag{A.18}$$

everywhere on the line joining $(0, x_2)$ and (L, x_2)[1]. Consequently the average $\langle \omega \rangle$ is also zero.

$$\left\langle \frac{\partial u_2}{\partial x_1} \right\rangle - \left\langle \frac{\partial u_1}{\partial x_2} \right\rangle = 0 \tag{A.19}$$

or,

$$\frac{\partial \langle u_1 \rangle}{\partial x_2} = \frac{\partial U_1}{\partial x_2} = 0 \tag{A.20}$$
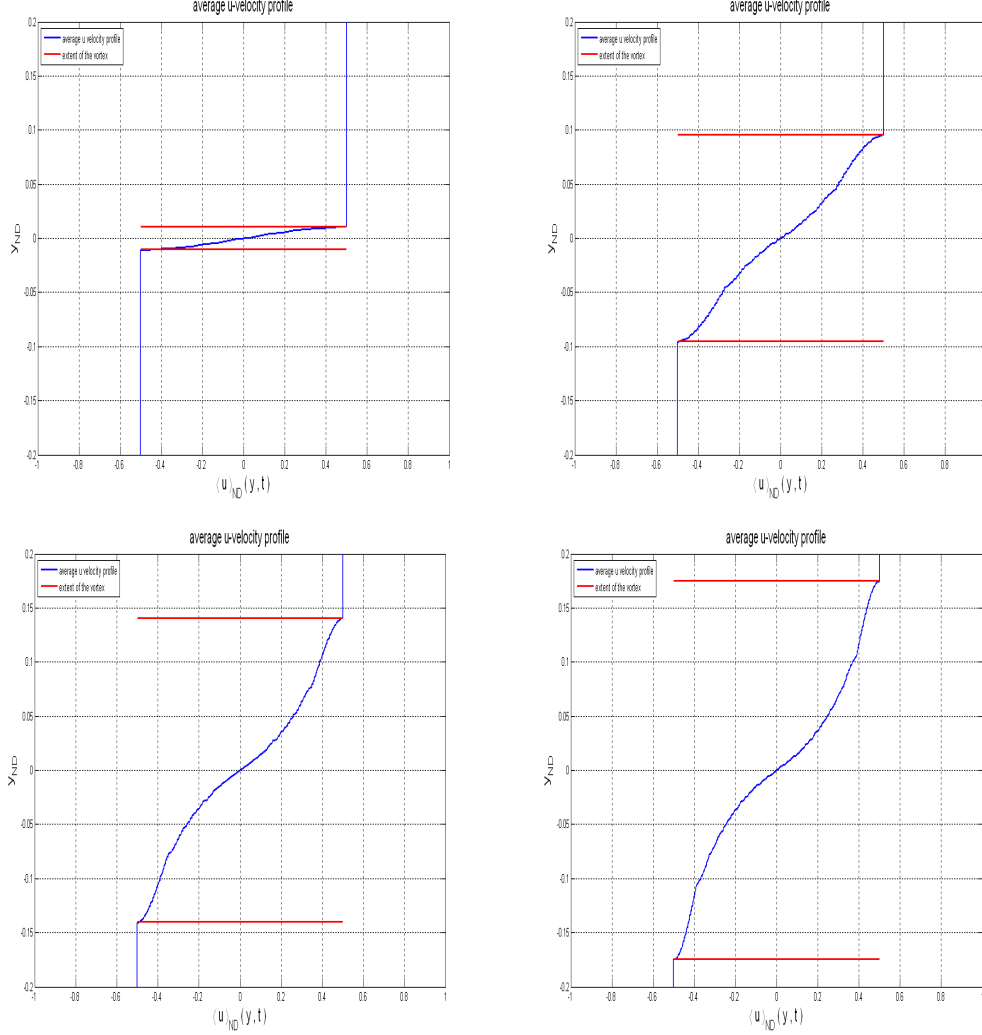
Figure A.4: Velocity profiles for $\frac{U_1}{2U}$ at $t_{ND} = 0, 0.7, 1.1080$ and 1.4160 respectively. The absolute value of $U_1 = U = 10$ outside the vortex region.

Since (A.20) is not true when x_2 lies within the vortex region, the profile of U_1 is not flat there. Also, $\frac{\partial U_i}{\partial x_i} = \frac{\partial U_1}{\partial x_1} + \frac{\partial U_2}{\partial x_2} = 0$. Substituting this in the continuity equation gives

$$\frac{\partial u'_i}{\partial x_i} = 0 \tag{A.21}$$

The averaged form of the Navier-Stokes equation are obtained as follows:

$$\frac{\partial (U_i + u'_i)}{\partial t} + (U_j + u'_j) \frac{\partial (U_i + u'_i)}{\partial x_j} = -\frac{\partial (P + p')}{\partial x_i} \tag{A.22}$$

---

[1] x_2 is such that the line does not intersect with the vortex sheet.

or,

$$\left\langle \frac{\partial (U_i + u_i')}{\partial t} + (U_j + u_j') \frac{\partial (U_i + u_i')}{\partial x_j} \right\rangle = - \left\langle \frac{\partial (P + p')}{\partial x_i} \right\rangle \tag{A.23}$$

or,

$$\frac{\partial U_i}{\partial t} + \frac{\partial \langle u_i' \rangle}{\partial t} + U_j \frac{\partial U_i}{\partial x_j} + U_j \left\langle \frac{\partial u_i'}{\partial x_j} \right\rangle + \langle u_i' \rangle \frac{\partial U_i}{\partial x_j} + \left\langle u_j' \frac{\partial u_i'}{\partial x_j} \right\rangle = -\frac{\partial P}{\partial x_i} - \frac{\partial p'}{\partial x_i} \tag{A.24}$$

or,

$$\frac{\partial U_i}{\partial t} + U_j \frac{\partial U_i}{\partial x_j} + \left\langle \frac{\partial (u_i' u_j')}{\partial x_j} \right\rangle = -\frac{\partial P}{\partial x_i} \tag{A.25}$$

We put $i = 1$ and $i = 2$ in the above equation respectively.

$$\frac{\partial U_1}{\partial t} + \frac{\partial}{\partial x_2} \langle u_1' u_2' \rangle = 0 \tag{A.26a}$$

$$\frac{\partial}{\partial x_2} \langle u_2' u_2' \rangle = -\frac{\partial P}{\partial x_2} \tag{A.26b}$$

While equation (A.26a) can be verified directly, equation (A.26b) is needed to compute the average pressure P. Equation (A.26a) can be further simplified

$$\frac{\partial U_1}{\partial t} + \frac{\partial}{\partial x_2} \langle u_1 u_2 \rangle = 0 \tag{A.27}$$

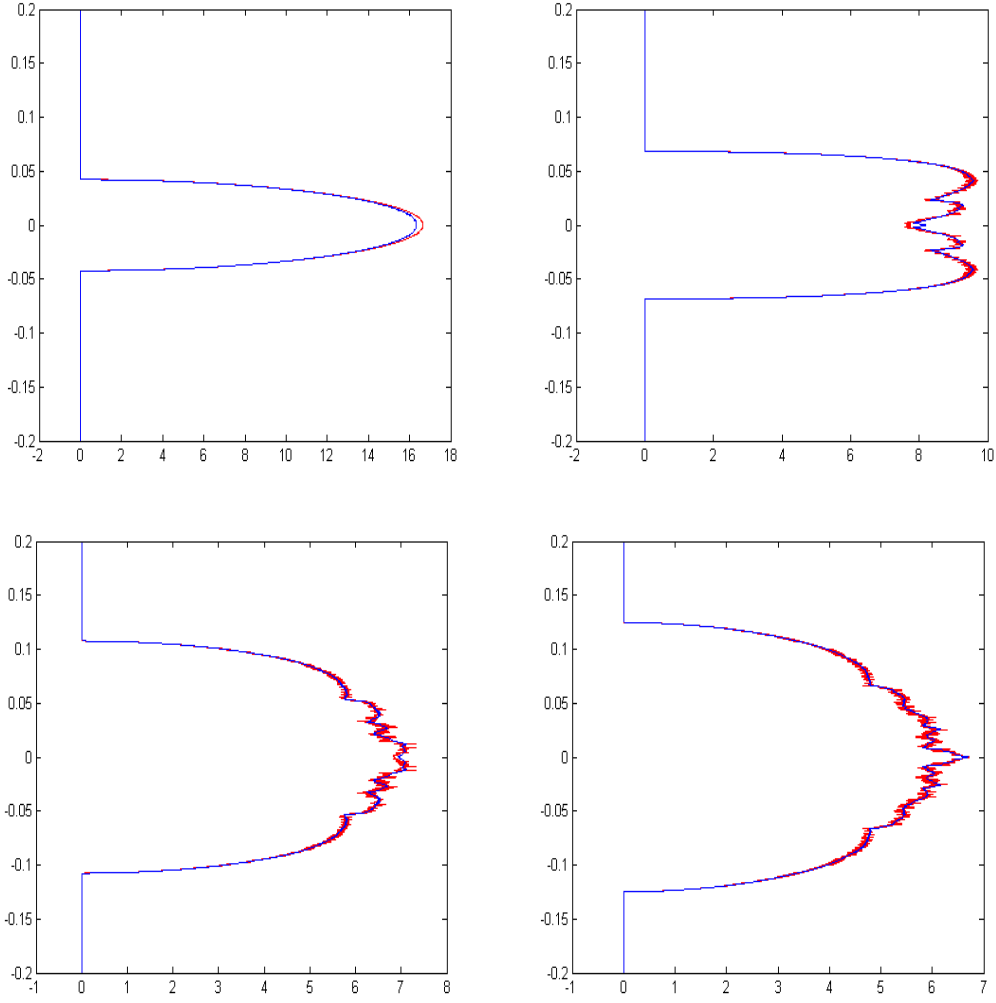The validity of (A.27) is shown in figure A.

Figure A.5: Profiles for $\langle u_1 u_2 \rangle$ in blue and $\int_{-\infty}^{x_2} \frac{\partial U_1}{\partial t} dx_2$ in red at $t_{ND} = 0.7, 0.888, 1.24$ and 1.372 respectively.

The averaged energy equation is obtained by multiplying the Navier-Stokes equation with u_i' and then taking the average.

$$\left\langle u_i' \frac{\partial (U_i + u_i')}{\partial t} + u_i'(U_j + u_j') \frac{\partial (U_i + u_i')}{\partial x_j} \right\rangle = -\left\langle u_i' \frac{\partial (P + p')}{\partial x_i} \right\rangle \tag{A.28}$$

or,

$$\left\langle u_i' \frac{\partial U_i}{\partial t} + u_i' \frac{\partial u_i'}{\partial t} + u_i' \left(U_j \frac{\partial U_i}{\partial x_j} + U_j \frac{\partial u_i'}{\partial x_j} + u_j' \frac{\partial U_i}{\partial x_j} + u_j' \frac{\partial u_i'}{\partial x_j} \right) \right\rangle = -\left\langle u_i' \frac{\partial P}{\partial x_i} + u_i' \frac{\partial p'}{\partial x_i} \right\rangle \tag{A.29}$$

or,

$$\langle u_i' \rangle \frac{\partial U_i}{\partial t} + \frac{\partial}{\partial t} \left\langle \frac{1}{2} u_i' u_i' \right\rangle + \langle u_i' \rangle U_j \frac{\partial U_i}{\partial x_j} + U_j \left\langle \frac{\partial}{\partial x_j} \left(\frac{1}{2} u_i' u_i' \right) \right\rangle + \langle u_i' u_j' \rangle \frac{\partial U_i}{\partial x_j} + \left\langle \frac{\partial}{\partial x_j} \left(\frac{1}{2} u_i' u_i' u_j' \right) \right\rangle$$
$$= -\langle u_i' \rangle \frac{\partial P}{\partial x_i} - \left\langle \frac{\partial (p' u_i')}{\partial x_i} \right\rangle \tag{A.30}$$

Let $u_i' u_i' = q^2$. This quantity represents the turbulent kinetic energy.

$$\frac{\partial}{\partial t} \left\langle \frac{q^2}{2} \right\rangle + U_j \left\langle \frac{\partial}{\partial x_j} \left(\frac{q^2}{2} \right) \right\rangle + \langle u_i' u_j' \rangle \frac{\partial U_i}{\partial x_j} + \left\langle \frac{\partial}{\partial x_j} \left(\frac{q^2}{2} u_j' \right) \right\rangle = -\left\langle \frac{\partial (p' u_i')}{\partial x_i} \right\rangle \tag{A.31}$$

Since q^2 and p' are periodic functions of x_1, equation (A.31) can be further simplified to

$$\frac{\partial}{\partial t}\left\langle \frac{q^2}{2}\right\rangle + \langle u_1' u_2'\rangle \frac{\partial U_1}{\partial x_2} + \frac{\partial}{\partial x_2}\left\langle \frac{q^2}{2}u_2'\right\rangle = -\frac{\partial}{\partial x_2}\langle p' u_2'\rangle \tag{A.32}$$

The vortex sheet equivalent for the conservation of mass and momentum are easier to verify. This is because the vortex sheet is a one dimensional structure. Various integral quantities are conserved during the evolution of two-dimensional vorticity distributions in an inviscid and incompressible fluid of uniform density as a direct consequence of Kelvin's theorem. Some of them have already been introduced earlier.

1. The total circulation

$$\Gamma = \sum_{i=1}^{N}\gamma_i \ell_i \tag{A.33}$$

2. The first order moments

$$M_x = \sum_{i=1}^{N}\gamma_i \ell_i x_{mi}, \quad M_y = \sum_{i=1}^{N}\gamma_i \ell_i y_{mi} \tag{A.34}$$

where $(x_{mi}, y_{mi}) = \left(\frac{x_i + x_{i-1}}{2}, \frac{y_i + y_{i-1}}{2}\right)$ is the midpoint of the ith segment.

3. The second order moment

$$J = \sum_{i=1}^{N}\gamma_i \ell_i \left[x_{mi}{}^2 + y_{mi}{}^2 + \frac{\ell^2}{12}\right] \tag{A.35}$$

The conservation of total circulation is automatically taken care of by the numerical simulation. The first order moments do not exhibit any systematic or significant variation. The initial values are: $M_{x0} = 2.38 \times 10^{-16}$ and $M_{y0} = -1.0099$. M_x attains a maximum magnitude of 2×10^{-12} and M_y varies by approximately $4.31 \times 10^{-7}\%$. The conservation of J fails due to the dissipative effect of viscosity. The second order moment decreases with time. It is not calculated or shown here, but the Hamiltonian is given in Appendix B.

Appendix B

Conservation of the Hamiltonian Function

The point vortex system is a Hamiltonian system for the conjugate variables $x_j N^{-\frac{1}{2}}$ and $y_j N^{-\frac{1}{2}}$; the Hamiltonian function is given by,

$$H(t) = \sum_{j=1}^{N} \sum_{k=1}^{N} {}' \Gamma_j \Gamma_k \log\left(\cosh 2\pi(y_j - y_k) - \cos 2\pi(x_j - x_k)\right) \tag{B.1}$$

The Hamiltonian is an invariant of motion and its value does not change with t.

The vortex sheet can be cast as a Hamiltonian system, but explicit representation of the Hamiltonian function H is difficult. The Hamiltonian is like interaction energy of the vortex sheet system and must depend only on relative locations of the vortex sheet elements, because H must remain invariant during rotation and translation of the system. Let H be a function of the form

$$H = \sum_{j=1}^{N} \sum_{k=1}^{N} {}' \Gamma_j \Gamma_k \, f(r_{jk}) \qquad \text{where} \qquad r_{jk} = |z_j - z_k| \tag{B.2}$$

The notation $\sum'$ implies excluding $j = k$ during summation. The Hamiltonian H and the function f are obtained from the following equation

$$\Gamma_j \frac{\mathrm{d}z_j^*}{\mathrm{d}t} = -2i \frac{\partial H}{\partial z_j} \tag{B.3}$$

of which splitting the real and imaginary parts lead to Hamilton's canonical equations

$$\Gamma_j \frac{\mathrm{d}x_j}{\mathrm{d}t} = -\frac{\partial H}{\partial y_j} \tag{B.4a}$$

$$\Gamma_j \frac{\mathrm{d}y_j}{\mathrm{d}t} = \frac{\partial H}{\partial x_j} \tag{B.4b}$$

Here $x_j \Gamma_j^{-\frac{1}{2}}$ is the generalized momentum and $y_j \Gamma_j^{-\frac{1}{2}}$ is the generalized coordinate. The time rate of the Hamiltonian is zero and H is an invariant quantity.

$$\begin{aligned} \frac{\mathrm{d}H}{\mathrm{d}t} &= \frac{\partial H}{\partial x_j} \frac{\mathrm{d}x_j}{\mathrm{d}t} + \frac{\partial H}{\partial y_j} \frac{\mathrm{d}y_j}{\mathrm{d}t} \\ &= \Gamma_j \frac{\mathrm{d}y_j}{\mathrm{d}t} \frac{\mathrm{d}x_j}{\mathrm{d}t} - \Gamma_j \frac{\mathrm{d}x_j}{\mathrm{d}t} \frac{\mathrm{d}y_j}{\mathrm{d}t} = 0 \end{aligned} \tag{B.5}$$

Since the motion equation (2.34) is a function of z_j's only, equation (B.3) can be solved for H

in principle.

$$\frac{\mathrm{d}z_j^*}{\mathrm{d}t} = -\sum_{k=1}^{N}{}' \frac{i\gamma_k}{2\pi} \left[\log \frac{\sin \pi(z_j - z_k - \ell_k e^{i\theta_k})}{\sin \pi(z_j - z_k)}\right] e^{-i\theta_k}$$

$$= -\sum_{k=1}^{N}{}' \frac{i\Gamma_k}{2\pi} \left[\log \frac{\sin \pi(z_j - z_k - \ell_k e^{i\theta_k})}{\sin \pi(z_j - z_k)}\right] \ell_k^{-1} e^{-i\theta_k}$$

$$= -\sum_{k=1}^{N}{}' \frac{i\Gamma_k}{2\pi} \left[\log \frac{\sin \pi(z_j - z_{k+1})}{\sin \pi(z_j - z_k)}\right] (z_{k+1} - z_k)^{-1} \tag{B.6}$$

Therefore,

$$\frac{\partial H}{\partial z_j} = \Gamma_j \sum_{k=1}^{N}{}' \frac{\Gamma_k}{4\pi} \left[\log \frac{\sin \pi(z_j - z_{k+1})}{\sin \pi(z_j - z_k)}\right] (z_{k+1} - z_k)^{-1} \tag{B.7}$$

The Hamiltonian is not conserved in general due to the process of desingularization. The final Hamiltonian is always smaller than the initial Hamiltonian due to dissipation of energy.
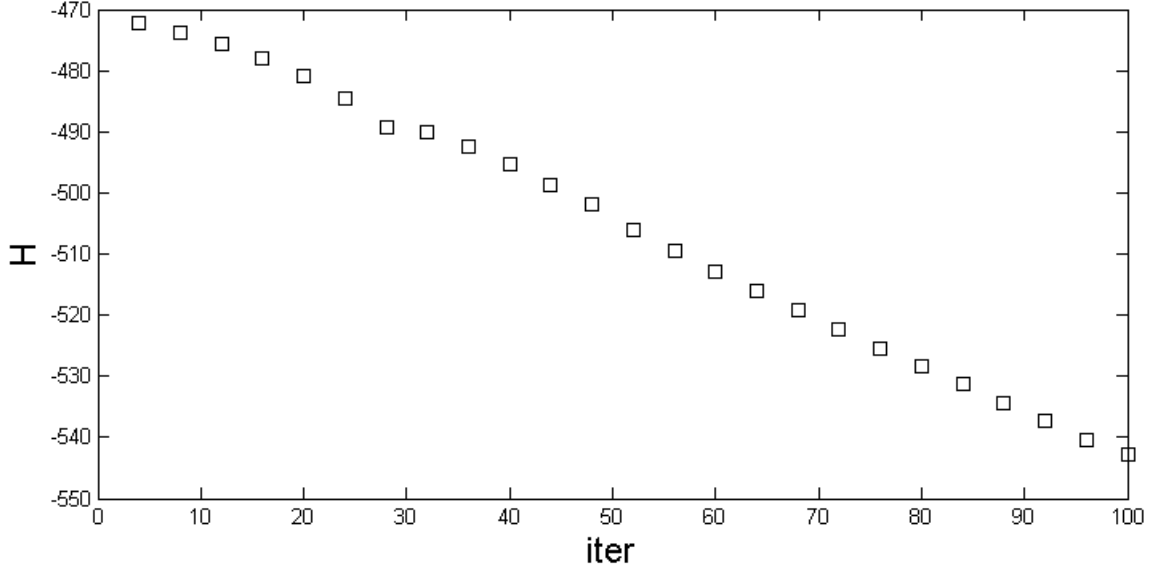

Figure B.1: The decrease of Hamiltonian function H due to loss of energy in the desingularization. The initial Hamiltonian is H_I = -472.1077 and the final Hamiltonian is H_F = -542.7209.

Bibliography

[1] Acton,E. 1976 The modelling of large eddies in a two-dimensional shear layer, *Journal of Fluid Mechanics* 76,3 561-592.

[2] Aref,H. and Siggia,E. 1979 Vortex dynamics of the two-dimensional turbulent shear layer, *Journal of Fluid Mechanics*, 100, 705-737.

[3] Baker,G. and Pham,L. 2006 A comparison of blob methods for vortex sheet roll-up, *Journal of Fluid Mechanics* 547, 297-316.

[4] Baker,G. and Shelley,M. 1990 On the connection between thin vortex layers and vortex sheets, *Journal of Fluid Mechanics* 215, 161-194.

[5] Basu,A., Narasimha,R. and Prabhu,A. 1994 Modelling plane mixing layers using vortex points and sheets, *Appl. Math. Modelling* 19, 66-75.

[6] Batchelor,G. 1969 *Phys. Fluids Suppl.* 12, 233-239.

[7] Beale,J. Kato,T. and Majda,A. 1984 Remarks on the breakdown of smooth solutions for the 3-D Euler equations *Comm. Math. Phys.* 94(1) 61–66.

[8] Bhattacharya,P. Manoharan,M. Govindarajan,R. and Narasimha,R. 2006 The critical Reynolds number of a laminar incompressible mixing layer from minimal composite theory, *Journal of Fluid Mechanics* 555, 105-114.

[9] Birkhoff,G. 1962 Helmholtz and Taylor instability, *Proceedings of Symposia in Applied Mathematics, American Mathematical Society, Providence* 55-76.

[10] Brady,M. and Pullin,D. 1999 On singularity formation in three-dimensional vortex sheet evolution, *Phys. Fluids.* 11, 3198

[11] Brown,G. and Roshko,A. 1974 On density effects and large structure in turbulent mixing layers, *Journal of Fluid Mechanics* 64,4 775-816.

[12] Caflisch,R. and Orellana,O. Singular solutions and ill posedness for the evolution of vortex sheets *Siam J.Math. Anal.* 20,2 293-307.

[13] Carazzo,G. Kaminski,E. and Tait,S. 2006 The route to self-similarity in turbulent jets and plumes, *Journal of Fluid Mechanics* 547, 137–148.

[14] Chavanis,P. Sommeria,J. and Robert,R. 1996 Statistical mechanics of two-dimensional vortices and collisionless stellar systems, *Astrophys. J.* 71, 385.

[15] Chorin,A. and Benard,P. 1973 Discretization of a vortex sheet, with an example of roll-up, *J. Comput. Phys.* 13, 423-429.

[16] Davidson,P. 2004 Turbulence: An Introduction for Scientists and Engineers, *Oxford University Press.*

[17] Delcourt,B. and Brown,G. 1979 The evolution and emerging structure of a vortex sheet in an inviscid and viscous fluid modelled by a point vortex method, *2nd Symp. Turb. Shear Flows, London.*

[18] Delort, 1991 Existence de nappes de tourbillon en dimension deux, *J. Am. Math. Soc.* 4, 553-586.

[19] Dhanak,M. 1994 Equation of motion of a diffusing vortex sheet, *Journal of Fluid Mechanics* 269, 265–281.

[20] Drazin,P. and Reid,W. 2004 Hydrodynamic stability, *Cambridge University Press.*

[21] Eyink,G. and Sreenivasan,K. 2006 Onsager and the theory of hydrodynamic turbulence *Rev. Mod. Phys.*

[22] Friedmann,A. and Poloubarinova,P. 1928 Über fortschreitende Singularitäten der ebenen Bewegung einer inkompressiblen Flüssigkeit, *Recueil de Géophysique* 9-23.

[23] Helmholtz,H von. 1868 Über discontinuirliche flüssigkeits-bewegungen, *Monats. Konigl Preuss. Akad. Wiss. Berlin* 215-228.

[24] Holm,D. Nitsche,M. and Putkaradze,V. 2006 Euler-alpha and vortex blob regularization of vortex filament and vortex sheet motion, *Journal of Fluid Mechanics* 555, 149–176.

[25] Hou,T. Lowengrub,J. and Shelley,M. 1997 The long time motion of vortex sheets with surface tension *Phys. Fluids* 9 1933–1954.

[26] Ishihara,T. and Kaneda,Y. 1995 Singularity formation in three-dimensional motion of a vortex sheet, *Journal of Fluid Mechanics* 300, 339-366.

[27] Ishihara,T. Kaneda,Y. Yokokawa,M. Itakura,K. and Uno,A. 2007 Small-scale statistics in high-resolution direct numerical simulation of turbulence: Reynolds number dependence of one-point velocity gradient statistics, *Journal of Fluid Mechanics.* 592, 335-366.

[28] Joyce,G. and Montgomery,D. 1973 Negative temperature states for the two-dimensional guiding-centre plasma, *J. Plasma Phys.* 10, 107-121.

[29] Krasny,R. 1986 A study of singularity formation in a vortex sheet by the point-vortex approximation, *Journal of Fluid Mechanics* 167, 65-93.

[30] Krasny,R. 1986 Desingularization of periodic vortex sheet roll up, *J. Comput. Phys* 65,2 292-313.

[31] Kolmogorov,A. 1941 The local structure of turbulence in incompressible viscous fluid for very large Reynolds numbers, *Dokl. Akad. Nauk SSSR* 30, 301-305.

[32] Kraichnan,R. 1967 Inertial ranges in two dimensional turbulence, *Phys. Fluids* 10, 1417-1423.

[33] Moore,D. 1978 The equation of motion of a vortex layer of small thickness, *Stud. Appl. Math.* 58,2 119–140.

[34] Moore,D. 1979 The spontaneous appearance of a singularity in the shape of an evolving vortex sheet, *Proceedings of the Royal Society* 365 1720.

[35] Moore,D. 1971 The discrete vortex approximation of a finite vortex sheet, *Califoria Institute of Technology Technical Report AFOSR*.

[36] Marchioro,C. and Pulvirenti,M. 1993 Mathematical theory of incompressible nonviscous fluids, *Springer*.

[37] Majda,A. and Bertozzi,A. 2002 Vorticity and incompressible flow, *Cambridge Text in Applied Mathematics*.

[38] Meiron,D. Baker,G. and Orszag,S. 1981 Analytic structure of vortex sheet dynamics. Part 1. Kelvin-Helmholtz instability, *Journal of Fluid Mechanics* 114, 283-298.

[39] Narasimha,R. and Basu,A. 1992 Vortex sheet simulation of a plane canonical mixing layer, *Computers and Fluids* 21, 1-30.

[40] Narasimha,R. and Prabhu,A. 1972 Equilibrium and relaxation in turbulent wakes, *Journal of Fluid Mechanics.* 54,1 1-17.

[41] Newton,P. 2001 The N vortex problem: analytical techniques, *Springer-Verlag, Applied Mathematical Sciences*.

[42] Nitsche,M. 2001 Singularity formation in a cylindrical and a spherical vortex sheet, *J. Comput. Phys.* 173, 208–230.

[43] Onsager,L. 1949 Statistical hydrodynamics, *Nuovo Cimento Suppl.*

[44] Paul,U. and Narasimha,R. 2013 The vortex sheet model for a turbulent mixing layer, *Phys. Scr.* T155.

[45] Pozrikidis,C. 2009 Fluid dynamics theory, computation and numerical simulation, *Springer*.

[46] Rosenhead,L. 1931 The formation of vortices from a surface of discontinuity, *Proc. R. Soc. Lond. A* 134,823 170-192.

[47] Saffman,P. 1977 Vorticity dynamics, *Cambridge University Press*.

[48] Sakajo,T. 2004 Analytic continuation of the Birkhoff–Rott equation in complex-time domain, *Euro. Jnl of Applied Mathematics* 15,1 39-53.

[49] Shelley,M. 1992 A study of singularity formation in vortex-sheet motion by a spectrally accurate vortex method, *Journal of Fluid Mechanics* 244, 493-526.

[50] Suryanaryanan,S. and Narasimha,R. 2014 Insights into turbulent free shear layer dynamics from vortex-gas computations and statistical mechanics, *JNCASR Thesis Report.*

[51] Suryanarayanan,S. Narasimha,R. and Haridass,N. 2014 Free turbulent shear layer in a point vortex gas as a problem in nonequilibrium statistical mechanics, *Phy.Rev. E.* E89, 013009.

[52] Townsend,A. 1956 The Structure of Turbulent Shear Flow *Cambridge University Press.*

[53] Tryggvason,G. Dahm,W. and Sbeih,W. 1991 Fine structure of vortex sheet rollup by viscous and inviscid simulation, *Journal of Fluid Engg* 31-36.

[54] Winant,C. and Browand,F. 1974 Vortex pairing: the mechanism of turbulent mixing-layer growth at moderate Reynolds number, *Journal of Fluid Mechanics* 63, 237–255.

[55] Wygnanski,I. Oster,D. Fiedler,H. and Dziomba,B. 1979 On the perseverance of a quasi two dimensional eddy structure in a turbulent mixing layer, *Journal of Fluid Mechanics* 93, 325-335.